

Nuclear matter at high density: Phase transitions, multiquark states, and supernova outbursts

M. I. Krivoruchenko, D. K. Nadyozhin, T. L. Rasinkova, Yu. A. Simonov, M. A. Trusov, A. V. Yudin
Institute for Theoretical and Experimental Physics, Moscow, Russia

Phase transition from hadronic matter to quark-gluon matter is discussed for various regimes of temperature and baryon number density. For small and medium densities, the phase transition is accurately described in the framework of the Field Correlation Method, whereas at high density predictions are less certain and leave room for the phenomenological models. We study formation of multiquark states (MQS) at zero temperature and high density. Relevant MQS components of the nuclear matter can be described using a previously developed formalism of the quark compound bags (QCB).

Partial-wave analysis of nucleon-nucleon scattering indicates the existence of $6Q_S$ which manifest themselves as poles of P -matrix. In the framework of the QCB model, we formulate a self-consistent system of coupled equations for the nucleon and $6Q_S$ propagators in nuclear matter and the G -matrix. The approach provides a link between high-density nuclear matter with the MQS components and the cumulative effect observed in reactions on the nuclei, which requires the admixture of MQS in the wave functions of nuclei kinematically.

$6Q_S$ determine the natural scale of the density for a possible phase transition into the MQS phase of nuclear matter. Such a phase transition can lead to dynamic instability of newly born protoneutron stars and dramatically affect the dynamics of supernovae. Numerical simulations show that the phase transition may be a good remedy for the triggering supernova explosions in the spherically symmetric supernova models. A specific signature of the phase transition is an additional neutrino peak in the neutrino light curve. For a Galactic core-collapse supernova, such a peak could be resolved by the present neutrino detectors. The possibility of extracting the parameters of the phase of transition from observation of the neutrino signal is discussed also.

PACS numbers: 12.38.Mh, 12.39.Mk, 26.30.-k, 25.75.Nq

Contents

I. Introduction	4
II. Quark-hadron phase transition in QCD	7
A. Gibbs' criterion	7
B. QCD phase diagram in FCM	8
C. Suppression of color superconductivity	11
D. Critical baryon chemical potential in cold nuclear matter	11
III. Density effect on confinement potential below phase transition	12
IV. Quark Compound Bag model	14
V. Effective Lagrangian of Quark Compound Bag model	18
VI. In-medium nucleon and dibaryon propagators	20
A. Nucleon propagators in ideal Fermi gas	20
B. Dibaryon propagators	21
C. In-medium dispersion law for interacting nucleons	22
D. Dyson equation for nucleon propagator	23
E. Bethe-Brueckner equation for dibaryon propagator	24
F. Link to optical potential model	24
VII. Dibaryons in phase shifts analysis of nucleon-nucleon scattering	25
A. Dibaryon self-energy operator in the vacuum	25
B. S matrix	26
C. P matrix. Dibaryons as P -matrix poles	27
D. P matrix and Castillejo-Dalitz-Dyson poles	29
E. Nucleon-nucleon scattering in the vacuum	30
1. 3S_1 channel	30
2. 1S_0 channel	32
3. 3P_1 and 1P_1 channels	33
4. 3P_0 channel	35
F. Discussion	35
VIII. Models of nuclear matter	35
A. Relativistic mean field models	37
B. Dirac-Brueckner-Hartree-Fock approximation	37
C. Variational approach	38
D. In-medium modifications of hadrons	39
IX. Nuclear matter with multiquark baryons. Nonrelativistic treatment	39
X. G matrix	41
A. Pauli blocking	41
B. Heterophase nuclear matter with a Bose condensate of dibaryons	43
XI. Nuclear phase transition in collapsed stellar cores	44
A. Equation of state	45
B. Initial model	46
C. Results of hydrodynamical calculations	46
D. Discussion	49
XII. Conclusions and outlook	50
Acknowledgments	51
XIII. Appendix A: The $6q$ description of 1S_0 and 3S_1 states	52

XIV. Appendix B: Transformation properties of dibaryon currents	52
A. Isospin C -parity	52
B. Lorentz C -parity:	53
C. Combined C -parity	53
D. Even and odd bilinear forms	54
References	55

I. INTRODUCTION

The problem of transition from the confined phase of hadronic matter to the deconfined quark-gluon phase is now widely discussed both on theoretical [1] and experimental levels [2] and also using lattice simulations [3]. The transition process is nonperturbative in nature and requires for a realistic description the use of nonperturbative models. Nambu-Jona-Lasinio (NJL) model and its generalizations describe successfully the spontaneous breaking of chiral symmetry but, unfortunately, do not lead to confinement and can not tell much about the deconfinement phase transition.

Recently the Field Correlator Method (FCM) [4], successfully applied earlier to the description of confinement and hadrons in the vacuum, has been extended for the description of hadron matter at nonzero temperature and density including phase transition into the deconfined phase. In this method, the quark-hadron phase transition occurs due to in-medium modifications of the QCD vacuum. The energy density of the QCD vacuum is determined by the gluonic condensate, and the colorelectric component of it is responsible for the confinement. In course of the quark-hadron phase transition, the colorelectric component evaporates, whereas the colormagnetic component stays intact (for a review see [5]).

In this way one obtains the critical transition temperature as a function of the quark flavors in agreement with the lattice data [6]. The phase diagram extrapolated to small temperatures points toward the critical quark chemical potentials of order $\mu_{cr} \cong 0.6$ GeV. This value is large enough to allow the ordinary nuclei to exist as collection of nucleons rather than quarks. The low-temperature phase transition gives rise to strong nonperturbative attraction in colorless channels [7] that provides dominance of the $q\bar{q}$ correlations over the diquark qq ones, making thereby conjecture on color superconductivity not quite realistic, in line with earlier findings [8]. In two-color QCD, where qq and $q\bar{q}$ are equivalent, superconducting phase of quark matter with colorless quark Cooper pairs [9–11] is confirmed by lattice simulations [12].

The low-temperature region of the phase diagram is, however, less certain because no interaction in the hadron medium (nuclear matter) was taken into account yet. The standard models of nuclear matter (see e.g. [13]) based on the realistic NN potentials predict energy per nucleon E/A depending rather sensitively on details of NN interaction.

An additional uncertainty comes from the $3N$ forces and nucleon-hyperon transitions, which make computation of equation of state (EoS) of the nuclear matter a rather complicated task, which calls for experimental verification. At this point an important piece of information can be obtained from astrophysics.

During the last decade, great progress is made in observational astrophysics towards the study of properties of neutron stars (see e.g. [14, 15] and, for a review, [16]). EoS of nuclear matter determined by the density dependence of E/A is important for calculation of structure and cooling rates of neutron stars and possible appearance of quark matter in interiors of neutron stars as was suggested for the first time by Ivanenko and Kurdgelaidze [17]. The current status of the quark stars hypothesis is discussed in Refs. [16, 18].

The recent interest to the nuclear matter EoS is also connected to new constraints obtained from the collective flow data and subthreshold kaon production in heavy-ion collisions [19, 20].

One of the main purposes of the present paper is to consider a generalized picture of NN interaction and of nuclear matter, which includes from the very beginning the quark degrees of freedom in the form of MQS. This implies a revision of the standard picture, based on the Yukawa mechanism of meson exchanges.

In 1935 Yukawa [21] proposed a hypothesis that the interaction between the nucleons may be due to the exchange of finite-mass meson. The experimental searches have led to the discovery of pions, heavier mesons, and eventually to the emergence of One Boson Exchange (OBE) model of nucleon-nucleon interaction. In this model, pions are responsible for long-range part of the nucleon-nucleon potential, while heavy mesons are responsible for the interaction at intermediate and short distances [22].

OBE models provide an accurate quantitative description of nucleon-nucleon interaction. The physical meaning of the meson exchange at short distances is, however, not entirely clear because of the finite size of nucleons and mesons. The values of the proton and pion charge radii $\langle r_p^2 \rangle^{1/2} = 0.875 \pm 0.007$ fm and $\langle r_\pi^2 \rangle^{1/2} = 0.659 \pm 0.025$ fm [23] indicate that the mechanism of pion exchange is justified at distances $r \gtrsim 1$ fm while at smaller distances there is overlap between hadrons, where the quark-gluon degrees freedom come into play and affect the dynamics.

Restrictions of this kind should be taken into account when calculating EoS of nuclear matter. The maximum density of nuclear matter below which the OBE models can be applied is determined by comparing the proton charge radius with the average distance between the nucleon with its nearest neighbor. The nearest neighbor is localized between r and $r + dr$, while the sphere of radius r with the probing nucleon in the center is empty. The probability distribution of the nearest neighbor is the probability of not finding a nucleon inside the sphere multiplied by the probability of finding a nucleon in the volume element $dV = 4\pi r^2 dr$. The probability do not find a nucleon inside the sphere is given by the Poisson law $P_0 = \exp(-\rho V)$, where ρ is nuclear matter density. For the saturation density $\rho_0 = 0.16$ fm⁻³, a simple calculation gives $\langle r \rangle = 1.02 \pm 0.37$ fm, where $\langle r \rangle$ is the mean distance, the second number is the standard error. When the density is close to saturation density, OBE mechanism, obviously, can not

be applied.

The problem of nuclear matter EoS is studied in the realistic OBE models of nucleon-nucleon interaction since the mid-1970's. One can distinguish three main approaches: A popular class of models based on the mean-field approximation [24, 25]. The field-theoretic Dirac-Brueckner-Hartree-Fock method goes beyond mean-field approximation (see [13] and references therein). Variational method is described in Ref. [26].

One should note that in all approaches of OBE-type additional fine tuning is required to obtain the realistic values of energies and densities, e.g., in the variational approach, $3N$ forces have to be added to the NN potentials.

OBE models are in reasonable agreement with laboratory data [19, 20], but predict a surprisingly low value of the maximum mass of neutron stars in the β -equilibrium, if one includes hyperons [27–31]. β -equilibrium leads to the occurrence of the hyperons when density increases to about $(2 \div 3)\rho_0$ and, consequently, leads to a softening of the nuclear matter EoS.

It has earlier been noted [32] that observational data on the rotation speed of X-ray transient XTE J1739-285, which point to a soft EoS, and mass of the pulsar PSR J1748-2021B, which points to a very stiff EoS, are almost mutually exclusive. In a recent study [33] data on compact sources 4U 1608-52, 1820-30 and 4U EXO 1745-248 were re-analyzed. The authors came to conclusion that only a very soft EoS is consistent with values of the mass and radius of the stars. A similar technique was used previously in the analysis of data from a compact source EXO 0748-676. In conjunction with the analysis [15], one can assume the existence of two classes of compact stars, e.g., neutron stars metastable against conversion to exotic stars, such as quark stars, strange stars, or perhaps dibaryon stars. The results of Refs. [15, 33] still require confirmation.

The difficulty in describing the massive neutron (hyperon) stars as well as the possibility of existence of various classes of compact objects stimulate the search for new concepts and models in which quark-gluon dynamics at short distances plays a more prominent role. One can expect that the microscopic models are more adequate at high density and can provide a physically satisfactory picture of the short-distance dynamics and high-density EoS.

The standard realistic NN forces (and also $3N$ forces) used for nuclear matter calculations exploit only baryonic and mesonic degrees of freedom. However, multi-quark states (MQS) can appear in nuclear matter also, yielding degrees of freedom of their own.

This idea is discussed, e.g., in Refs. [34–36]. In most papers, it is associated with multi-quark bags similar to the MIT bags [37], where only perturbative interquark forces act inside bags. This invokes immediately the idea of deconfined pieces of matter inside of hadrons and the quark-hadron phase transition caused by the increased number of multi-quark bags and their final overlap.

However, the MIT bag is only a crude model of hadrons. Lattice and other analytical models show that the correlation length in the QCD vacuum is very small ~ 0.1 fm. This fact is due to large mass of nonperturbative structures called gluelumps (for a review see [38]). The string (confinement) between quarks acts therefore already at distances ~ 0.1 fm or less and instead of multi-quark bags one gets for MQS strongly bound systems with inner density growing with the number of quarks and a radius twice smaller than in the MIT bag model [39]. Moreover, a detailed study of the dependence of the confinement potential on the density [40] showed that the medium effects lead to an additional attraction, as a result of which MQS are becoming smaller and lighter. A growing admixture of MQS can produce another minimum in the curve of E/A vs density providing a phase transition into the heterophase nuclear matter with substantial MQS component or the quark matter.

MQS can play an important role in the so-called cumulative and subthreshold processes i.e., reactions on nuclei that cannot proceed on single nucleons [41]. The corresponding cumulative number N_{cum} defines the minimal number of nucleons needed kinematically for the reaction. It is clear, that MQS are appropriate objects to provide the cumulative effect. The MQS density enters directly cross-sections of the cumulative and subthreshold reactions. There is a close connection between the MQS density in nuclei and neutron star interiors.

Multi-quark configurations that appear first when overlap of nucleons becomes significant can be considered as a kind of dibaryons. The experimental searches of dibaryons in the past did not give conclusive results. Recently, resonance behavior of the double pionic fusion reaction $pn \rightarrow d\pi^0\pi^0$ measured at CELSIUS-WASA has been interpreted as evidence for a $\Delta\Delta$ dibaryon [42]. Such dibaryon has, however, more features in common with deuteron rather than a compact 6QS.

The possibility for occurrence of a Bose condensate of dibaryons in nuclear matter is discussed in Refs. [34, 35, 43–48]. The ground state of the heterophase nucleon-dibaryon matter is stable for a wide range of parameters of the models discussed and nuclear matter densities. Using the mean-field approximation of the OBE models, constraints for the ω - and σ -meson coupling constants with dibaryons were extracted from properties of nuclear matter at saturation, stability condition of the binary mixture of nucleons and dibaryons, and from the existence of massive neutron stars.

To give a quantitative method for study of the nucleon and dibaryon fields, we are using the so-called Quark Compound Bag (QCB) model [49], appeared in the development of the P -matrix formalism of Jaffe and Low [50]. Jaffe and Low proposed to identify MQS with the so-called "primitives" which appear as poles of P matrix rather than S matrix. The P -matrix formalism was used to yield an accurate description of the nucleon-nucleon systems in

Ref. [51] (see also [49, 52–55]).

The dynamical character of the QCB model allows to apply it for the description of nucleon-nucleon interaction at finite density and temperature and for the study of nuclear matter EoS.

It should be noted also that the QCB model is very economical since it uses only a few parameters, such as mass and radius of the MQS with a fixed orbital and total angular momentum of quarks.

The average orbital momentum of a nucleon pair in the nuclear matter can be estimated as $L \lesssim rp_F = 1.4 \pm 0.5$. This estimate does not depend on the density. The s -channel dibaryon exchange as the mechanism of nucleon-nucleon interaction is therefore restricted in nucleon matter by a few lowest partial waves. An additional suppression of the high partial waves appears in the low-density limit because of the threshold behavior $\sim a(p_F)^L$ of the partial wave amplitudes, where a is the scattering length. The S -wave interaction is therefore dominant in the low-density limit.

The comparison of the observational data with the calculations of static properties of neutron stars and the dynamic simulations of core-collapse supernovae rise questions which have not found a definite answer yet. One such issue is the quantitative properties of the phase transition. The inclusion of MQS in the NN interaction dynamics, e.g., in the QCB model is an alternative approach to describe nuclear forces and nuclear matter EoS. In this approach, the modeling of heterophase states of high-density baryonic matter is possible.

The physical conditions that appear at the final stages of the core collapse in interiors of newly born hot proton-neutron stars are unique to constrain parameters of the quark-hadron phase transition, which cannot be constrained otherwise from laboratory data (see, e.g., [56]). Observation of neutrino bursts from supernovae, which may genetically be related to a phase transition, will play an important role in the identification of physical nature and properties of the exotic states of nuclear matter at high density.

Massive stars end their life with gravitational collapse of iron central cores that according to astronomical observations must result in the explosion of so-called core-collapse supernovae (SN). However, an extensive hydrodynamic modeling during already more than thirty years has demonstrated that in case of spherical symmetry it is very hard to simulate the explosion: stellar envelope would not separate and finally fell back on the collapsed core. Therefore, the SN theorists began to concentrate special attention on basically nonspherical effects such as rotation, magnetic fields, large scale convection, jet streams, etc (e. g., see [57, 58] and references therein).

Here, we discuss the calculations of gravitational collapse that was undertaken to estimate the effect of the nuclear phase transition on the core collapse dynamics. Although the property of phase transition to destabilize the hydrostatic equilibrium of stars and giant planets is well known for a long time [59–63] the hydrodynamic consequences of such a destabilization were yet rarely addressed in the investigation of SN mechanism. For a historical review and as the starting point for understanding the instability induced by phase transition, remarkable essays by Seidov [64, 65] can be recommended. It was understood that the phase transition onset in stellar center can generate a shock wave [66, 67]. However the hydrodynamic effects on the SN mechanism expected from such a shock required further detailed study. Recently there appeared a detailed research of possible phase transition influence on the dynamics of the collapse and SN mechanism [68, 69]. The research is based on sophisticated hydrodynamic code including neutrino transport and quark-hadron phase transition simulated with the aid of the MIT bag model. It was shown that an additional neutrino peak appears in the neutrino light curve as a specific signature of the phase transition. For the core-collapse supernovae of our Galaxy, this peak could be resolved by the existing neutrino detectors.

The QCD phase transitions may be a good remedy for triggering the SN explosion in spherically symmetric SN models, while the detected neutrinos can provide important information on physical nature and parameters of the QCD phase transition.

This work reviews phenomenological and microscopic approaches to NN interactions and nuclear matter properties with inclusion of quark-gluon degrees of freedom, quark-hadron phase transitions and influence of phase transitions on physics of neutron stars, supernova outbursts and neutrino signals from supernovae.

In Sect. II we discuss the $\mu - T$ QCD phase diagram, give estimates of critical temperature of the deconfinement phase transition at low baryon chemical potentials, and discuss the role of diquark correlations in cold quark matter. In Sect. III we discuss modification of the confinement force at nonzero chemical potential and estimate critical density above which formation of MQS becomes energetically preferable. In Sect. IV the QCB model is introduced in its original nonrelativistic form, while Sects. V-VII are devoted to the relativistic formulation of QCB and the accurate description of NN data in the QCB framework. In Sect. VIII the EoS of nuclear matter are given in the standard OBE form, in Sect. IX in a simplified nonrelativistic QCB form, while section X is devoted to the relativistic mean field treatment based on the QCB model of Sect. V. In Sect. X we provide equations to calculate the G -matrix and describe qualitative features of the phase transition to the new MQS phase. In Sect. XI astrophysical aspects of (proto) neutron star dynamics are given and the evolution of the supernova outbursts is presented based on detailed calculations. Section XII is devoted to conclusions and perspectives of the present approach. Appendices contain technical details necessary to derive some of the equations in the text.

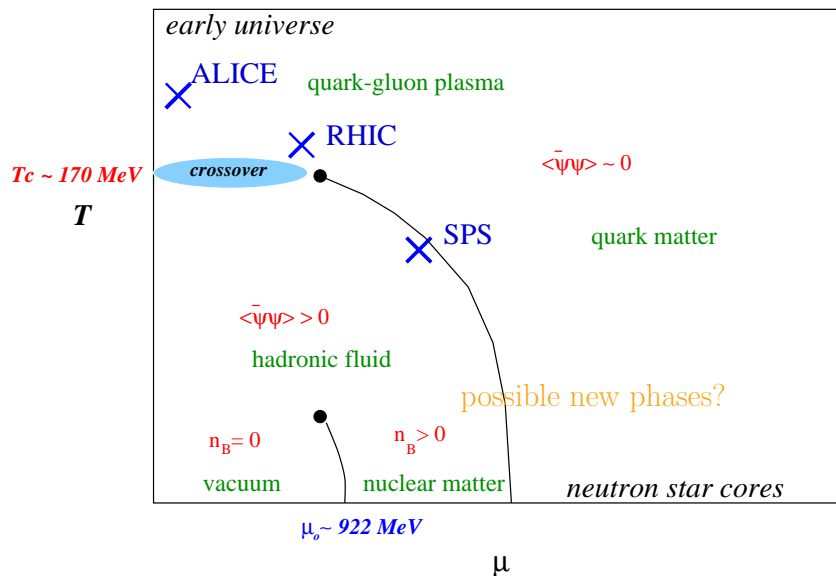


FIG. 1: QCD phase diagram in the temperature-chemical potential plane. First-order phase transitions are shown by solid lines. Filled circles are second-order phase transitions. Crossover at $\mu \approx 0$ shows transition from hadronic phase to quark-gluon plasma. Crosses depict heavy-ion collision experiments.

II. QUARK-HADRON PHASE TRANSITION IN QCD

In Fig. 1 one can see the generic picture of the phase transition expected in QCD. Only the low- μ region is accessible to lattice QCD, while mostly NJL-type models are used to predict the phase curve and the superconducting phases. We shall show below that the phase curve can be obtained from the Field Correlator method (FCM) [4, 5] and indeed looks like in Fig. 1, whereas the superconducting phases are unlikely. We shall also find the critical values T_c and μ_c for symmetric nuclear matter ($\mu_p = \mu_n \equiv 3\mu_q$) with switched off weak interactions in terms of the gluon condensate, following [6].

A. Gibbs' criterion

According to the Gibbs' criterion, two phases in thermodynamic equilibrium have the same temperatures, pressures, and balanced chemical potentials. Phase with highest pressure is thermodynamically preferred provided other conditions are equal. Chemical equilibrium leads to a set of relations for the chemical potentials of constituents. If weak interactions are switched off, chemical equilibrium for the substance with n_f flavors reduces to

$$\mu_A = C_A^a \mu_a, \quad (\text{II.1})$$

where μ_A and μ_a are the chemical potentials in the hadron phase with $A = p, n, \Lambda, \dots, \pi^\pm$ - and π^0 -mesons, etc. and in the quark phase with $a = u, d$ -quarks for $n_f = 2$ and u, d, s -quarks for $n_f = 3$. The matrix C_A^a determines the composition of particles in the hadron phase and, in particular, allows to express electric charge of particles in the hadron phase e_A in terms of electric charge of the constituents e_a : $e_A = C_A^a e_a$. If leptons appear in the substance then A and a run over the leptons too. For a representative set of hadrons and electrons and muons C_A^a has the form

$$C_A^a = \begin{array}{c} a \rightarrow \\ \downarrow \\ A \end{array} \begin{array}{c} u \quad d \quad s \quad e \quad \mu \\ p \\ n \\ \Sigma^- \\ \pi^- \\ e \\ \mu \\ \vdots \end{array} \left\| \begin{array}{c} 2 \quad 1 \quad 0 \quad 0 \quad 0 \\ 1 \quad 2 \quad 0 \quad 0 \quad 0 \\ 0 \quad 2 \quad 1 \quad 0 \quad 0 \\ -1 \quad 1 \quad 0 \quad 0 \quad 0 \\ 0 \quad 0 \quad 0 \quad 1 \quad 0 \\ 0 \quad 0 \quad 0 \quad 0 \quad 1 \\ \vdots \end{array} \right\|.$$

The critical temperature without the lepton component depends on the n_f chemical potentials of the quarks, that are independent parameters.

If the relaxation time is longer than the typical time scale of the weak processes, the weak interactions come into play. This is the case of phase transitions in neutron stars whose lifetimes are comparable with the age of our Galaxy. Even in supernovae the free fall time is much longer than time needed to keep substance under the chemical equilibrium with respect to the weak interactions.

The weak interactions modify the matching conditions (II.1). The lepton component appears in the substance and the electric neutrality is to be imposed. The modified conditions look like (see e.g. [70])

$$\mu_A = C_A^a \mu_a + e_A V, \quad (\text{II.2})$$

where e_A is electric charge of particle A , the indices A and a run over leptons also. The chemical equilibrium generates at the boundary of two phases a jump of the electrostatic potential V formed by a double layer of leptons to match chemical potentials under the condition of the bulk electroneutrality. The similar jump exists e.g. at boundaries of two different metals in contact. The chemical equilibrium with respect to the weak interactions and the electroneutrality condition leave each phase with one free parameter only that can be chosen to be, e.g., the neutron chemical potential in the hadron phase and the d -quark chemical potential in the quark phase. The matching conditions (II.2) are reduced to one equation for μ_n and μ_d at the phase transition. The critical temperature is thereby a function of one parameter only.

Below we start with the system of quarks and gluons without weak interactions and where interaction in the hadron phase is also switched off, as it happens in the large N_c limit. One can as a first step neglect also interaction between quarks and gluons as compared to their interaction with vacuum fields. This approximation can be called the Vacuum Dominance Model (VDM).

B. QCD phase diagram in FCM

The basic notion for the phase transition in QCD is the nonzero vacuum energy density ε_{vac} introduced in QCD sum rules [71]. The conformal anomaly gives

$$\varepsilon_{vac} = 1/4\theta_{\mu\mu} = \frac{\beta(\alpha_s)}{16\alpha_s} \langle (F_{\mu\nu}^a)^2 \rangle \cong -\frac{(11 - \frac{2}{3}n_f)}{32} G_2^{(n_f)} \quad (\text{II.3})$$

where [71, 72]

$$G_2 = (0.01 \pm 0.002) \text{ GeV}^4. \quad (\text{II.4})$$

The quark-hadron phase transition occurs due to reconstruction of the vacuum in the course of which the colorelectric part of ε_{vac} , ensuring confinement, is thermodynamically not advantageous and therefore vanishes in the temperature-affected QCD vacuum [73].

In the confining phase the pressure looks like

$$P_1(T, \mu_1) = \varepsilon_{vac} + T^4 \chi_1(T, \mu_1), \quad (\text{II.5})$$

where μ_1 denotes the set of the chemical potentials, the second term stands for pressure of the hadron gas. In the deconfined phase, the colorelectric confining correlator $D^E(x) = 0$ [73], as confirmed by lattice data [74], so that the vacuum energy density ε_{vac}^{dec} is decreased by about a factor of two, $\Delta G_2 \approx \frac{1}{2}G_2$ within 10%.

The pressure of the deconfined phase equals

$$P_2(T, \mu_2) = \varepsilon_{vac}^{dec} + T^4 \chi_2(T, \mu_2) \quad (\text{II.6})$$

where μ_2 is the set of the quark chemical potentials, $\chi_2(T, \mu_2) = p_{gl} + p_q$ is a function weakly depending on T for low chemical potentials, $p_i = P_i/T^4$ are reduced gluon and quark pressures.

The Gibbs' criterion,

$$P_1(T_c, \mu_1) = P_2(T_c, \mu_2), \quad (\text{II.7})$$

together with the matching conditions (II.1) allow to find T_c in terms of $\Delta\varepsilon_{vac} \sim \Delta G_2$. By neglecting the hadron pressure $\chi_1(T, \mu_2)$, which is $O(10\%)$ of $\Delta\varepsilon_{vac}$ for low chemical potentials, one gets

$$T_c = \left(\frac{\Delta\varepsilon_{vac}}{\chi_2(T_c, \mu_2)} \right)^{1/4}. \quad (\text{II.8})$$

$\chi_1(T, \mu_2)$ is, however, important for the order of quark-hadron phase transition.

Next step is the evaluation of p_q and p_{gl} . It is shown in [76], that in VDM the main dynamical contribution to quark and gluon pressure can be written in the form of the Polyakov line (II.9), creating effective selfenergies $V_1(\infty, T)$ for quarks and $\frac{9}{4}V_1(\infty, T)$ for gluons, and otherwise quarks and gluons are free. The resulting expressions for p_{gl}, p_q are in (II.10), (II.11). Neglecting quark mass one obtains the form (II.12), where $\Phi_{+,-}^{(k)}$ are given in (II.13).

Equations (II.10), (II.12) contain all necessary dynamical information for quark-hadron phase transition and dynamics of quark-gluon plasma (QGP). Basic quantity is the potential $V_1(\infty, T)$, entering Polyakov line (II.9), which is calculated on lattice and analytically see [77].

$$|L_{fund}| = \exp\left(-\frac{V_1}{2T}\right). \quad (\text{II.9})$$

$$p_{gl} = \frac{16}{\pi^2} L_{adj}(T) = \frac{16}{\pi^2} \exp\left(-\frac{9V_1(\infty, T)}{8T}\right) \quad (\text{II.10})$$

$$p_q = \frac{12n_f}{\pi^2} \sum_{n=1}^{\infty} \frac{(-)^{n+1}}{n^4} (L_f)^n \varphi_q^{(n)}(T) \cosh \frac{\mu n}{T} \quad (\text{II.11})$$

$$\begin{aligned} p_q(m_q = 0) &= \frac{12n_f}{\pi^2} \sum_{n=1}^{\infty} \frac{(-)^{n+1}}{n^4} L_f^n \cosh \frac{\mu n}{T} = \\ &= \frac{n_f}{\pi^2} \left[\Phi_-^{(3)}\left(\frac{\mu - \frac{V_1}{2}}{T}\right) + \Phi_+^{(3)}\left(\frac{\mu + \frac{V_1}{2}}{T}\right) \right] \end{aligned} \quad (\text{II.12})$$

$$\Phi_-^{(k)}(z) = \int_0^{\infty} \frac{x^k dx}{e^{x-z} + 1}; \quad \Phi_+^{(k)}(z) = \int_0^{\infty} \frac{x^k dx}{e^{x+z} + 1}. \quad (\text{II.13})$$

Now one can compute $T_c(\mu)$ for different n_f from Eq. (II.8), where $\frac{11}{32}\Delta G_2 \rightarrow \frac{(11-\frac{2}{3}n_f)}{32}\frac{1}{2}G_2$ and $p_q \sim n_f$ in (II.11). In this way one obtains a simple formula for the transition temperature

$$T_c \simeq \left(\frac{(11 - \frac{2}{3}n_f)G_2}{64(p_{gl} + p_q)}\right)^{1/4} \quad (\text{II.14})$$

where $p_{gl}(p_q)$ are gluon (quark) pressure divided by T^4 in the deconfined phase, calculated in the same method (see [5] for details). This simple formula yields for different number of flavors n_f correct values $T_c(n_f)$, in good agreement with lattice data [6].

In doing so one assumes that temperature and moderate density do not affect strongly the vacuum fields in G_2 and for the latter one can use the same phenomenological values as for zero temperature, i.e. $G_2 \cong 0.01 \text{ GeV}^4$.

Proceeding in this way one obtains the phase diagram in the $\mu_q - T$ plane [6], see Fig. 2, where the critical value $\mu_{cr} = \mu_q(T=0) \cong 0.6 \text{ GeV}$. This value is large enough and it will be shown below that vacuum structure is affected by the chemical potential μ_q and confinement is modified. As it is, one has for small T the first order density phase transition to the deconfined quark-gluon matter with strong np attraction in the white systems [7] preferring $q\bar{q}$ system over diquarks and thus making the proposal of quark superconductivity not very realistic, in line with earlier criticism of [8].

Then one obtains the numbers in Table I, where the asterisk corresponds roughly to 1/2 of standard condensate. The values $T_c(n_f = 0) = 0.27 \text{ GeV}$ and $T_c(n_f = 2) = 0.19 \text{ GeV}$ are in good agreement with numerous lattice data, while $\mu_c \approx 0.6 \text{ GeV}$ cannot be obtained on the lattice. The resulting curves $T_c(\mu)$ are shown in Fig. 2.

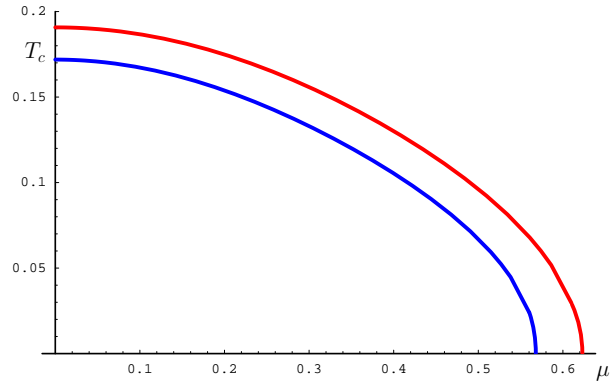
The critical density of the phase transition into the strange quark matter ($n_f = 3$) at zero temperature gets positive. This means that the strange quark matter is not absolutely stable. The condition of absolute stability of the strange quark matter restricts the critical temperature for vanishing chemical potentials by $T_c(n_f = 3) < 122 \pm 7 \text{ MeV}$ [75]. According to the lattice data, this restriction is not satisfied with a large certainty.

TABLE I: Critical values of T and μ for various n_f and ΔG_2

★

$\frac{\Delta G_2}{0.01 \text{ GeV}^4}$	0.191	0.341	0.57	1
T_c (GeV) $n_f = 0$	0.246	0.273	0.298	0.328
T_c (GeV) $n_f = 2$	0.168	0.19	0.21	0.236
T_c (GeV) $n_f = 3$	0.154	0.172	0.191	0.214
μ_c (GeV) $n_f = 2$	0.576	0.626	0.68	0.742
μ_c (GeV) $n_f = 3$	0.539	0.581	0.629	0.686

In the derivation of the phase curve in Fig. 2 it was assumed, that the pressure of the hadronic phase can be given with good accuracy by the vacuum fields only (the Vacuum Dominance Model (VDM)), while the contribution of the hadronic gas is neglected. This approximation is reasonable for $\mu = 0$, where the effect of pionic gas is around 10%, but maybe crude for large μ , where hadronic matter is dense nuclear matter. Therefore the region of large μ and small T can be modified, when interaction in nuclear matter is properly taken into account. Since the main emphasis of the present paper is the treatment of the possible new phase of MQS at smaller μ , it will be reasonable to reconsider the hadron-quark phase transition with account of possible MQS contribution.

FIG. 2: Phase transition curves in (T, μ) plane. T and μ are in GeV. Upper curve: $n_f = 2$; lower curve: $n_f = 3$.

C. Suppression of color superconductivity

As was shown in [77, 78] the diquark nonperturbative interaction is expressed via $V_1(r, T)$ as follows (for a large size superconducting diquark)

$$V_{QQ}(r) = \frac{1}{2}V_1(\infty, T) + \frac{1}{2}V_1(r, T) \rightarrow V_1(\infty, T_c) \approx 0.5\text{GeV} \quad (\text{II.15})$$

For each quark it gives the factor

$$L_q(T) = \exp\left(-\frac{V_1(\infty, T)}{2T}\right). \quad (\text{II.16})$$

Hence each quark carries Boltzmann factor

$$L_q \approx \exp\left(-\frac{0.25\text{GeV}}{T}\right). \quad (\text{II.17})$$

Assuming that the dependence on μ is weak one expects that approximately the same factor holds for $\mu \rightarrow \mu_{crit}$. For the white $QQ\bar{Q}$ system this factor is missing [78], hence one expects

$$\frac{\langle V_{QQ\bar{Q}} \rangle}{\langle V_{QQ} \rangle} \approx L_q^2 \approx \exp\left(-\frac{0.5\text{GeV}}{T}\right) \ll 1 \quad (\text{II.18})$$

Therefore one expects $Q\bar{Q}$ pairing, and not QQ pairing, in qgp .

D. Critical baryon chemical potential in cold nuclear matter

One can expand (II.13) for $T \rightarrow 0$, $a \rightarrow \infty$

$$\Phi_-^{(3)}(a \rightarrow \infty) = \frac{a^4}{4} + \frac{\pi^2}{2}a^2 + \frac{7\pi^4}{60} + \dots, \quad a = \frac{\mu \mp \frac{V_1}{2}}{T}; \quad (\text{II.19})$$

For the pressure one obtains

$$P = \frac{n_f}{4\pi^2} \left(\left(\mu - \frac{V_1}{2} \right)^4 + \left(\mu + \frac{V_1}{2} \right)^4 + \dots \right) \quad (\text{II.20})$$

and for the density

$$\rho_q \equiv \frac{N_q}{V} = \frac{n_f}{\pi^2} \left\{ \left(\mu - \frac{V_1}{2} \right)^3 + \left(\mu + \frac{V_1}{2} \right)^3 \right\}. \quad (\text{II.21})$$

The critical μ at small T has an expansion

$$\mu_c(T \rightarrow 0) = \frac{V_1(T_c)}{2} + (48)^{1/4} T^{(0)} \left(1 - \frac{\pi^2}{2} \frac{T^2}{\left(\mu_c - \frac{V_1(T_c)}{2} \right)} + \dots \right). \quad (\text{II.22})$$

For $V_1(T_c) = 0.5 \text{ GeV}$ and $n_f = 2$ one has: $\mu_c(T = 0) \cong 0.6 \text{ GeV}$.

The critical density from (II.21), (II.22) is

$$\rho_q(\text{crit}) \cong \frac{2n_f m_c}{\pi^2} \left(\mu - \frac{V_1}{2} \right) \approx 0.12 \text{ GeV}^3 = 15 \text{ fm}^{-3} \quad (\text{II.23})$$

so that baryon number density is

$$\rho_{Bar}^{crit} = \frac{\rho_q}{3} \cong 5 \text{ fm}^{-3} \quad (\text{II.24})$$

This is 30 times normal nuclear density, $n_0 = \frac{1}{6} \text{ fm}^{-3}$ and the pressure is very high, $P_{crit}^q \cong 125 P_{nucl}(2n_0)$. It is clear that nuclear matter cannot exist as usual baryon matter for density of 5 baryons in fm^3 .

III. DENSITY EFFECT ON CONFINEMENT POTENTIAL BELOW PHASE TRANSITION

Consider a white system of a quark and a heavy antiquark \bar{Q} , which in baryon can be replaced by the string junction. Then in the partition function $Z = \int DAD\psi \exp(\bar{\psi}(\hat{D} + m_q)\psi)$ one can average over DA and keep the quadratic in A_μ term in the exponent, which yields $Z = \int D\psi \exp \int \bar{\psi}(x)\psi(x)\bar{\psi}(y)\psi(y)J(x,y)dx dy..$ Here $J(x,y)$ is proportional to the quadratic correlator $D^E(x)$, $J(x,y) = \int_0^x du \int_0^y dv D^E(u-v)$.

In case of confinement ($D^E \neq 0$), $J(x,x) \sim x$ at large x and as shown in [79] this property yields simultaneously confinement and chiral symmetry breaking (CSB). As was shown in [79], the effective quark mass M_s° (growing at large x due to confinement) and quark propagator S are found from the system of equations (we neglect emission of pions)

$$M_s^{(0)}(x,y) = \bar{J}_{\mu\mu}(x,y) Tr S_q(x,y) \quad (III.25)$$

$$iS_q(x,y) = \langle x | (\hat{\partial} + m_q + M_s^{(0)})^{-1} | y \rangle. \quad (III.26)$$

Solutions of (III.25), (III.26) are different for light or heavy quark q . For heavy quark, $m_q \rightarrow \infty$, one neglects $M_s^{(0)}$ in S_q and has

$$S_q(x,y)(m_q \rightarrow \infty) \sim \delta^{(3)}(\mathbf{x} - \mathbf{y}) \quad (III.27)$$

$$M_s^{(0)}(x,y) \rightarrow \bar{J}(\mathbf{x}, \mathbf{x}) \sim \sigma |\mathbf{x} - \mathbf{x}(\bar{Q})| \quad (III.28)$$

For light quark q one solves the system using relativistic WKB for Dirac particles and again obtains CSB and confinement for large x . That was done in [79] for the case of zero density (vanishing μ_q).

Now we turn to the case of nonzero $\mu_q \equiv \mu$. As will be seen, for heavy quarks nothing happens -linear confinement at all r , unless $\mu \sim m_q$ (for standard nuclear density $\mu \cong 0.3$ GeV.).

Let us study now the case of light quarks, following the paper [80]. The effective light quark mass can be written as

$$\bar{M}(\mathbf{x}, \mathbf{y}; \mu) = J(\mathbf{x}, \mathbf{y}) \gamma_4 \Lambda(\mathbf{x}, \mathbf{y}; \mu) \quad (III.29)$$

where $\gamma_4 \Lambda(\mathbf{x}, \mathbf{y}, \mu)$ is the time-independent quark Green's function, cf. (III.25). It can be written in terms of one-particle eigenfunctions $\psi_n(\bar{x})$ as

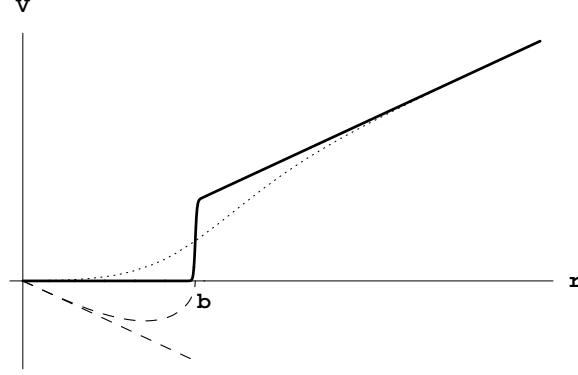
$$\begin{aligned} \Lambda(\mathbf{x}, \mathbf{y}; \mu) &= \sum_n \psi_n(\mathbf{x}) \text{sign}(\varepsilon_n - \mu) \psi_n^+(\mathbf{y}) = \\ &= \Lambda_0(\mathbf{x}, \mathbf{y}) - \Delta\Lambda(\mathbf{x}, \mathbf{y}) \end{aligned} \quad (III.30)$$

In [80] $\psi_n(\mathbf{x})$ are found in the relativistic WKB method and the approximate summation over n can be performed, yielding for $\Lambda_0(\mathbf{x}, \mathbf{y})$ the smeared δ -function form for large $|\mathbf{x}|, |\mathbf{y}|$ and $|\mathbf{x} - \mathbf{y}| \ll |\mathbf{x}|, |\mathbf{y}|$. In [80] also the term $\Delta\Lambda(\mathbf{x}, \mathbf{y})$ in (III.30) was calculated in the same way, which is nonzero for $\mu \neq 0$, and distorts the linear confinement at distances $r \leq \mu/\sigma$, where $\sigma = 0.18$ GeV² is the standard string tension. The resulting picture for the averaged $\bar{M}(r) = \int d^3\mathbf{r}' \bar{M}(\mathbf{r}, \mathbf{r}', \mu)$ is given in Fig 3, where $\bar{M}(r)$ is split into a Lorentz scalar and vector parts,

$$\bar{M}_{scal} = \sigma r \theta(\sigma r - \mu), \quad \bar{M}_{vect}(r) = -2\sigma r \theta(\mu - \sigma r). \quad (III.31)$$

In MQS we shall for simplicity consider all quarks attached to the same string junction (this is not crucial for quarks in the modified confining potential, since near the string junction the scalar part vanishes, but the vector part can be rewritten in the form of pairwise potentials [81]). Consider now a system of N quarks around one string junction in the nuclear medium of ordinary nucleons. Using the local limit for interactions of a light quark with string junction, Eq. (III.31), one can calculate the change of masses of white states due to density.

FIG. 3: Interactions $\bar{M}_{scal}(r)$ (solid line) and $\bar{M}_{vect}(r)$ (dashed line) as functions of distance r , with $b = \mu/\sigma$. Dotted line and dashed line show the qualitative smoothed form of both terms respectively.



Assuming that multiquark states located at different string junction points do not overlap (see below the note on states radii), one can associate the parameter μ for a given quark with the largest value of ε_n , occupied by other quarks, belonging to the same string junction point. In what follows we shall show, that in some situations it will be advantageous for two or more nucleons (with different string junctions) to coalesce into a common state with one string junction, building in this way the contracted potential (III.31).

Note, that for one nucleon (3 quarks) the contraction mechanism does not work and μ can be taken at zero value, since no forbidden states exist for each quark of a given color. This, again, is true, provided one-quark states do not overlap at the given density. The situation changes, however, for two nucleons, since e.g. one can add to the first nucleon, i.e. 3 quarks in S-states, 3 quarks in P-states relative to the same string junction point. The latter will move in the scalar part of the potential $\Lambda(\mathbf{x}, \mathbf{y})$, with μ being equal to the S-state Dirac eigenvalue ε_S , thus the energy $\varepsilon_P(\mu = \varepsilon_S)$ may become less than $\varepsilon_S(\mu = 0)$:

$$\varepsilon_P(\mu = \varepsilon_S) < \varepsilon_S(\mu = 0) \quad (\text{III.32})$$

The same type of inequality may occur for higher L states, when more nucleons coalesce to the same Multiquark State. This would imply instability of nuclei with respect to transition to MQS matter.

Note, that $\mu_B \neq 3\mu$, since μ is attributed to MQS string junction and does not grow with μ_B unless different MQS start to overlap. Hence for $\mu_B > 0$ (III.32) should be replaced by

$$\varepsilon_P(\mu = \varepsilon_S) < \varepsilon_S(\mu = 0) + \varepsilon_B(\text{Fermi}). \quad (\text{III.33})$$

To check (III.33) in [80] ε_S and ε_P were computed numerically with the potential (III.31), and in perturbation theory, considering the change of potential in (III.31) as a small perturbation. The results are given in Tables II,III. The calculated quantities are $\Delta M_S = 3\Delta\varepsilon_n(S)$ and $\Delta M_P(3q) = 2\Delta\varepsilon_n(S) + \Delta\varepsilon(P)$, where $\Delta\varepsilon_n = \varepsilon_n(\mu) - \varepsilon_n(0)$. One should note at this point, that the vector part of interaction written in (III.31) for the case of light quark with heavy antiquark, and for the case of 3 quarks interacting with string junction the vector part is transformed as an addition to the color Coulomb potential with coefficient 1/2 (see [81] for explicit derivation of scalar and vector interaction in the nucleon). This prescription was used for our calculations.

From these numbers one can obtain $\varepsilon_S(\mu_q = 0) \approx 0.52$ GeV, $\varepsilon_P(\mu_q = 0) = 0.77$ GeV, $\varepsilon_P(\mu_q = 0.52 \text{ GeV}) = 0.57$ GeV. This is close to the $\varepsilon_S(\mu_q = 0)$, i.e. one can expect the formation of MQS for ε_B (Fermi)=50 MeV, which corresponds to critical density $\rho \cong 3\rho_0$.

Also, the average radii of S - and P -wave quark states were computed (see Tables II,III) and it is found the radius is decreasing with a rise of μ , at least for the moderate μ values, so it is reasonable to neglect in the first approximation the possible overlapping of multiquark state wavefunctions attached to different string junction points.

As we shall discuss below, this might be important for new heavy-ion colliders (FAIR, NICA,...), and crucial for neutron stars and supernovae. However, we have still neglected interaction between baryons in nuclear matter. In the next sections we show that this interaction can be described in terms of MQS formation in the intermediate states, and a new theory of nuclear matter based on MQS can be formulated.

TABLE II: Mass shifts of $3q$ system with all quarks in the S -state (purely numerically, and perturbatively, for comparison) and the S -wave average radius, due to nonzero μ_q

μ , MeV	ΔM_{exact} , MeV	$\Delta M_{\text{pert.}}$, MeV	$\langle r \rangle_S$, fm
100	-5.8	-5.7	0.505
200	-75	-70	0.487
300	-290	-265	0.460
400	-630	-603	0.464
500	-1008	-1020	0.501

TABLE III: Mass shifts of $3q$ system with two quarks in the S -state and one quark in the P -state (purely numerically, and perturbatively, for comparison), and the P -wave average radius, due to nonzero μ_q

μ , MeV	ΔM_{exact} , MeV	$\Delta M_{\text{pert.}}$, MeV	$\langle r \rangle_P$, fm
100	-4.0	-3.9	0.613
200	-53	-50	0.605
300	-221	-199	0.558
400	-530	-481	0.473
500	-917	-873	0.448

IV. QUARK COMPOUND BAG MODEL

In this section we describe the general two-channel formalism of the nucleon-nucleon interaction that provides dynamical framework for the P -matrix formalism and is used in Sect. VI to build the relativistic formalism and to construct in Sect. X the Bethe-Goldstone G operator for nucleons in nuclear matter.

For simplicity we consider a hadronic channel consisting of two spinless nonrelativistic hadrons, which is coupled to another channel, where any number of quarks and gluons are present. We denote the hadronic channel with a subscript h and the quark channel with a subscript q . The wave function is a column with two components (Ψ_h, Ψ_q) , while the interaction term in the Hamiltonian is a 2×2 matrix.

$$\hat{V} = \begin{pmatrix} V_{hh} & V_{hq} \\ V_{qh} & V_{qq} \end{pmatrix}. \quad (\text{IV.1})$$

We do not specify the quark dynamics and even the type of variables, on which V_{qq} is acting. At this point we can take the description of the quark-gluon system as general as possible and we shall use only the property of confinement, i.e. that the eigenstates of the quark Hamiltonian are discrete states confined to a finite region in space whatever the binding energy is.

The coupled dynamical equations for Ψ_h, Ψ_q are

$$(T_h + V_{hh} - E)\Psi_h = -V_{hq}\Psi_q, \quad (\text{IV.2})$$

$$L_q\Psi_q + V_{qh}\Psi_h = E\Psi_q, \quad (\text{IV.3})$$

where L_q is some quark-gluon operator (its exact form is irrelevant for our purposes) and T_h is the kinetic operator for hadrons and E is the full energy, $E = \sqrt{s}$; V_{hh} is in general a nonlocal energy-dependent operator. T_h in general is a relativistic operator.

One can solve formally equation (IV.3) to express Ψ_q in terms of Ψ_h :

$$\Psi_q = -G_q V_{qh} \Psi_h \quad (\text{IV.4})$$

where the quark Green function has a spectral representation

$$G_q = \sum_{\nu} \frac{\Psi_q^{\nu} \bar{\Psi}_q^{\nu}}{E_{\nu} - E}. \quad (\text{IV.5})$$

The quark eigenstates Ψ_q^ν and eigenvalues E_ν belong only to a discrete spectrum because of the confinement. Using (IV.4) one can exclude the quark channel and rewrite the hadronic equation (IV.2) as

$$(T_h + V_{hh} + V_{hqh})\Psi_h = E\Psi_h \quad (\text{IV.6})$$

where

$$V_{hqh} = -V_{hq}G_qV_{qh} = -\sum_\nu \frac{V_{hq}\Psi_q^\nu\bar{\Psi}_q^\nu V_{qh}}{E_\nu - E}. \quad (\text{IV.7})$$

Let us discuss the structure of the quark-induced hadronic interaction V_{hqh} .

1. It does not contain any quark or gluon degrees of freedom, which are present in Ψ_q^ν and V_{hq} . Indeed, in (IV.7) the summation over all quark degrees of freedom is implied by the repeated subscript q , so that the only remaining coordinates are hadronic relative distances, entering via V_{hq} and V_{qh} .
2. V_{hqh} is separable Hermitian interaction; if we denote

$$f_\nu(r) \equiv V_{hq}\Psi_q^\nu, \quad (\text{IV.8})$$

V_{hqh} has the form

$$V_{hqh} = \sum_\nu \frac{f_\nu(r)f_\nu^*(r')}{E - E_\nu}. \quad (\text{IV.9})$$

3. The numerator of (IV.9) depends in general case on energy E through the quark-hadron interaction V_{qh} . The most characteristic energy dependence enters through the denominator in (IV.9); for E near E_ν the quark-induced potential V_{hqh} can be infinitely large.
4. Since quarks are not allowed outside the bag the function $f_\nu(r)$ should be nonzero only inside the bag. Hence it can be easily approximated there by any series on a finite interval of r .

We assume now that the solution of the hadronic problem (IV.6) without V_{hqh} is known; the corresponding regular at origin scattering wave functions and the Green function we denote by $X(r)$ and G_h respectively. In terms of these pure hadronic quantities we can rewrite the full coupled quark-hadron equation (IV.6) as

$$\Psi_h(r) = X(r) + \sum_\nu \frac{(G_h f_\nu)(f_\nu \Psi_h)}{E_\nu - E} \quad (\text{IV.10})$$

where we have used the notation

$$\begin{aligned} (G_h f_\nu) &\equiv \int G_h(r, r') f_\nu(r') dr' \\ (f_\nu \Psi_h) &\equiv \int \Psi_h(r) f_\nu^*(r) dr. \end{aligned} \quad (\text{IV.11})$$

The constants $(f_\nu \Psi_h)$ are to be found from the system of linear algebraic equations

$$(f_\nu \Psi_h) = (f_\nu X) + \sum_\mu \frac{(f_\nu G_h f_\mu)(f_\mu \Psi_h)}{E_\mu - E} \quad (\text{IV.12})$$

where

$$(f_\nu G_h f_\mu) \equiv \int \int f_\nu^*(r) G_h(r, r') f_\mu(r') dr dr'.$$

The resulting picture is particularly simple when E is close to some eigenvalue E_μ and all other terms in the sum in (IV.10) with $\nu \neq \mu$ can be neglected. In this case we have

$$\Psi_h(r) = X(r) + \frac{G_h f_\mu (f_\mu X)}{E_\mu - E - (f_\mu G_h f_\mu)}. \quad (\text{IV.13})$$

At this point it is possible to discuss the general properties of our solution $\Psi_h(r)$. First of all, multiplying both sides of (IV.13) with $f_\mu^*(r)$ and integrating over dr , we obtain

$$(f_\mu \Psi_h) = 0, \quad \text{for } E = E_\mu. \quad (\text{IV.14})$$

This property does not mean that Ψ_h vanishes inside the bag, where $f_\mu(r)$ is nonzero. Indeed, $\Psi_h(r)$, being complex, may have no zeros at all inside the bag, still the condition (IV.14) can be satisfied. One example of this kind obtains if we take $f_\mu(r) = \theta(R - r)$ and $V_{hh} \equiv 0$. No definite consequences can be deduced for the observables in that case. At this point we make an ansatz, that hadrons are coupled to the QCB degrees of freedom only on the surface of the compound bag. As we shall see below, this assumption immediately leads to explicit expressions for the wave function and the observables. It is crucial for all results of the paper. Moreover we show below that this assumption leads naturally to the P matrix formalism of Jaffe and Low [50] and therefore experimental evidence in favor of that formalism presented in [50] justifies our assumption. Moreover in Refs. [49, 51] additional experimental evidence is presented in favor of the stated ansatz.

From theoretical point of view the assumption, that the hadrons effectively are not coupled with the bag constituents inside the bag, but only at the surface, is not new. In the framework of the nuclear cluster models, (see the book [82]) it is well known that the region near the surface of the compound nucleus plays the crucial role.

In [83] an additional support is given to the assumption in terms of quark cluster models. The general character of these considerations allows to apply it also to the quark systems. Accordingly we assume the following simplified form for $f_\mu(r)$:

$$f_\mu(r) = c_\mu \delta(r - b) \quad (\text{IV.15})$$

where b is connected to the QCB radius R and c_μ is some constant. With the choice (IV.15) the solution $\Psi_h(r)$ simplifies:

$$\Psi_h(r) = X(r) + \frac{G_h(r, b)X(b)}{\frac{E_\mu - E}{\gamma_\mu} - G_h(b, b)}, \quad (\text{IV.16})$$

where $\gamma_\mu \equiv |c_\mu|^2$.

From (IV.16) follows an important property of $\Psi_h(r)$, namely

$$\Psi_h(r) \equiv 0, \quad \text{for } r \leq b \text{ and } E = E_\mu, \quad (\text{IV.17})$$

since

$$G_h(r, r') = X(r_{<})Y(r_{>}) \quad (\text{IV.18})$$

where $Y(r)$ is a nonvanishing at $r = 0$ solution of the purely hadronic equation (IV.2) with $V_{hq} = 0$. It is convenient to choose $X(r), Y(r)$ with the asymptotics $X(r)_{r \rightarrow \infty} \sim \frac{\sin(kr + \delta_0(k))}{k}$

$$Y(r)_{r \rightarrow \infty} \sim 2\mu \exp[i(kr + \delta_0(k))], \quad (\text{IV.19})$$

where μ is the reduced mass (reduced energy in relativistic case).

Let us define the factor $F(E)$ as follows

$$|\Psi_h(r)|^2 = F(E)|X(r)|^2, \quad r \leq b. \quad (\text{IV.20})$$

$F(E)$ shows how much $\Psi_h(r)$ decreases inside the bag because of the presence of the quark states; exact form of $F(E)$ is:

$$F(E) = \left| \frac{E_\mu - E}{E_\mu - E - \gamma_\mu G_h(b, b)} \right|^2. \quad (\text{IV.21})$$

From (IV.16) we immediately conclude that the logarithmic derivative of $\Psi_h(r)$ at $r = b$ should be meromorphic in E , namely

$$\frac{\Psi'_h(b)}{\Psi_h(b)} = \frac{X'(b)}{X(b)} + \frac{2\mu\gamma_\mu}{E - E_\mu}. \quad (\text{IV.22})$$

To obtain (IV.22) we use the property of the solution X, Y : $X(r)Y'(r) - X'(r)Y(r) = -2\mu$.

An important quantity entering (IV.21) and (IV.16), $G_h(b, b)$, can be expressed through $P_0 \equiv \frac{X'(b)}{X(b)}$ (the latter can be extracted from the experimental data, see [49]). Assuming that there is no interaction beyond $r = b$, we can use (IV.19) as the exact values of $X(r)$ and $Y(r)$ for $r \geq b$, and obtain from (IV.18):

$$G_h(b, b) = \frac{2\mu}{k} \sin^2(kb + \delta_0)(\cot(kb + \delta_0) + i). \quad (\text{IV.23})$$

On the other hand we have $P_0 = k \cot(kb + \delta_0)$ so that

$$G_h(b, b) = \frac{2\mu}{P_0 - ik}. \quad (\text{IV.24})$$

It is instructive to evaluate $\gamma_\nu G_h(b, b)$ which enters (IV.16). For NN scattering from the analysis of [49] we have $P_0 \approx 0.4$ GeV, $\gamma_\nu \approx 0.1$ GeV. Therefore e.g. at $E = 0.1$ GeV, $\gamma_\nu G_h(b, b) = (0.15 + i0.12)$ GeV.

The ratio $F(E)/F(0)$ is effectively zero for positive energy, e.g. for $E = 0.05$ GeV this ratio is ~ 0.01 . Let us now consider many quark eigenstates instead of one.

In this case the general result (IV.10) for Ψ_h is valid where $(f_\nu \Psi_h)$ are to be found from the solution of the system of equations (IV.12). The results simplify very much if we use the ansatz analogous to (IV.15):

$$f_\nu(r) = c_\nu \delta(r - b), \quad \nu = 1, 2, \dots, N \quad (\text{IV.25})$$

with the same range b for all quark eigenstates.

The ansatz (IV.25) can be approximately true for those bag eigenstates where the number of quarks and energy eigenvalues do not change much.

Taking into account (IV.25) we obtain $(f_\nu g_h f_\mu) = c_\nu^* G_h(b, b)$ and $(f_\nu \Psi_h) = c_\nu^* \Psi_h(b)$. Inserting these values we rewrite Eq. (IV.10) as follows:

$$\Psi_h(r) = X(r) + \frac{G_h(r, b) X(b) \sum_\nu \frac{\gamma_\nu}{E_\nu - E}}{1 - G_h(b, b) \sum_\nu \frac{\gamma_\nu}{E_\nu - E}} \quad (\text{IV.26})$$

where $\gamma_\nu = |c_\nu|^2$.

From (IV.26) one can see that whenever E approaches some eigenvalue E_ν , the hadronic wave function vanishes for $r \leq b$. In this way the property (IV.17) generalizes to the many quark eigenstates case: the form of the wave function (IV.26) is similar to the one-state case (IV.16) if in the latter one replaces $\frac{E_\nu - E}{\gamma}$ in the denominator by the quantity

$\left(\sum_\nu \frac{\gamma_\nu}{E_\nu - E}\right)^{-1}$. Under the same condition as in (IV.25) we obtain the following expression for P matrix

$$P = k \cot(kb + \delta_0(k)) + \sum_\nu \frac{2\mu\gamma_\nu}{E - E_\nu} \quad (\text{IV.27})$$

and all arguments about the correspondence of the quark eigenstates (“the primitives” the terminology of Jaffe and Low [50]) and poles of the P matrix remain true. Here $\delta_0(k)$ is the phase due to interaction V_{hh} which is assumed to vanish for $r > b$.

In practical calculations one is using the potential of the form [49, 83]

$$V = V_{hgh} + V_{hh}\theta(r - b) \quad (\text{IV.28})$$

and V_{hgh} for arbitrary NN angular momentum l is

$$V_{hgh}(\mathbf{r}, \mathbf{r}') = \frac{1}{rr'} \sum_m Y_{jmls}^* \frac{f_\nu^*(r, E) f_\nu(r', E)}{E - E_\nu} Y_{jmls}, \quad (\text{IV.29})$$

while $f_\nu(r, E)$ can be represented as

$$f_\nu(r, E) = -c_\nu \delta(r - b) + x_\nu(E_\nu - E) \eta_\nu(r), \quad (\text{IV.30})$$

where $\eta_\nu(r)$ describe the relative NN motion inside the MQS' and are chosen in the form

$$\eta_\nu(r) = N_\nu j_l(\beta_\nu r) \beta_\nu r, \quad \int \eta_\nu^2(r) dr = 1. \quad (\text{IV.31})$$

TABLE IV: Even and odd operators O .

Even	Odd		
even	odd	even-odd	odd-odd-odd
1	τ^α	$\tau^\alpha i\gamma_5$	$\tau^\alpha i\gamma_5 \sigma_{\mu\nu} i \overleftrightarrow{\partial}_\nu$
$i\gamma_5$	γ_μ	$i\gamma_5 i \overleftrightarrow{\partial}_\mu$	
$\overleftarrow{\gamma_5} \gamma_\mu$	$\sigma_{\mu\nu}$	$(\overleftarrow{\partial} + \overrightarrow{\partial})_\nu \sigma_{\mu\nu}$	
$(\overleftarrow{\partial} + \overrightarrow{\partial})_\mu$	$i\gamma_5 \sigma_{\mu\nu}$	$(\overleftarrow{\partial} + \overrightarrow{\partial})_\nu i\gamma_5 \sigma_{\mu\nu}$	
	$i \overleftrightarrow{\partial}_\mu$		

Finally, all coefficients are to be fitted to the experimental phases, usually in the interval $[0; 500 \div 800 \text{ MeV}]$. As a first approximation we shall assume, that $V_{hh} \equiv 0$ and only V_{hqh} is retained; as is shown in [49, 51] in this way one obtains a good fit to experimental NN S phases for energies up to $\sim 500 \text{ MeV}$. In Fig. 9 comparison to the experimental phases is given for the 1S_0 and 3S_1 states obtained from relativistic-expressions of Sect. VII.

We thus introduced in the NN system the interaction due to MQS (IV.29), which can alone (or in combination with usual OBEP) describe NN force, and the same in $3N, 4N\dots$ systems. At this stage f_n, E_n are found phenomenologically from NN phases, and due to [40] are changing with matter density. One can use V_{hqs} changing with matter density. One can use V_{hqs} both to reactions. At the next stage one should calculate f_n, E_n microscopically from QCD Lagrangian (e.g. in the framework of the FCM).

V. EFFECTIVE LAGRANGIAN OF QUARK COMPOUND BAG MODEL

In this section, we construct effective relativistic QCB Lagrangian for the description of nucleon-nucleon interaction.

Two-nucleon currents entering the effective Lagrangian are constructed as bilinear combinations of the nucleon wave functions:

$$J(x) = \bar{\Psi}_c(x) O \Psi(x). \quad (\text{V.1})$$

The nucleon wave functions, $\Psi(x)$, carry bispinor and isospin indices, $\Psi_c(x) = C \bar{\Psi}^T(x)$ is C -conjugated wave function, $\bar{\Psi}_c \equiv (\bar{\Psi}_c) = -\Psi^T C$, and $C = i\tau^2 i\gamma^2 \gamma^0$ in the standard representation [84]. The currents (V.1) annihilate dibaryons. The creation currents have the form

$$J^+(x) = \bar{\Psi}(x) \bar{O} \Psi_c(x). \quad (\text{V.2})$$

The matrix O admits expansion over the Dirac γ -matrices and the Pauli τ^α -matrices. Many terms of the formal expansion vanish, since $\Psi(x)$ anticommute. Under the permutation of two nucleon fields $J(x)$ transforms identically provided

$$C^T O^T C = -O. \quad (\text{V.3})$$

Transformation properties of the operators O and the nucleon fields under the C -conjugation are given in Appendix B.

Matrices O entering the effective Lagrangian are therefore antisymmetric (odd) under the C -conjugation. In Table IV we show elementary even and odd matrices and the composite odd ones which obey (V.3). They are combined further with the first-order differential operators $i \overleftrightarrow{\partial}_\mu = i(-\overleftarrow{\partial} + \overrightarrow{\partial})_\mu$ (odd one) and $(\overleftarrow{\partial} + \overrightarrow{\partial})_\mu$ (even one).

The matrices $\tau^\alpha \gamma_5 \gamma_\mu$ and $\tau^\alpha \sigma_{\mu\nu} i \overleftrightarrow{\partial}_\nu$ are not shown, since currents they produce with free nucleons represent full derivatives:

$$\bar{\Psi}_c \tau^\alpha \gamma_5 \gamma_\mu \Psi = \frac{1}{m} \partial_\mu (\bar{\Psi}_c \tau^\alpha i\gamma_5 \Psi), \quad (\text{V.4})$$

$$\bar{\Psi}_c \tau^\alpha \sigma_{\mu\nu} i \overleftrightarrow{\partial}_\nu \Psi = 2\partial_\mu (\bar{\Psi}_c \tau^\alpha \Psi). \quad (\text{V.5})$$

Full derivatives shifted to the dibaryon vector fields give vanishing contributions to the Lagrangian.

We restrict ourselves with scalar and vector dibaryon currents of positive and negative parity. This is sufficient to provide the phenomenological description of the NN scattering in $J = 0^\pm, 1^\pm$ channels (S - and P -wave scattering).

The list of possible two-nucleon currents is shown in Table V.

TABLE V: Two-nucleon currents, associated dibaryon fields, and their quantum numbers.

Current	Dibaryon	(I, J^P)
$\bar{\Psi}_c \tau^\alpha \Psi$	φ_-^α	$(1, 0^-)$
$\bar{\Psi}_c \tau^\alpha i \gamma_5 \Psi$	φ_+^α	$(1, 0^+)$
$\bar{\Psi}_c i \overleftrightarrow{\partial}_\mu \Psi$	$\chi_{+\mu}$	$(0, 1^+)$
$\partial_\nu (\bar{\Psi}_c \sigma^{\mu\nu} \Psi)$	$\chi_{+\mu}$	$(0, 1^+)$
$\bar{\Psi}_c i \gamma_5 i \overleftrightarrow{\partial}_\mu \Psi$	$\chi_{-\mu}$	$(0, 1^-)$
$\partial_\nu (\bar{\Psi}_c i \gamma_5 \sigma^{\mu\nu} \Psi)$	$\chi_{-\mu}$	$(0, 1^-)$
$\bar{\Psi}_c \tau^\alpha i \gamma_5 \sigma^{\mu\nu} i \overleftrightarrow{\partial}_\nu \Psi$	$\chi_{-\mu}^\alpha$	$(1, 1^-)$

A third vector current $\bar{\Psi}_c \gamma_\mu \Psi$ with quantum numbers $(0, 1^+)$ can be expressed in terms of the two ones listed in Table V using the Gordon's expansion

$$\bar{\Psi}_c \gamma_\mu \Psi = \frac{1}{2m} \bar{\Psi}_c i \overleftrightarrow{\partial}_\mu \Psi + \frac{1}{2m} \partial_\nu (\bar{\Psi}_c \sigma^{\mu\nu} \Psi).$$

The vector dibaryons are characterized by two coupling constants. Recall that photon couplings with the nucleons are characterized by two coupling constants also.

In the channel $(0, 1^+)$, the pseudovector coupling with the current $\bar{\Psi}_c i \overleftrightarrow{\partial}_\mu \Psi$ gives vanishing contribution at two-nucleon threshold, so the S -wave NN scattering length is determined completely by the pseudotensor coupling $(0, 1^+)$. In what follows, we neglect by the pseudovector coupling.

In the channel $(0, 1^-)$, a linear combination of two currents enters the P -wave NN scattering length, so we set the vector coupling equal to zero and redefine the tensor coupling.

Finally, every dibaryon is coupled to one two-nucleon current.

The dibaryon fields φ_P^α , $\chi_{P\mu}$ and $\chi_{P\mu}^\alpha$ carry (suppressed) indices of radial excitations, index $P = \pm 1$ stands for the parity, α is isospin index, and μ is the Lorentz index:

$$\varphi^\alpha = \begin{pmatrix} \varphi_{1-}^\alpha \\ \varphi_{1+}^\alpha \\ \varphi_{2-}^\alpha \\ \varphi_{2+}^\alpha \\ \vdots \end{pmatrix}, \quad \chi_\mu = \begin{pmatrix} \chi_{1+\mu} \\ \chi_{1-\mu} \\ \chi_{2+\mu} \\ \chi_{2-\mu} \\ \vdots \end{pmatrix}, \quad \chi_\mu^\alpha = \begin{pmatrix} \chi_{1+\mu}^\alpha \\ \chi_{1-\mu}^\alpha \\ \chi_{2+\mu}^\alpha \\ \chi_{2-\mu}^\alpha \\ \vdots \end{pmatrix}.$$

The coupling constants are defined accordingly:

$$g = \begin{pmatrix} g_{1-} \\ g_{1+} \\ g_{2-} \\ g_{2+} \\ \vdots \end{pmatrix}, \quad h = \begin{pmatrix} h_{1+} \\ h_{1-} \\ h_{2+} \\ h_{2-} \\ \vdots \end{pmatrix}, \quad h' = \begin{pmatrix} h'_{1+} \\ h'_{1-} \\ h'_{2+} \\ h'_{2-} \\ \vdots \end{pmatrix}. \quad (\text{V.6})$$

The effective Lagrangian splits into free and interaction parts:

$$\mathcal{L} = \mathcal{L}^{[0]} + \mathcal{L}_{int}^{[1]} + \mathcal{L}_{int}^{[2]}. \quad (\text{V.7})$$

$\mathcal{L}_{int}^{[1]}$ describes interaction of dibaryons with nucleons, while $\mathcal{L}_{int}^{[2]}$ describes a four-fermion contact interaction. The free part has the form

$$\begin{aligned} \mathcal{L}^{[0]} &= \bar{\Psi} (i \hat{\nabla} - m) \Psi \\ &+ \partial_\mu \varphi^{\alpha+} \partial_\mu \varphi^\alpha - \varphi^{\alpha+} M_{10}^2 \varphi^\alpha \\ &- \partial_\nu \chi_\mu^+ \partial_\nu \chi_\mu + \chi_\mu^+ M_{01}^2 \chi_\mu \\ &- \partial_\nu \chi_\mu^{\alpha+} \partial_\nu \chi_\mu^\alpha + \chi_\mu^{\alpha+} M_{11}^2 \chi_\mu^\alpha. \end{aligned} \quad (\text{V.8})$$

The interaction parts are as follows

$$\mathcal{L}_{int}^{[1]} = \varphi^{\alpha+} \bar{\Psi}_c \tau^\alpha \Gamma \Psi g + g^+ \bar{\Psi} \tau^\alpha \Gamma \Psi_c \varphi^\alpha \quad (\text{V.9})$$

$$\begin{aligned} & - \partial_\nu \chi_\mu^+ \bar{\Psi}_c \Gamma \sigma_{\mu\nu} \Psi \frac{h}{2m} - \frac{h^+}{2m} \bar{\Psi} \Gamma \sigma_{\mu\nu} \Psi_c \partial_\nu \chi_\mu \\ & + \chi_\mu^{\alpha+} \bar{\Psi}_c \tau^\alpha \Gamma \sigma^{\mu\nu} i \overleftrightarrow{\partial}_\nu \Psi \frac{h'}{2m} + \frac{h'^+}{2m} \bar{\Psi} \tau^\alpha \Gamma \sigma^{\mu\nu} i \overleftrightarrow{\partial}_\nu \Psi_c \chi_\mu^\alpha, \\ \mathcal{L}_{int}^{[2]} & = \lambda_{10} (\bar{\Psi} \tau^\alpha \Gamma \Psi_c) (\bar{\Psi}_c \tau^\alpha \Gamma \Psi) \\ & + \lambda_{01} (\bar{\Psi} \Gamma \sigma_{\mu\nu} \Psi_c) (\bar{\Psi}_c \Gamma \sigma_{\mu\nu} \Psi) \\ & + \lambda_{11} (\bar{\Psi} \tau^\alpha \Gamma \sigma^{\mu\nu} i \overleftrightarrow{\partial}_\nu \Psi_c) (\bar{\Psi}_c \tau^\alpha \Gamma \sigma^{\mu\nu} i \overleftrightarrow{\partial}_\nu \Psi). \end{aligned} \quad (\text{V.10})$$

Here, m is the nucleon mass, M_{IJ} are dibaryon masses (matrices) diagonal in the radial and parity quantum numbers and

$$\Gamma = \begin{pmatrix} 1 & 0 & 0 & 0 & \cdots \\ 0 & i\gamma_5 & 0 & 0 & \cdots \\ 0 & 0 & 1 & 0 & \cdots \\ 0 & 0 & 0 & i\gamma_5 & \cdots \\ \vdots & \vdots & \vdots & \vdots & \ddots \end{pmatrix}.$$

The coupling constants g , h , h' , and λ_{IJ} depend on the radial and parity quantum numbers as indicated e.g. by Eq. (V.6). \mathcal{L} is Hermitian by the construction.

There exists six various vertices for the Lorentz structures: $\{1, \gamma_\mu, \sigma_{\mu\nu}, i\gamma_5, \gamma_5 \gamma_\mu, i\gamma_5 \sigma_{\mu\nu}\}$. The vector and tensor ones correspond to two spin-1 fields, vector and pseudovector ones. So, we have at most two spin-0 fields with parity $P = \pm 1$ and two spin-1 fields with parity $P = \pm 1$, altogether four fields. The isospin degrees of freedom provide two additional structures, so we might have eight dibaryons. However, not all of them are coupled to the NN channel. The system of two nucleons may carry quantum numbers shown in Table VI.

TABLE VI: Two-nucleon states with lowest quantum numbers.

$^{2S+3}L_J$	(I, J^P)
3S_1	$(0, 1^+)$
1S_0	$(1, 0^+)$
3P_1	$(1, 1^-)$
1P_1	$(0, 1^-)$
3P_0	$(1, 0^-)$

We thus have five possible dibaryons $(I, J^P) = (1, 0^\pm), (0, 1^\pm), (1, 1^-)$. Missing are three dibaryons with the exotic quantum numbers $(0, 0^\pm), (1, 1^+)$, that do not correspond to two-nucleon states. From other hand, states $(0, 0^\pm)$ have the vanishing couplings with the NN channel, since $\bar{\Psi}_c \Psi = \bar{\Psi}_c i\gamma_5 \Psi = 0$. In the $(1, 1^+)$ channel one has, in addition, $\bar{\Psi}_c \tau^\alpha \gamma_\mu \Psi = \bar{\Psi}_c \tau^\alpha \sigma_{\mu\nu} \Psi = 0$.

The $(1, 1^-)$ channel is not exotic. It is included into the effective Lagrangian through the vertex $\bar{\Psi}_c \tau^\alpha i\gamma_5 \sigma_{\mu\nu} \overleftrightarrow{\partial}_\nu \Psi$. The vertex $\bar{\Psi}_c \tau^\alpha \sigma_{\mu\nu} \overleftrightarrow{\partial}_\nu \Psi$ is full derivative according to Eq. (V.5).

VI. IN-MEDIUM NUCLEON AND DIBARYON PROPAGATORS

We consider symmetric nuclear matter with equal proton and neutron fractions.

A. Nucleon propagators in ideal Fermi gas

The in-medium nucleon propagator is defined by

$$iS_F(x) = \langle T \Psi(x) \bar{\Psi}(0) \rangle. \quad (\text{VI.1})$$

The propagator depends on the Fermi momentum p_F . In the momentum representation,

$$S_F(p) = \int dx e^{ipx} S_F(x) \quad (\text{VI.2})$$

We need the in-medium nucleon propagator constructed out of the C -conjugated nucleon fields

$$iS_F^c(x) = \langle T \Psi_c(x) \bar{\Psi}_c(0) \rangle. \quad (\text{VI.3})$$

The momentum representation of $S_F^c(x)$ is derived from Eq. (VI.2). The propagators are related by

$$S_F^c(x) = C^T S_F^T(-x) C, \quad (\text{VI.4})$$

$$S_F^c(p) = C^T S_F^T(-p) C. \quad (\text{VI.5})$$

The C -conjugation matrix is defined in Appendix A.

In the momentum representation, the propagators of the ideal gas have the form

$$S_F(p) = S_F^c(p) = \frac{1}{\hat{p} - m}. \quad (\text{VI.6})$$

The signs of imaginary parts of the pole positions on the complex energy plane should be specified separately.

The poles of $S_F(p)$ approach the real axis from the upper half of the complex p_0 -plane for $\Re p_0 < \mu = +\sqrt{m^2 + p_F^2}$ and from the lower half of the complex p_0 -plane for $\Re p_0 > \mu$. $S_F^c(p)$ has poles shifted to the upper half-plane for $\Re p_0 < -\mu$ and to the lower half-plane otherwise.

$S_F(x)$ describes therefore propagation of nucleons in presence of the Fermi sphere made up of nucleons. $S_F^c(x)$ describes propagation of nucleons in presence of the Fermi sphere, however, made up of antinucleons, the Fermi momentum being the same.

The plane waves expansion of the in-medium propagators has the form

$$iS_F(x) = \int \frac{d\mathbf{p}}{(2\pi)^3} [e^{-ipx} \Lambda_+(\mathbf{p}) (\theta(x_0)\theta(|\mathbf{p}| - p_F) - \theta(-x_0)\theta(p_F - |\mathbf{p}|)) + e^{ipx} \Lambda_-(\mathbf{p})\theta(-x_0)], \quad (\text{VI.7})$$

$$iS_F^c(x) = \int \frac{d\mathbf{p}}{(2\pi)^3} [e^{ipx} \Lambda_-(\mathbf{p}) (\theta(-x_0)\theta(|\mathbf{p}| - p_F) - \theta(x_0)\theta(p_F - |\mathbf{p}|)) + e^{-ipx} \Lambda_+(\mathbf{p})\theta(x_0)], \quad (\text{VI.8})$$

where $p = (E(\mathbf{p}), \mathbf{p})$, $E(\mathbf{p}) = +\sqrt{m^2 + \mathbf{p}^2}$, and

$$\Lambda_{\pm}(\mathbf{p}) = \frac{\pm \hat{p} + m}{2E(\mathbf{p})} \quad (\text{VI.9})$$

are projection operators that obey

$$C^T \Lambda_{\pm}(\mathbf{p})^T C = \Lambda_{\mp}(\mathbf{p}). \quad (\text{VI.10})$$

B. Dibaryon propagators

The dibaryon propagators with quantum numbers $(1, 0^{\pm})$, $(0, 1^{\pm})$, $(1, 1^{-})$ are defined, respectively, by

$$i\Delta'^{\alpha\beta}(x-y) = \langle T \varphi^{\alpha}(x) \varphi^{\beta+}(y) \rangle, \quad (\text{VI.11})$$

$$iD'_{\mu\nu}(x-y) = \langle T \chi_{\mu}(x) \chi_{\nu}^{\dagger}(y) \rangle, \quad (\text{VI.12})$$

$$iD'_{\mu\nu}{}^{\alpha\beta}(x-y) = \langle T \chi_{\mu}^{\alpha}(x) \chi_{\nu}^{\beta+}(y) \rangle. \quad (\text{VI.13})$$

The radial indices are suppressed. The coupling to the NN channel produces mixing of the radial excitations.

The free propagators are given by

$$\Delta^{\alpha\beta}(p) = \frac{1}{p^2 - M_{10}^2} \delta^{\alpha\beta}, \quad (\text{VI.14})$$

$$D_{\mu\nu}(p) = \frac{-g_{\mu\nu} + p_{\mu} p_{\nu} / p^2}{p^2 - M_{01}^2}, \quad (\text{VI.15})$$

$$D_{\mu\nu}{}^{\alpha\beta}(p) = \frac{-g_{\mu\nu} + p_{\mu} p_{\nu} / p^2}{p^2 - M_{11}^2} \delta^{\alpha\beta}. \quad (\text{VI.16})$$

Tensor structures of the dressed propagators can be factored out

$$\Delta'^{\alpha\beta}(p) = \delta^{\alpha\beta} \Delta'(p), \quad (\text{VI.17})$$

$$D'_{\mu\nu}(p) = (-g_{\mu\nu} + p_\mu p_\nu / p^2) D'(p), \quad (\text{VI.18})$$

$$D'^{\alpha\beta}_{\mu\nu}(p) = \delta^{\alpha\beta} (-g_{\mu\nu} + p_\mu p_\nu / p^2) D'_1(p). \quad (\text{VI.19})$$

C. In-medium dispersion law for interacting nucleons

In systems with interaction, self-energy operators of fermions appear. They can be expanded over the γ -matrices:

$$\hat{\Sigma}(p) = \hat{\Sigma}_V(p) + \Sigma_S(p), \quad (\text{VI.20})$$

$$\hat{\Sigma}^c(p) = \hat{\Sigma}_V^c(p) + \Sigma_S^c(p), \quad (\text{VI.21})$$

where $\hat{\Sigma}_V(p) = \Sigma_V^\mu(p) \gamma_\mu$ and $\hat{\Sigma}_V^c(p) = \Sigma_V^{c\mu}(p) \gamma_\mu$. The C -conjugation gives (cf. (VI.5))

$$\hat{\Sigma}^c(p) = C^T \hat{\Sigma}^T(-p) C. \quad (\text{VI.22})$$

We thus obtain

$$\Sigma_V^{c\mu}(p) = -\Sigma_V^\mu(-p), \quad (\text{VI.23})$$

$$\Sigma_S^c(p) = \Sigma_S(-p), \quad (\text{VI.24})$$

and

$$\hat{\Sigma}^c(p) = \gamma_5 \hat{\Sigma}(-p) \gamma_5.$$

The diagram representation of the self-energy operator arising due to the dibaryon-induced nucleon-nucleon interaction is shown in Fig. 4. Its non-relativistic version is $U_2(\mathbf{p}, \rho)$ defined by Eq. (IX.17). Equation (IX.18) is the analogue of the one-loop approximation shown in Fig. 4.

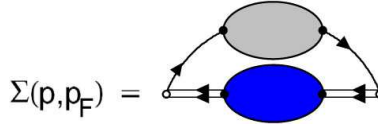


FIG. 4: Nucleon self-energy operator. The double solid line with the shaded blob shows the dressed dibaryon propagator, the single solid line the shaded blob shows the dressed nucleon propagator.

The in-medium propagators have the form

$$S'_F(p) = \frac{1}{\hat{p} - m - \hat{\Sigma}(p)} = \frac{\hat{p} + m + \hat{\Sigma}^c(-p)}{\phi(p)},$$

$$S'^c_F(p) = \frac{1}{\hat{p} - m - \hat{\Sigma}^c(p)} = \frac{\hat{p} + m + \hat{\Sigma}(-p)}{\phi_c(p)},$$

where

$$\begin{aligned} \phi(p) &= (p - \Sigma_V(p))^2 - (m + \Sigma_S(p))^2, \\ \phi_c(p) &= (p - \Sigma_V^c(p))^2 - (m + \Sigma_S^c(p))^2. \end{aligned}$$

Using Eqs. (VI.23) and (VI.24) we find

$$\phi_c(p) = \phi(-p). \quad (\text{VI.25})$$

The dispersion laws of elementary excitations of nucleons are determined from equation

$$\phi(p) = 0. \quad (\text{VI.26})$$

This equation gives two solutions $p_0 = \pm E_\pm(\mathbf{p})$ with positive and negative energies of the excitations. Respectively, positive and negative energy solutions of equation $\phi_c(p) = 0$ are $p_0 = \pm E_\mp(\mathbf{p})$. In the ideal Fermi gas, $E_\pm(\mathbf{p}) = +\sqrt{m^2 + \mathbf{p}^2}$.

The plane waves expansion of the in-medium propagators has the form

$$iS'_F(x) = \int \frac{d\mathbf{p}}{(2\pi)^3} [e^{-ip+x} \Lambda'_+(\mathbf{p}) (\theta(x_0)\theta(|\mathbf{p}| - p_F) - \theta(-x_0)\theta(p_F - |\mathbf{p}|)) + e^{ip-x} \Lambda'_-(\mathbf{p})\theta(-x_0)], \quad (\text{VI.27})$$

$$iS'_{F_c}(x) = \int \frac{d\mathbf{p}}{(2\pi)^3} [e^{ip+x} \Lambda'^c_+(\mathbf{p}) (\theta(-x_0)\theta(|\mathbf{p}| - p_F) - \theta(x_0)\theta(p_F - |\mathbf{p}|)) + e^{-ip-x} \Lambda'^c_-(\mathbf{p})\theta(x_0)], \quad (\text{VI.28})$$

where $p_{\pm} = (E_{\pm}(\mathbf{p}), \mathbf{p})$ and

$$\Lambda'_{\pm}(\mathbf{p}) = \frac{\pm \hat{p}_{\pm} + m + \hat{\Sigma}^c(\mp p_{\pm})}{\pm \phi'(\pm p_{\pm})}, \quad (\text{VI.29})$$

$$\Lambda'^c_{\mp}(\mathbf{p}) = \frac{\pm \hat{p}_{\mp} + m + \hat{\Sigma}(\mp p_{\mp})}{\pm \phi'_c(\pm p_{\mp})}, \quad (\text{VI.30})$$

with $\phi'(p) = d\phi(p)/dp_0$ and $\phi'_c(p) = d\phi_c(p)/dp_0$. In the ideal Fermi gas, Eqs. (VI.7) and (VI.8) are recovered.

D. Dyson equation for nucleon propagator

$\Sigma(p)$ is calculated to one loop, contributions of the antinucleons are neglected. The loops are formed thereby by nucleons and nucleon holes in the Fermi sphere. Such approximation is close to the mean-field approximation.

Shown in Fig. 5 is the system of Dyson equations,

$$S'_F = S_F + S_F \Sigma S'_F, \quad (\text{VI.31})$$

for the in-medium nucleon propagator. The virtual dibaryons in the loop contribute to the self-energy operator. The four-fermion interaction will be included later.

Starting from Lagrangian (V.7) one gets

$$\begin{aligned} \frac{1}{4} \hat{\Sigma}(p) &= \int \frac{d^4 p_c}{(2\pi)^4} g^+ \tau^\alpha \Gamma \Delta'^{\alpha\beta}(p - p_c) i S'^c_F(p_c) \tau^\beta \Gamma g \\ &- \int \frac{d^4 p_c}{(2\pi)^4} \frac{h^+}{2m} i \sigma_{\mu\tau}(p_c - p) \tau \Gamma D'_{\mu\nu}(p - p_c) i S'^c_F(p_c) \Gamma i \sigma_{\nu\sigma}(p_c - p) \sigma \frac{h}{2m} \\ &+ \int \frac{d^4 p_c}{(2\pi)^4} \frac{h'^+}{2m} i \sigma_{\mu\tau}(p + p_c) \tau \tau^\alpha i \gamma_5 D'^{\alpha\beta}_{\mu\nu}(p - p_c) i S'^c_F(p_c) \tau^\beta i \gamma_5 i \sigma_{\nu\sigma}(-p_c - p) \sigma \frac{h'}{2m}. \end{aligned} \quad (\text{VI.32})$$

In Eq. (VI.32) summation over the radial numbers and parity states ($\Gamma = 1, i\gamma_5$) is assumed. The integrals over the timelike component of p_c can be calculated assuming $\phi(p)$ has simple zeros in the complex energy plane at $p_0 = \pm E_{\pm}(\mathbf{p})$. The negative energy states are neglected. The remaining three-dimensional integrals describe contributions to the self-energy operators from the nucleon holes.

The self-energy can be expanded over the different channels

$$\hat{\Sigma}(p) = \sum_{I, J^P} \hat{\Sigma}_{I, J^P}(p). \quad (\text{VI.33})$$

The separate contributions for $(I, J^P) = (1, 0^{\pm}), (0, 1^{\pm}), (1, 1^{-})$ are given in Appendix B.

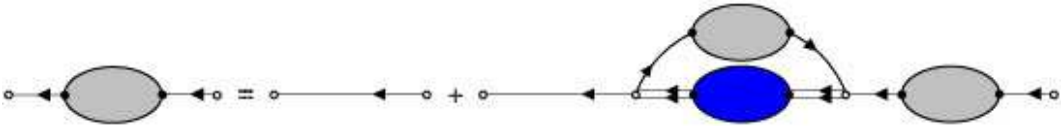


FIG. 5: System of Dyson equations for nucleon propagator $S'_F(p)$. The single and double solid lines show the nucleon and dibaryon propagators. The shaded blobs indicate the dressed propagators. Summation over dibaryons in the loop is assumed.

E. Bethe-Brueckner equation for dibaryon propagator

Dibaryon self-energy operator to one loop is determined by two-body nucleon Green function, its diagram representation is shown in Fig. 6. The system of equations of Fig. 6 is equivalent to Eqs. (IX.1) which determine two-nucleon scattering in the vacuum (T -matrix) and in the medium (G -matrix). The potential V_2 is the analogue of the dibaryon propagator in the vacuum, $G_2(W)$ is the analogue of the dressed dibaryon propagator, $Q_2 e_2^{-1}$ is the dibaryon self energy shown in Fig. 6.

The corresponding analytical expressions have the form

$$\begin{aligned}\Pi^{\beta\alpha}(p, p_F) &= -2i \int \frac{d^4 p_c}{(2\pi)^4} g \text{Sp}[\tau^\beta \Gamma S'_F(p + p_c, p_F) \tau^\alpha \Gamma S'_{F_c}(p_c, p_F)] g^+, \\ \Pi_{\nu\mu}(p, p_F) &= -2i \int \frac{d^4 p_c}{(2\pi)^4} \frac{h}{2m} \text{Sp}[(-i\sigma_{\nu\sigma} p_\sigma) \Gamma S'_F(p + p_c, p_F) i\sigma_{\mu\tau} p_\tau \Gamma S'_{F_c}(p_c, p_F)] \frac{h^+}{2m}, \\ \Pi_{\nu\mu}^{\beta\alpha}(p, p_F) &= -2i \int \frac{d^4 p_c}{(2\pi)^4} \frac{h'}{2m} \text{Sp}[(-\tau^\beta i\gamma_5 i\sigma_{\nu\sigma} (p + 2p_c)_\sigma) S'_F(p + p_c, p_F) i\sigma_{\mu\tau} (p + 2p_c)_\tau \tau^\alpha i\gamma_5 S'_{F_c}(p_c, p_F)] \frac{h'^+}{2m}.\end{aligned}$$

Here, $\text{Sp}[\dots]$ is taken over isospin and bispinor indices. The self-energy operators are diagonal in (I, J^P) and represent matrices in the radial numbers.

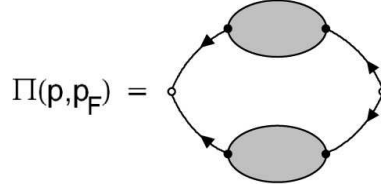


FIG. 6: Dibaryon self-energy operator. The single solid lines with the shaded blobs are the dressed nucleon propagators. The loop produces mixing between dibaryons with different radial quantum numbers.

The system of Dyson equations for the dibaryon propagators has the form:

$$\begin{aligned}\Delta'^{\alpha\beta}(p) &= \Delta^{\alpha\beta}(p) + \Delta^{\alpha\sigma}(p) \Pi^{\sigma\gamma}(p) \Delta'^{\gamma\beta}(p), \\ D'_{\mu\nu}(p) &= D_{\mu\nu}(p) + D_{\mu\tau}(p) \Pi_{\tau\sigma}(p) D'_{\sigma\nu}(p), \\ D'^{\alpha\beta}_{\mu\nu}(p) &= D^{\alpha\beta}_{\mu\nu}(p) + D^{\alpha\delta}_{\mu\tau}(p) \Pi^{\delta\gamma}_{\tau\sigma}(p) D'^{\gamma\beta}_{\sigma\nu}(p).\end{aligned}$$

These equations are depicted in Fig. 7.

F. Link to optical potential model

Probing particles acquire new decay channels in the medium, connected to collisions with the surrounding particles, and become unstable. Phenomenologically, the in-medium spin-1/2 particles are described by the Dirac equation

$$(i\hat{\nabla} - m_1 + \frac{i}{2}\Gamma)\Psi = 0, \quad (\text{VI.34})$$

where Γ is collision width

$$\Gamma = \rho\sigma v\gamma. \quad (\text{VI.35})$$

Here, v is velocity and γ Lorentz factor. The cross section can be expressed in terms of the forward scattering amplitude with the help of the optical theorem

$$\sigma = \frac{4\pi}{p^*} \text{Im}f(\theta = 0). \quad (\text{VI.36})$$

The self-energy operator and the forward scattering amplitude are analytical functions. Given the imaginary part is known, the real part can be restored using the dispersion relations. If, however, the scattering amplitude is known, one can write

$$\Sigma(p) = -\rho \frac{2\pi\sqrt{s}}{m_1 m_2} f(\theta = 0). \quad (\text{VI.37})$$

where m_2 is mass of the particles of the medium.

Near the threshold, one can expand the amplitude over the partial waves and keep the lowest order $L = 0$ terms: $f(\theta = 0) \approx e^{i\delta(s)} \sin \delta(s)/p^*$ where $\delta(s)$ is the S -wave phase shift. If probing particle is identical with particles of the medium, one has $m_1 = m_2 = m$, $f(\theta = 0) \approx 2e^{i\delta(s)} \sin \delta(s)/p^*$ and

$$\Sigma(p) = -\rho \frac{8\pi}{mp^*} e^{i\delta(s)} \sin \delta(s). \quad (\text{VI.38})$$

The symmetric nuclear matter consists of the two types of the particles, so the statistical factors modify Eq. (VI.38).

Let a spin-up proton scatters on the in-medium protons in the $(1, 0^+)$ channel. The in-medium protons have spin down. The statistical weight of the configuration $\uparrow\downarrow$ in the $S = 0$ spin wave function is $1/2$. The proton-proton collisions contribute to the self-energy operator with the weight $1/2 \times \rho/4$, where $\rho/4$ is the spin-down proton density. A spin-up proton scatters on the in-medium neutrons also, with the weight factor $1/2$ for the $I = 1$ channel and the weight factor $1/2$ for the spin-down neutrons. The spin-isospin factor in the $I = 1$ channel becomes $1/4 \times 1/2 \times 1/2 = 1/16$. The in-medium protons and neutrons contribute altogether with the factor $1/8 + 1/16 = 3/16$. We therefore replace $\rho \rightarrow 3\rho/16$ in Eq. (VI.38). The $(0, 1^+)$ channel can be analyzed in the similar fashion.

From other hand, in the low-density limit of the symmetric matter, Eqs.(VI.32) give

$$\Sigma_{IJ^P}(p) = -\rho \frac{3\pi}{2mp^*} e^{i\delta_{IJ^P}(s)} \sin \delta_{IJ^P}(s) \frac{\gamma_0 + 1}{2} + \dots,$$

where $(I, J^P) = (1, 0^+)$ and $(0, 1^+)$ in agreement with the optical potential model.

It is instructive to compare the nucleon self-energy with the Relativistic Mean Field (RMF) model [24, 25], according to which

$$\Sigma(p) = \rho \frac{g_\omega^2}{m_\omega^2} \gamma^0 - \rho \frac{g_\sigma^2}{m_\sigma^2}. \quad (\text{VI.39})$$

The first term describes the ω -meson exchange between the nucleons, the second one originates from the σ -meson exchange. In the RMF models $\Sigma(p) \sim \gamma^0 - 1$ (numerically). The strong cancellation of the large vector and the large scalar mean fields is the typical feature of the RMF models.

In our model, the nucleon self-energy in the low density limit is proportional to $\gamma_0 + 1$. The first term can be interpreted as the vector mean field, the second one as the scalar mean field. The mean fields are of the same sign and of the same order.

VII. DIBARYONS IN PHASE SHIFTS ANALYSIS OF NUCLEON-NUCLEON SCATTERING

In order to describe the in-medium properties of nucleons and dibaryons, one has to fix parameters entering the effective Lagrangian. Those parameters determine the NN scattering phase shifts which are known experimentally.

A. Dibaryon self-energy operator in the vacuum

The dibaryon self-energy operators are matrices proportional gg^+ , hh^+ , and $h'h'^+$. Such a circumstance allows to factorize the radial numbers and the parity structures. Also, the isospin and Lorentz structures of the self-energy operators can be factored out:

$$\Pi^{\beta\alpha}(p) = \delta^{\beta\alpha} g \Pi_{10^P}(p) g^+, \quad (\text{VII.1})$$

$$\Pi_{\nu\mu}(p) = (-g_{\nu\mu} + \frac{p_\nu p_\mu}{p^2}) h \Pi_{01^P}(p) h^+, \quad (\text{VII.2})$$

$$\Pi_{\nu\mu}^{\beta\alpha}(p) = \delta^{\beta\alpha} (-g_{\nu\mu} + \frac{p_\nu p_\mu}{p^2}) h' \Pi_{11^-}(p) h'^+, \quad (\text{VII.3})$$

where

$$\Pi_{IJ^P}(p) = \frac{1}{(2\pi)^4} \int d^4 q_c d^4 p_c \delta^4(p - q_c - p_c) \frac{\varphi_{IJ^P}(q_c, p_c)}{(q_c^2 - m^2 + i0)(p_c^2 - m^2 + i0)}. \quad (\text{VII.4})$$

The functions $\varphi_{IJ^P}(q_c, p_c)$ have the form

$$\begin{aligned} \varphi_{10^P}(q_c, p_c) &= -\frac{2i}{3} \text{Sp}[\tau^\alpha \Gamma(\hat{q}_c + m) \tau^\alpha \Gamma(-\hat{p}_c + m)], \\ \varphi_{01^P}(q_c, p_c) &= -\frac{2i}{3} \frac{1}{4m^2} (-g_{\nu\mu} + \frac{p_\nu p_\mu}{p^2}) \text{Sp}[\Gamma(-i\sigma_{\nu\sigma} p_\sigma)(\hat{q}_c + m) i\sigma_{\mu\tau} p_\tau \Gamma(-\hat{p}_c + m)], \\ \varphi_{11^-}(q_c, p_c) &= -\frac{2i}{9} \frac{1}{4m^2} (-g_{\nu\mu} + \frac{p_\nu p_\mu}{p^2}) \text{Sp}[\tau^\alpha i\gamma_5 (-i\sigma_{\nu\sigma}(q_c - p_c)_\sigma)(\hat{q}_c + m) i\sigma_{\mu\tau}(q_c - p_c)_\tau \tau^\alpha i\gamma_5 (-\hat{p}_c + m)]. \end{aligned}$$

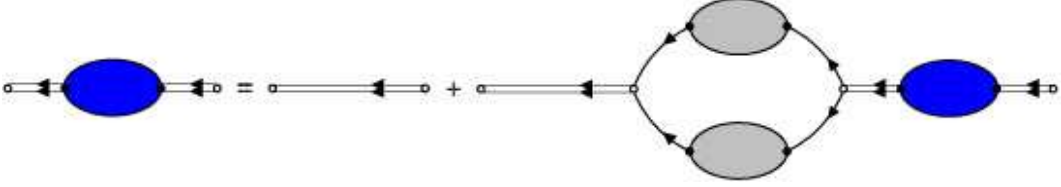


FIG. 7: Systems of Dyson equations for the dibaryon propagators shown by the double solid lines. The single solid lines show the nucleon propagator. The shaded blobs indicate dressed propagators.

The discontinuity over the cut $(4m^2, +\infty)$ can be found to be

$$\Pi_{IJ^P}(s + i0) - \Pi_{IJ^P}(s - i0) = -\frac{1}{4\pi^2} \Phi_2(s) \varphi_{IJ^P}(q_c, p_c),$$

where q_c and p_c are the on-mass-shell nucleon momenta and $\Phi_2(s)$ is two-body phase space

$$\Phi_2(s) = \frac{\pi p^*(s)}{\sqrt{s}},$$

where $p^*(s) = \sqrt{s/4 - m^2}$. In what follows, $p^*(s + i0) \equiv k > 0$ above the threshold and $p^*(s - i0) = -k$.

The functions $\varphi_{IJ^P}(q_c, p_c)$ are given in Table VII. They show the correct threshold behavior $\sim k^{2L}$. The imaginary part of $\Pi_{IJ^P}(s)$ is negative and corresponds to positive transition probabilities.

TABLE VII: $\varphi_{IJ^P}(q_c, p_c)$ and κ_{IJ^P} is different channels.

$2S+3 L_J$	(I, J^P)	$\varphi_{IJ^P}(q_c, p_c)$	κ_{IJ^P}
3S_1	$(0, 1^+)$	$8is(1 + p^{*2}/(3m^2))$	$\pi b/(2m)$
1S_0	$(1, 0^+)$	$8is$	$\pi b/(2m)$
3P_1	$(1, 1^-)$	$64ip^{*2}/3$	$\pi mb^3/12$
1P_1	$(0, 1^-)$	$16ip^{*2}s/(3m^2)$	$\pi mb^3/12$
3P_0	$(1, 0^-)$	$32ip^{*2}$	$\pi mb^3/18$

B. S matrix

We consider first the scalar dibaryons. The dressed propagator can be written as follows

$$\Delta'^{\alpha\beta}(p) = \delta^{\alpha\beta} \Delta'(p).$$

In the one-loop approximation, the system of Dyson equations can be solved to give

$$\Delta'(p) = \Delta(p) + \frac{\Delta(p)g\Pi_{10^P}(p)g^+\Delta(p)}{1 - \Lambda_{10^P}^{-1}(p)\Pi_{10^P}(p)}.$$

Here, $\Delta(p)$ is the bare dibaryon propagator diagonal in the radial numbers,

$$\begin{aligned}\Lambda_{10^P}^{-1}(s) &= g^+ \Delta(p) g = g^+ \frac{1}{s - M_{10^P}^2} g \\ &= \sum_r g_r^* \frac{1}{s - M_{r10^P}^2} g_r,\end{aligned}\tag{VII.5}$$

where $s = p^2$, the sum is taken over the radial numbers.

The model described in Sect. V is the relativistic extension of the Quark Compound Bag model [49]. $\Lambda_{01^P}^{-1}(s)$ is, in particular, the function defined in Eq. (5) of Ref. [49]. The poles of $\Lambda_{01^P}^{-1}(s)$ correspond to the compound $6q$ states i.e. dibaryons, whereas poles of $\Lambda_{01^P}(s)$ are the Castillejo-Dalitz-Dyson (CDD) poles [85]. The model described in Sect. V can also be considered as a version of the Dyson model [86], which is, in turn, a version of the Lee model [87].

The four-point Green function of the nucleons is shown in Fig. 8. The scattering amplitude is proportional to

$$g^+ \Delta'(p) g = \frac{1}{\Lambda_{10^P}(p) - \Pi_{10^P}(p)}.$$

Extension to the vector dibaryons is straightforward. In general case, the S -matrix can be written as follows:

$$S_{IJ^P} = e^{2i\delta_{IJ^P}(s)} = \frac{\Lambda_{IJ^P}(s) - \Pi_{IJ^P}(s - i0)}{\Lambda_{IJ^P}(s) - \Pi_{IJ^P}(s + i0)}.\tag{VII.6}$$

C. P matrix. Dibaryons as P -matrix poles

The experimental searches of exotic MSQ did not give conclusive results. Jaffe and Low [50], therefore, proposed to identify exotic MSQ with so-called "primitives", i.e., the poles of the P matrix, not S matrix. The primitives manifest themselves in the form of zeros of D functions on the unitary cut. Analysis of the phase shifts of meson-meson scattering and nucleon-nucleon scattering [88] showed the presence of primitives with masses close to those expected in the MIT bag model.

The method of Jaffe and Low is basically heuristic and can hardly be extended to modified external conditions e.g. at finite temperature or density. In this sense, the dynamical P matrix developed by Simonov [49] is perfectly suited for studying collective properties of nuclear matter. Earlier, it has been applied successfully for description of nucleon-nucleon interaction in the vacuum [49, 51–54].

Since the P -matrix formalism is phenomenologically successful, it is desirable for any model to have a link with it. As noticed by Simonov [49], the P matrix has poles at primitive masses provided the interaction between nucleons and dibaryons is restricted to the surface of a radius b . In the coordinate space, the form factor entering the $\bar{N}\bar{N}D$ vertex represents a delta-function $\delta(r - b)$.

In the momentum representation, we have to use therefore, in the partial L -wave,

$$\mathcal{F}_L(s) = \left(\frac{s}{4m^2}\right)^{1/4} \frac{(2L+1)!! j_L(kb)}{(kb)^L}.\tag{VII.7}$$

The partial wave scattering amplitudes of the pointlike nucleons and dibaryons discussed so far already have the correct threshold behavior. The denominator $(kb)^L$ in Eq. (VII.7) is thus introduced not to violate that feature. The additional dependence on $s/(4m^2)$ is introduced to simplify calculations of the dibaryon self-energy operators. The common factor is chosen to fulfill

$$\mathcal{F}_L(s = 4m^2) = 1.$$

In the nonrelativistic limit, $\mathcal{F}_L(s) \equiv 1$ for pointlike interaction with $b = 0$.

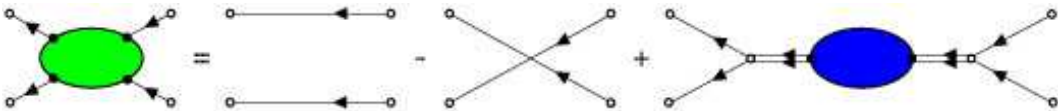


FIG. 8: Four-point Green function of nucleons.

Let us consider function

$$f_L(z) = z j_L(z) h_L^{(1)}(z),$$

where $j_L(z)$, $y_L(z)$, and $h_L^{(1)}(z) = j_L(z) + i y_L(z)$ are, respectively, the 1-st, 2-nd and 3-rd spherical Bessel functions defined as Ref. [89]. One has, for $z > 0$,

$$\begin{aligned} j_L(z) - j_L(-z) &= \begin{cases} 0, & \text{even } L, \\ 2j_L(z), & \text{odd } L, \end{cases} \\ y_L(z) - y_L(-z) &= \begin{cases} 2y_L(z), & \text{even } L, \\ 0, & \text{odd } L \end{cases} \end{aligned}$$

and, as a consequence,

$$f_L(z) - f_L(-z) = 2z j_L^2(z). \quad (\text{VII.8})$$

The form factor modifies the discontinuity of $\Pi_{IJ^P}(s)$:

$$\begin{aligned} \varphi_{IJ^P}(q_c, p_c) &\rightarrow \varphi_{IJ^P}(q_c, p_c) \mathcal{F}_L^2(s) \\ &= \varphi_{IJ^P}(q_c, p_c) \left(\frac{s}{4m^2} \right)^{1/2} \left(\frac{(2L+1)!!}{(kb)^L} \right)^2 \frac{f_L(kb) - f_L(-kb)}{2kb}. \end{aligned} \quad (\text{VII.9})$$

$\Pi_{IJ^P}(s)$ can be reconstructed using the dispersion integral.

In order to simplify calculations, we replace the ratio $\varphi_{IJ^P}(q_c, p_c)/(kb)^{2L}$ by its threshold value. Such a procedure can be viewed as a redefinition of the form factor $\mathcal{F}_L(s)$ which is a phenomenological element of the model. One can easily verify that the discontinuity has the correct form for the expression

$$\Pi_{IJ^P}(s) = -\frac{1}{16\pi b m} \varphi_{IJ^P}(q_c, p_c) \left(\frac{(2L+1)!!}{(kb)^L} \right)^2 f_L(s),$$

where $f_L(s) \equiv f_L(p^*(s))$. $\Pi_{IJ^P}(s)$ defined this way is analytical function in the complex s -plane with the cut $(4m^2, +\infty)$. On the first Riemann sheet, $\Pi_{IJ^P}(s) \rightarrow 0$ for $s \rightarrow \infty$. Equation for $\Pi_{IJ^P}(s)$ can be written as

$$\kappa_{IJ^P} \Pi_{IJ^P}(s) = -i f_L(s), \quad (\text{VII.10})$$

with coefficients κ_{IJ^P} listed in Table VII.

P matrix is defined as the logarithmic derivative of two-nucleon radial wave function:

$$P = \left. \frac{d \ln \chi_L(r)}{d \ln r} \right|_{r=b}. \quad (\text{VII.11})$$

Here, we suppress indices of the channel except for L .

One can express S matrix in terms of P matrix and $\Lambda(s)$, P matrix in terms of S matrix and $\Lambda(s)$, and $\Lambda(s)$ in terms of S and P matrices.

Firstly, using Eq. (VII.11) and Eqs. (VII.6) and (VII.10) one gets

$$S = -\frac{h_L^{(2)}(z)P - (zh_L^{(2)}(z))'}{h_L^{(1)}(z)P - (zh_L^{(1)}(z))'} \quad (\text{VII.12})$$

$$= \frac{\kappa\Lambda - izj_L(z)h_L^{(2)}(z)}{\kappa\Lambda + izj_L(z)h_L^{(1)}(z)}, \quad (\text{VII.13})$$

where $z = kb$ (see e.g. [90], problem 82).

Secondly, P matrix can be found to be

$$P = \frac{(zh_L^{(2)}(z))' + S(zh_L^{(1)}(z))'}{h_L^{(2)}(z) + S h_L^{(1)}(z)} \quad (\text{VII.14})$$

$$= P_{free} + \kappa^{-1} \Lambda^{-1}, \quad (\text{VII.15})$$

where

$$P_{free} = \frac{(z j_L(z))'}{j_L(z)}. \quad (\text{VII.16})$$

Equation (VII.15) is equivalent to Eq. (IV.27) with $\delta_0 = 0$. P matrix can be modified in general by adding to P matrix of the noninteracting particles new poles with positive residues. The negative ones are not allowed since they bring the corresponding D function out of the class of generalized R functions. The free P matrix has residues

$$r_p = 8 \left(\frac{a_L}{b} \right)^2,$$

where $a_0 = \pi$, $a_1 = 4.49$ etc. are zeros of the Bessel functions.

Equation (VII.15) can be used for the extraction from experimental phase shifts the information on masses of the compound states which show up as P -matrix poles on the real axis of the complex s -plane.

Thirdly, Λ is expressed through S and P matrices:

$$\kappa \Lambda = -iz j_L(z) \frac{S h_L^{(1)}(z) + h_L^{(2)}(z)}{S - 1} \quad (\text{VII.17})$$

$$= (P - P_{free})^{-1}. \quad (\text{VII.18})$$

Poles of Λ are the CDD poles.

D. P matrix and Castillejo-Dalitz-Dyson poles

Castillejo, Dalitz and Dyson [85] introduced the so-called CDD poles to parameterize the uncertainty of the amplitudes which satisfy the correct analytic properties in the complex energy plane, the unitarity relation and are solutions of the scattering Low's equation. The physical meaning of the CDD poles has been clarified by Dyson [86] who showed, using one of the earlier versions of the Lee model [87], that CDD poles correspond to bound states and resonances. New type of CDD pole is associated with primitives [92].

The CDD poles are poles of Λ and D functions defined by the denominator of Eq. (VII.6):

$$D(s) = \Lambda(s) - \Pi(s), \quad (\text{VII.19})$$

where the indices (I, J^P) are suppressed. The CDD poles are localized between zeros of $\Lambda(s)$, i.e., between $M_{rIJ^P}^2$ and $M_{r+1IJ^P}^2$.

D function we discuss is the generalized R function [85]. It has no zeros on the first Riemann sheet of the complex s -plane. It has no zeros on the real half-axis $(-\infty, s_0)$, corresponding to bound states, also provided $D(s_0) < 0$ and $s_0 < M_{rIJ^P}^2$.

Resonances are simple roots of equation

$$D(s) = 0, \quad (\text{VII.20})$$

located on the second Riemann sheet below the unitary cut. In the limit of small g_α , roots of Eq. (VII.20) are localized in the neighborhood of $s = M_{rIJ^P}^2$. $\Re s$ gives the resonance mass, $\Im s$ determines the decay width $\Gamma_\alpha = g_\alpha^2 \Im D(M_\alpha^2) / M_\alpha$.

At the CDD poles $\delta(s) = 0 \pmod{\pi}$, the phase shift crossed the level with a positive slope. Indeed, let s_γ be a CDD pole. Equations (VII.5) and (VII.6) imply $\Lambda^{-1}(s_\gamma) = 0$ and $\Lambda^{-1}(s_\gamma)' < 0$. Expanding the D function around $s = s_\gamma$ and using Eq. (VII.6), one finds

$$\delta(s_\gamma)' = -\Im D(s_\gamma) \Lambda^{-1}(s_\gamma)' > 0.$$

The same behavior is implied by the Breit-Wigner formula, according to which on isolated resonances phase shift increases by π . In the theory of potential scattering, growth of phase is associated with attraction.

Models such as the Dyson-Lee model [86, 87] apply directly to systems where the phase shifts increase with energy.

Nucleon-nucleon interaction, on the contrary, points toward the dominance of repulsion, that results in decrease of phase shifts with increasing energy. It may seem that the Dyson-Lee models are not applicable to the problem of nucleon-nucleon scattering. However, this is not true. A delicate generalization allows one to extend the CDD methodology of constructing analytical unitary amplitudes to systems with repulsion:

In the earlier studies it was always assumed that $\Im D(s)$ is strictly positive [85, 86]. Simonov [49] showed that the softening of this constraint to $\Im D(s) \geq 0$ is sufficient to ensure that systems with repulsive interactions got into the class of Dyson-Lee models.

The scattering of two nucleons through compound 6QS, dibaryons, can be described with a form factor $\mathcal{F}_L(s)$ that has simple zero(s) at $s = s_p > s_0 = 4m^2$ like in Eq. (VII.7). As a consequence, $\Im D(s) \sim (s - s_p)^2$ in the vicinity of s_p .

If $\Re D(s_p) \neq 0$, the phase touches at $s = s_p$ one of the levels $\delta(s) = 0 \pmod{\pi}$ without crossing.

However, if the real and imaginary parts of the equation (VII.20) vanish simultaneously at one point, the phase crosses one of the levels *with negative slope*. One can verify this by expanding the D function in the neighborhood of $s = s_p$. Given the equation (VII.6) and the conditions $\Im D(s_p)'' > 0$ and $\Re D(s_p)' > 0$, we obtain the following inequality

$$\delta(s_p)' = -\frac{\Im D(s_p)''}{2\Re D(s_p)'} < 0.$$

In the theory of potential scattering, negative slope of phase is associated with repulsion.

The compound MQS show up as poles of the P matrix. By their physical characteristics, poles of P matrix can be divided into two groups:

The first group is a group of bound states and resonances:

Provided that $D(s_0) > 0$ there is always one bound state. Other bound states are generated by the compound states with masses $M_\alpha < \sqrt{s_0}$.

A distinctive feature of resonance is the condition $\mathcal{F}_L(s) \neq 0$ in the neighborhood of $s = M_{rIJP}^2$ on the second sheet of the Riemann surface. Equation (VII.20) can then be used to find the simple poles of the scattering matrix.

The roots of Eq. (VII.20), which lie on the real half-axis $(-\infty, s_0)$ of the second sheet of the Riemann surface, define virtual states. Their position is determined by the masses of the compound states and interaction.

The poles of the second group are associated with the roots of Eq. (VII.20) *on the unitary cut* in the neighborhood of $s = M_{rIJP}^2$. Such poles do not lead to resonant behavior of the scattering cross sections, they do not generate poles in the S -matrix and are not resonances. Jaffe and Low have proposed to call such states "primitives" [50]. When resonance hits the unitary cut, its singular effect on the S matrix disappears. In contrast to the resonances, primitives drive phase shifts down and mimic repulsion.

Resonances and primitives do not exist as asymptotic states. In the diagram technique of Feynman, propagators of primitives are multiplied by form factors of the vertices. Such a combination has no poles at $s = M_{rIJP}^2$. Primitives, thus, do not propagate, although produce a direct impact on the dynamics.

In the general case, therefore, CDD poles correspond to bound states, resonances, and primitives. The last ones are P -matrix poles associated with the zeros of D functions on the unitary cut, which do not manifest themselves as poles of S matrix. The primitive-type CDD poles arise in systems with repulsion.

E. Nucleon-nucleon scattering in the vacuum

Techniques developed in Ref. [85] can be used to parameterize the nucleon-nucleon scattering amplitudes by functions with correct analytical properties within the QCB model.

1. 3S_1 channel

The most striking feature of the 3S_1 nucleon-nucleon phase shift is the vanishing of the phase shift at $T_{lab} = 354$ MeV. S -matrix according to Eq.(VII.6) is unit in two cases: $\Lambda(s) = \infty$ (a CDD pole) or $\Im \Pi(s) = 0$.

At the CDD poles $\delta(s) = 0 \pmod{\pi}$ with a positive slope, whereas the slope at $T_{lab} = 354$ MeV is negative. The CDD poles generate resonances for $\Im \Pi(s) < 0$.

Let us consider the primitive-type CDD poles. The imaginary part of $\Pi(s)$ is related to dibaryon decay width, so it must be nonpositive. According to Eq.(VII.10),

$$\Im \kappa \Pi(s) = -z j_L(z)^2 \leq 0. \tag{VII.21}$$

$\Im \kappa \Pi(s)$ has second order zeros, connected to the simple zeros of $j_L(z)$. If $\Lambda(s) - \Re \Pi(s)$ is finite, then $\delta(s) = 0 \pmod{\pi}$ but the phase does not cross the horizontal axes $0, \pm\pi, \dots$. If, however, $\Lambda(s) - \Re \Pi(s) = 0$ and s is a simple zero, the phase crosses the horizontal axes $\delta(s) = 0 \pmod{\pi}$ *with a negative slope*.

A negative slope of the phase is associated with the repulsion. If we want to describe the repulsion, we have to fulfill Eq. (VII.20) both for real and imaginary parts at real $s = s_p > s_0 = 4m^2$. The condition $\Im\Pi(s) \leq 0$ gives third equation

$$\Im\Pi(s_p)' = 0,$$

which is, however, fulfilled automatically.

$T_{lab} = 354$ MeV corresponds to $k = 408$ MeV. Equation $\Im D(s) = 0$ simplifies to $kb = \pi$. We thus fix $b = 1.52$ fm. This value is close to $b = 1.41 - 1.44$ fm obtained in Ref. [49]. The zero of the phase alone thus determines $\Pi(s)$.

In the S -wave,

$$\kappa\Pi(s + i0) = -\frac{\sin z}{z}e^{iz},$$

and we observe that $\Re\Pi(s) = 0$ for $s = s_p$. Eq. (VII.20) simplifies therefore to $\Lambda(s) = 0$. The inverse Λ function has a pole at $s = s_p$. Equation $\Lambda(s) = 0$ allows to find the dibaryon mass $M = 2\sqrt{k^2 + m^2} = 2047$ MeV. This value is close to the dibaryon mass $M = 2071 - 2081$ MeV found in Ref. [49]. It is related to the primitive-type CDD pole at $M = 3203$ MeV as shown below.

We set

$$\gamma = -\Re\kappa\Pi(s = s_d) > 0,$$

where $s_d = M_d^2$ is the deuteron pole. In the case of one dibaryon, one can write

$$\kappa^{-1}\Lambda^{-1} = c_p\left(\frac{r_p}{s - s_p} - \frac{r_p}{s_d - s_p}\right) - \frac{1}{\gamma}, \quad (\text{VII.22})$$

where c_p is a free positive definite parameter such that $\kappa c_p r_p = g^2$.

The constant term entering Λ^{-1} describes the four-fermion contact interaction between the nucleons.

The parameterization (VII.22) ensures the existence of zero of D function and of a pole of S matrix at $s = s_d$, respectively.

To eliminate unphysical zeros of the D function, one has to constrain c_p . We write the D function in form of the dispersion integral

$$D(s) = \Lambda(s) - \frac{1}{\pi} \int_{4m^2}^{+\infty} \frac{\Im\Pi(s')}{s' - s - i0} ds'.$$

The imaginary part of D can be represented as follows

$$\Im D(s) = \Im s \left(\frac{\Lambda^2(s)}{|s - s_p|^2} \kappa c_p r_p - \frac{1}{\pi} \int_{s_0}^{+\infty} \frac{\Im\Pi(s')}{|s' - s|^2} ds' \right).$$

Since $\Im\Pi(s') \leq 0$, the bracket is positive for $c_p > 0$, in which case $D(s)$ has no complex roots in the complex s -plane modulo the half-axis $(-\infty, s_0)$.

It remains to check the half-axis $(-\infty, s_0)$. The derivative

$$D(s)' = \frac{\Lambda^2(s)}{(s - s_p)^2} \kappa c_p r_p - \frac{1}{\pi} \int_{s_0}^{+\infty} \frac{\Im\Pi(s')}{(s' - s)^2} ds'$$

is positive below the threshold. $D(s)$ crosses the real axis at $s = s_d < s_0$. This is the unique root of the D function provided $\Lambda(s)$ has no poles at $s < s_0$. Let us investigate therefore roots of $\Lambda^{-1}(s)$. Since $\kappa^{-1}\Lambda^{-1}(s_d) = -1/\gamma < 0$, $\Lambda^{-1}(s)' < 0$ and $\Lambda^{-1}(s)$ has no poles at $s < s_p$ by the construction, the condition $\Lambda^{-1}(-\infty) < 0$ is sufficient to exclude unphysical roots below the threshold. The parameter c_p should finally be subjected to the constraint

$$0 < c_p < c_p^{\max} = \frac{s_p - s_d}{\gamma r_p}. \quad (\text{VII.23})$$

In Fig. 9 (a) we show the 3S_1 phase shift versus kinetic energy of the proton in the laboratory system for $c_p = 0.9c_p^{\max}$. In Fig. 9 (c) $\Re D(s)$ and $\Im D(s)$ as functions of T are shown. We recall that for pn system $s = s_0 + 2m_n T_{lab}$ where m_n is the neutron masses. $\Re D(s)$ has one zero below the two-nucleon threshold, which corresponds to the deuteron.

If the number of dibaryons is greater than one, the constraint VII.23 reads

$$\sum_p c_p \frac{r_p}{s_p - s_d} < \frac{1}{\gamma},$$

where c_p are positive.

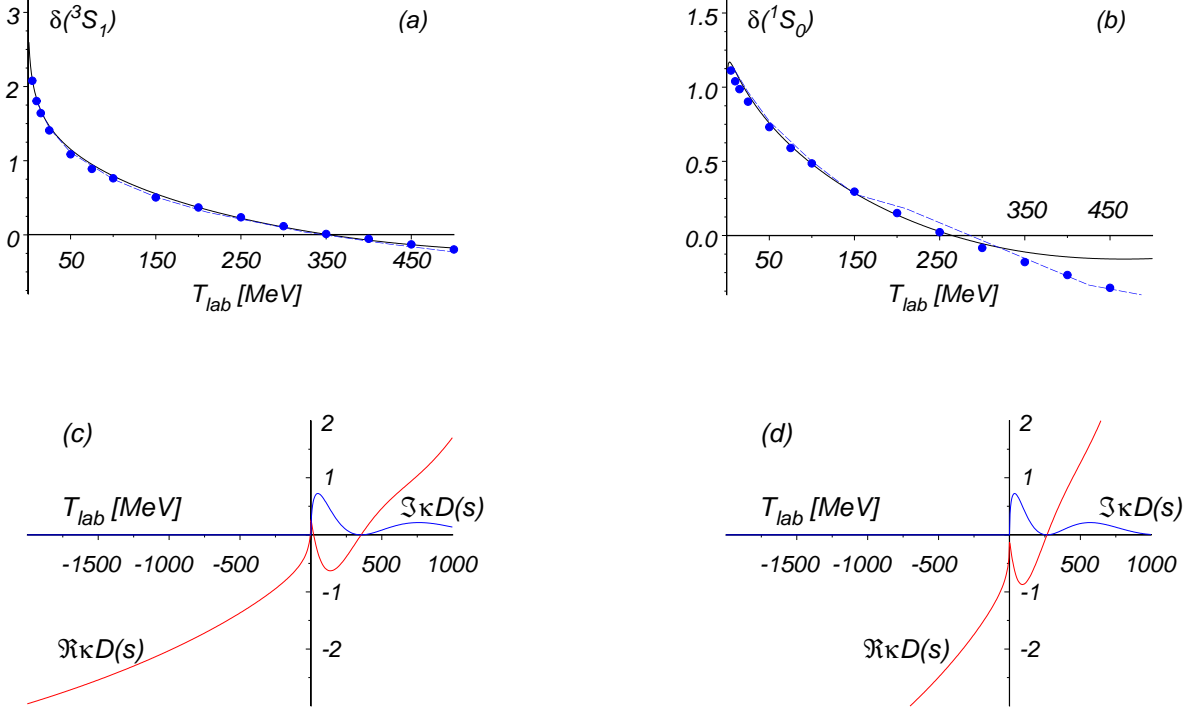


FIG. 9: (color online) 3S_1 and 1S_0 scattering phase shifts in radians (upper panel) and real and imaginary parts of the D functions (lower panel) versus the proton kinetic energy. The long-dashed curves are parameterizations of the QCB model from Ref. [49], the solid curves are parameterizations of the relativistic QCB model. The experimental phase shifts [93] are shown by the circles.

2. 1S_0 channel

The scattering phase vanishes at $T_{lab} = 265$ MeV. Arguments similar to the ones used for the 3S_1 channel lead us to the estimates $b = 1.76$ fm and $M = 2006$ MeV. The numbers are close to those obtained in Ref. [49] $b = 1.44$ fm and $M = 2112$ MeV. The CDD pole is localized at $M = 2916$ MeV.

The inverse Λ function has the form of Eq.(VII.22) with s_d replaced by $s_0 = 4m^2$, where m is the average mass of proton and neutron. Near two-nucleon threshold, $\kappa D(s) = -\gamma + 1 + ikb + \dots$. From other hand, $D(s) \sim 1 - i\delta(k) + \dots = 1 - ika + \dots$, where $a = 23.56$ fm is the scattering length. One has to require

$$\gamma = -\kappa\Pi(s_0) + \frac{b}{a}, \quad (\text{VII.24})$$

with $\Pi(s_0) = -1$.

D function of the 1S_0 channel has no roots for the complex values of s and its derivative is positive on the real half-axis below two-nucleon threshold. In order to avoid the unphysical poles of S matrix, it is sufficient to require

$$\kappa D(-\infty) = \frac{1}{-\frac{c_p r_p}{s_0 - s_p} - \frac{1}{\gamma}} < \kappa D(s_0) = 1 - \gamma < 0.$$

Since $\gamma > 1$, the second inequality is fulfilled. The first one gives

$$c_p < \min\left(c_p^{\max}, \frac{c_p^{\max}}{\gamma - 1}\right), \quad (\text{VII.25})$$

where $c_p^{\max} = (s_p - s_0)/(\gamma r_p)$. Since $b \ll a$, it reduces to $c_p < c_p^{\max}$.

In Fig. 9 (b) we show our fit of the 1S_0 phase shift versus the proton kinetic energy with $c_p = 0.9c_p^{\max}$. In Fig. 9 (d), real and imaginary parts of the D function are shown on the real T_{lab} -axis. $\Re D(s)$ has no zeros below the threshold. $\Im D(s)$ is positive definite above two-nucleon threshold. At $s = s_p$ both the real and imaginary parts of the D function vanish.

3. 3P_1 and 1P_1 channels

The 3P_1 and 1P_1 phase shifts do not cross the real axis. So, we have to use other methods to estimate the parameter b and the dibaryon mass.

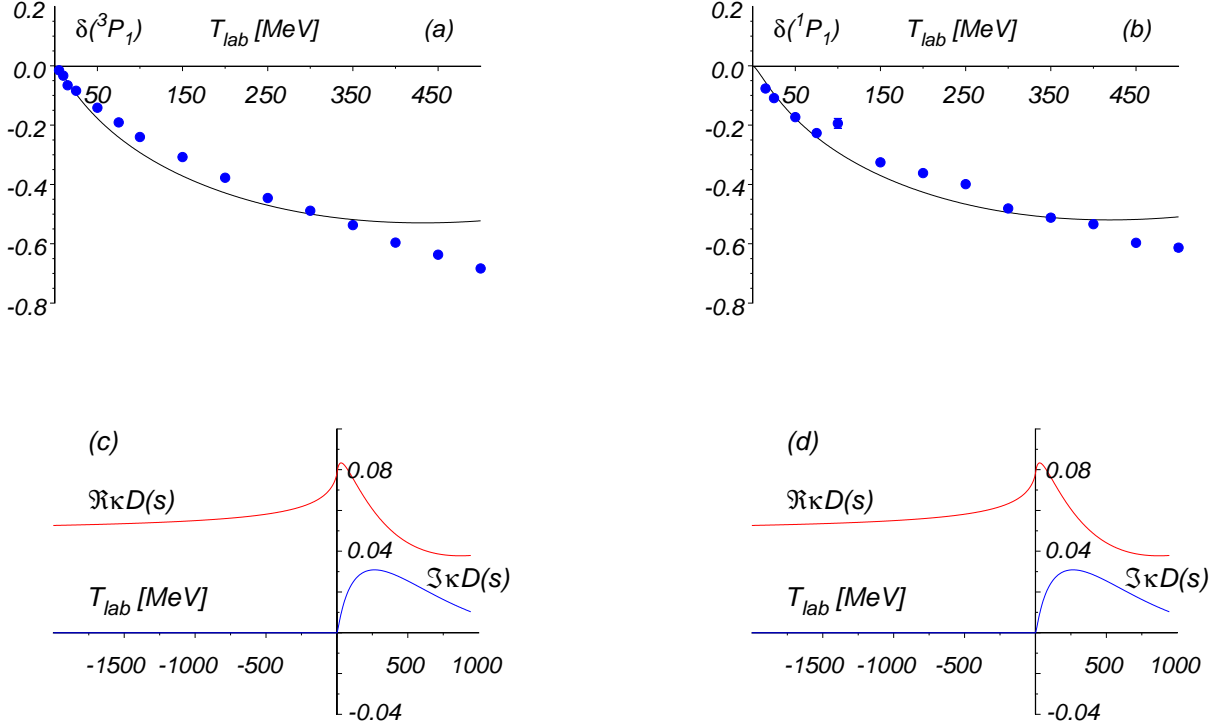


FIG. 10: (color online) 3P_1 and 1P_1 scattering phase shifts in radians (upper panel) and real and imaginary parts of the D functions (lower panel) versus the proton kinetic energy. The solid curves are parameterizations within the relativistic QCB model. The experimental phase shifts [93] are shown by circles.

The inverse Λ function can be taken in the form of Eq.(VII.22) with s_d replaced by $s_0 = 4m^2$. At the threshold, $\kappa D(s) = -\gamma - \kappa\Pi(s_0) + \frac{i}{9}k^3b^3 + \dots$. From other hand, $D(s) \sim 1 - i\delta(k) + \dots = 1 - ik^3a + \dots$, where $a = -1.5 \times 10^{-7}$ MeV $^{-3}$ for the 3P_1 channel and $a = -3 \times 10^{-7}$ MeV $^{-3}$ for the 1P_1 channel. To provide correct threshold behavior one has to require

$$\gamma = -\kappa\Pi(s_0) + \frac{b^3}{9a}. \quad (\text{VII.26})$$

Since a is negative, $\kappa D(s_0) = -\kappa\Pi(s_0) - \gamma > 0$. In order to remove unphysical poles, it is sufficient to require

$$0 < \kappa D(-\infty) = \frac{1}{\frac{c_p r_p}{s_p - s_0} - \frac{1}{\gamma}} < \kappa D(s_0) = -\kappa\Pi(s_0) - \gamma.$$

In the case of $\gamma < 0$, this equation provides no constraints on c_p . In the case $0 < \gamma < -\kappa\Pi(s_0)$, $\kappa^{-1}\Lambda^{-1}(s_0) = -\frac{1}{\gamma} < 0$, $\kappa^{-1}\Lambda^{-1}(-\infty) = \frac{c_p r_p}{s_p - s_0} - \frac{1}{\gamma} > 0$, and $\Lambda^{-1}(s)' < 0$. There is therefore a pole in the D function, and zero of the D function on the real half-axis $(-\infty, s_0)$. The case of $0 < \gamma < -\kappa\Pi(s_0)$ is thus not useful.

Let us assume $\gamma = 0$. The value of b for the 3P_1 channel can be found to be $b = 1.51$ fm. The dibaryon of mass $M = 2214$ MeV that makes $\Lambda(s_p)$ to vanish ensures the crossing of the level $\delta(s) = -\pi$ at $T_{lab} = 732$ MeV. In such a case, the repulsion is largely overestimated. The linear interpolation of the experimental data e.g. gives $\delta(s_p) \sim -1$. If $M \neq 2214$ MeV, the phase remains negative and touches one of the levels $\delta(s) = 0 \pmod{\pi}$ at $s = s_p$. A better description is possible for lower value of b and greater value of M , respectively. However, lower values of b require positive γ which is not acceptable.

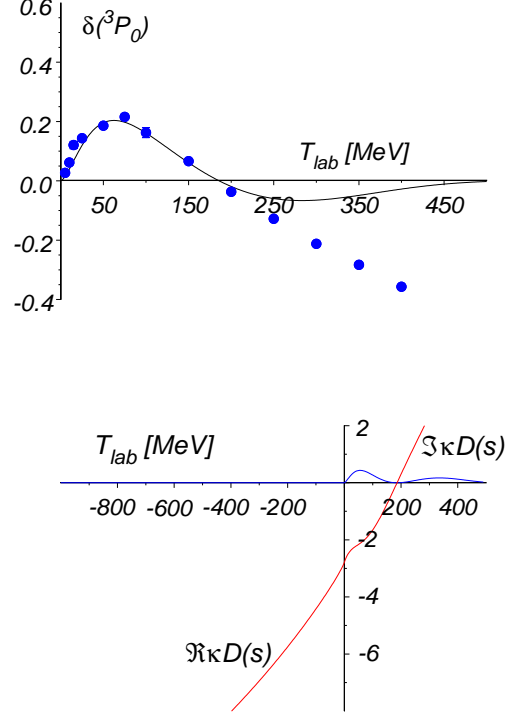


FIG. 11: (color online) 3P_0 scattering phase shifts in radians (upper panel) and real and imaginary parts of the D functions (lower panel) versus the proton kinetic energy. The solid curves are parameterizations within the relativistic QCB model. The experimental phase shifts [93] are shown by circles.

We thus consider more general expression for the imaginary part of $\Pi(s)$:

$$\kappa \Im \Pi(s) = -z j_l(z)^2 \frac{\varkappa^2}{\varkappa^2 + z^2}, \quad (\text{VII.27})$$

where \varkappa is a parameter. $\Pi(s)$ is restored from the dispersion integral. The explicit analytical expression for $\Pi(s)$ can be found e.g. with the help of MAPLE. For $\varkappa = \infty$, we recover previous formulas. A finite \varkappa leads to reduced values of $\Pi(s_0)$ in the absolute value and the parameter b , respectively, keeping γ negative. For $L = 1$,

$$\kappa \Pi(s_0) = \frac{1}{6\varkappa^3} (-3 + 3\varkappa^2 - 2\varkappa^3 + 3(1 + \varkappa)^2 e^{-2\varkappa}).$$

One can notice that $0 \leq -\kappa \Pi(s_0) \leq 1/3$.

The same arguments as before lead us to the conclusion of absence of unphysical poles of the S -matrix in the complex s -plane for negative γ .

A reasonable fit in the 3P_1 channel can be obtained without the CDD poles and primitives. $c_p = 0$ implies that the only important interaction is the contact four-fermion interaction described by γ . We use $\gamma = -1/20$, $b = 0.93$ fm and $\varkappa^2 = 1/3$ which corresponds to $\kappa \Pi(s_0) = -0.028$.

In Fig. 10 (a) we show phase shift of the 3P_1 channel. Shown in Fig. 10 (c) are real and imaginary parts of the D function.

The phase shift in the 1P_1 channel behaves similar to the phase shift in the 3P_1 channel. We use therefore precisely the same set of the parameters. The scattering length appears to be a factor of two lower than the experimental one, however, the overall description of the data is better than with the increased scattering length. In Fig. 10 (b) the phase shift in the 1P_1 channel is shown. In Fig. 10 (d) the real and imaginary parts of the D function are shown.

4. 3P_0 channel

The parameterization of the phase shift in the 3P_0 channel is similar to that in the 1S_0 channel. Here, we do not modify $\Im\Pi(s)$ and set $\varkappa = \infty$. The values of $b = 3$ fm and the dibaryon mass $M = 1969$ MeV are found from the position $T_{lab} = 186$ MeV of zero of the phase shift. The primitive-type CDD pole appears at $M = 2650$ MeV. The parameter (cf. Eq. (VII.26))

$$\gamma = \frac{1}{3} + \frac{b^3}{9a} \quad (\text{VII.28})$$

can be fixed by the scattering length $a = 2.8 \times 10^{-7} \text{ MeV}^{-3}$. We consider, however, the scattering length as a fitting parameter. The general agreement with the data is better when slope of the phase shift at $T_{lab} = 0$ is two times lower than the experimental one. Fig. 11 (a) shows the phase shift as compared to the experimental data as functions of the proton kinetic energy. Shown in Fig. 11 (b) are the real and imaginary parts of the D function.

F. Discussion

In Sects. V-VII we constructed and analyzed the effective Lagrangian to describe the two-nucleon forces based on their s -channel dibaryon exchange mechanism. Dibaryons in our approach are the primitives, and not resonances. They manifest themselves as poles of P matrix or, equivalently, as zeros of D functions on the unitary cut. Resonances with the energy-dependent width have similar properties, when the width vanishes at the resonance mass, while far from the mass of the resonance the width is finite. The effective Lagrangian was formulated for the nucleons, which are well-defined asymptotic states, and for the primitives, which are decoupled of the two-nucleon channel on the mass shell, and, apparently, are not asymptotic states. Note that although the resonances are not asymptotic states, they are often included in effective Lagrangians. Despite the unusual properties of the primitives, there is no intrinsic difficulty in applying the diagram technique for calculation of various processes involving primitives, based on their effective Lagrangian.

In Sect. V we gave a complete list of relativistic two-nucleon currents with the angular momentum $J = 0, 1$, through which the primitives are coupled to two nucleons in the low- J partial waves. We found five primitives with the lowest quantum numbers $(I, J^P) = (0, 1^\pm), (1, 0^\pm),$ and $(1, 1^-)$ and discussed their effect on the nucleon-nucleon interaction in Sect. VII. In the various versions of the QCB model, the S -wave nucleon-nucleon phase shifts are fitted by the primitives excellently and we confirm it again. We considered the P -wave scattering also. We found good qualitative agreement with the experiment. The description of the channels 3P_1 and 1P_1 requires the contact four-fermion interaction only, without primitives, whereas the channel 3P_0 gives an evidence for the primitive. We suppose more accurate parameterization of the experimental phases can be achieved by means of the s -channel dibaryon exchange only without invoking the t -channel meson-exchange mechanism.

P -matrix analysis has been successful in describing the various processes, including nucleon-nucleon interaction. This formalism is built into the effective Lagrangian with an appropriate choice of nucleon-nucleon-dibaryon form factors and four-fermion vertices.

In the limit of low density we reproduce results of optical potential model. Lorentz structure of the nucleon self-energy operator is different from the OBE RMF models. In our approach, vector and scalar parts of the self-energy operator are of the same order of magnitude.

Solutions of the self-consistent system of equations for the nucleon and dibaryon propagators and G -matrix in nuclear matter will be presented elsewhere [94].

VIII. MODELS OF NUCLEAR MATTER

The nuclei are known to be stable under normal conditions on Earth, while the collection of nuclei forms the ground state in QCD at finite baryon charge.

The range of densities and temperatures $\rho \sim 10^{39} \text{ cm}^{-3}$ and $T \sim 10^{12} \text{ K}$, where the phase transition in nuclear matter takes place with chiral symmetry restoration and deconfinement, can be studied experimentally in heavy-ion collisions. Supercold nuclear matter exists in the interiors of massive neutron stars.

Quark matter appears in compression of nuclear matter. New forms of nuclear matter can exist at intermediate densities, such as hyperon matter, crystalline neutron matter, pion and kaon condensation and a Bose condensation of dibaryons.

In the field of atomic physics, modifications of the properties of ordinary atoms at density $\rho \sim 10^{10} - 10^{18} \text{ cm}^{-3}$ and temperature $T \sim 10^4 \text{ K}$ are studied since the mid-1930's (for a review see [96, 97]).

To ensure the stability of nuclear matter under conditions $T \lesssim 10 \div 20 \text{ MeV}$ and $\rho \sim 0.16 \div 0.30 \text{ fm}^{-3}$, the NN forces must satisfy necessary and sufficient saturation conditions (see, e.g., the review of F. Caloggero and Yu. A. Simonov [98]). For local and velocity-independent potentials these conditions require a strong repulsive core at small distances, $r \lesssim 0.4 \text{ fm}$.

The quark-hadron phase transition in nuclear matter has been discussed first by Zel'dovich [99]. By comparing pressures of the ideal Fermi gases of nucleons and quarks, he arrived at a conclusion that the composite structure of the nucleons requires a short-range repulsion between the nucleons. His discussion was based on the Le-Shatelie - Brown principle. Earlier he showed that the stiffest, consistent with causality nuclear matter EoS corresponds to exchange by a massive vector particle between the nucleons [100]. The ω -meson exchange mechanism is the most typical and challenging feature of the modern OBE models.

As discussed above, at short distances NN force becomes nonlocal – in OBE picture due to finite size of nucleons and mesons – and in the QCB picture due to formation of MQS. It is remarkable that nonlocal NN interaction, even when everywhere attractive, easily passes the requirements of saturation, while in the local OBE case one needs a very large coupling of ω -meson, producing repulsive core.

The realistic OBE models of nuclear matter split into three groups:

Relativistic mean field (RMF) models are based on the mean-field approximation to account for the meson-exchange interactions between nucleons, σ - and ω -mesons ensure the saturation property. The mean field models are the phenomenological ones.

Dirac-Brueckner-Hartree-Fock (DBHF) approach is a field-theoretic scheme, which is based on accurate experimental data of nucleon-nucleon interaction. Nuclear many-body problem is solved microscopically by the summation of wide subclass of Feynman diagrams. The scheme claims to be parameter-free description of the nuclear matter EoS.

The variational approach is proposed in [26]. This uses the potentials of the nucleon-nucleon interaction, whose characteristics are extracted from the nucleon-nucleon scattering and descriptions of light nuclei. Ground-state wave function of infinite nuclear matter is constructed with the use of the variational principle. Nuclear EoS is claimed to be parameter-free as well.

The DBHF models and the variational approach are successful in the description of nuclear matter at saturation starting essentially from the first principles, however, with an additional tuning, e.g., of $3N$ forces in the variational approach.

In addition to the above three methods, the non-relativistic BHF calculations [101], phenomenological theories with density dependent interactions such as Gogny or Skyrme forces [102] and various modifications of the RMF scheme are widely used for modeling nuclear matter also.

A critical test of nuclear models is possible on the basis of astrophysical observations on the properties of massive neutron stars.

The most massive pulsars reported in the literature are PSR B1516+02B with the mass of $1.96_{-0.12}^{+0.09} M_{\odot}$ and PSR J1748-2021B with the mass of $2.74 \pm 0.22 M_{\odot}$ [103]. The mass of rapidly rotating neutron star in the low mass X-ray binary 4U 1636-536 is found to be $M = 2.0 \pm 0.1 M_{\odot}$ [14]. The mass of the X-ray source EXO 0748-676 is limited to $M \geq 2.10 \pm 0.28 M_{\odot}$. These observations indicate clearly that the β -equilibrated nuclear matter EoS is stiff and, furthermore, eliminate the soft EoS constructed, e.g., on the basis of the classical Reid soft core model [26].

The new degrees of freedom lower the energy of matter and make EoS softer. Scenarios with phase transitions shift the masses to the region of even smaller values. Existence of quark matter and other forms of exotic matter in the cores of neutron stars was questioned [15] (see, however, [33]).

The so-called realistic models of neutron stars usually ignore hyperon channels, for example, the reactions $\Sigma^{-} \rightarrow n + e + \bar{\nu}_e$. In the RMF models [27, 28, 104], which take hypernuclear data into account, the inclusion of the β -equilibrium balance for hyperons reduces the limiting mass of neutron stars by $0.5 \div 0.8 M_{\odot}$. These results are in agreement with recent calculations [29–31]. The β -equilibrium brings thus difficulties to reproduce the observed high masses of neutron stars.

The problem can be solved by assuming the existence of light weakly interacting bosons, the possibility of the existence of which is discussed in some generalizations of the Standard model [32]. A more conventional and perhaps more realistic approach is to modify the baryon-baryon interaction at short distances, taking the quark-gluon degrees

of freedom into account. It is based on the formalism of the P matrix and QCB model discussed in the previous sections.

A. Relativistic mean field models

Development of many-body theory in nuclear physics was motivated by the problem of describing heavy nuclei and, since 1970's, neutron stars. The change in mass of the nucleon in nuclear matter has been introduced in the pioneering work of Walecka [24]. Mean-field (MF) and relativistic mean field (RMF) approximations were proposed to describe the dense nuclear matter self-consistently to all orders in density, but in tree level of perturbation theory. MF and RMF were very successful in describing the basic properties of finite nuclei and nuclear matter near saturation density. RMF models are currently the most popular models of nuclear matter, although they do not provide a strict connection with the phenomenology of nucleon-nucleon scattering.

Since mid-1970's, RMF models have been improved in many directions: by including nonlinear self-interactions of σ -, ρ -, and δ -mesons, introduction of the density-dependent coupling constants and vertices with higher derivatives, in order to describe the energy, radius, surface thickness of nuclei, neutron skins, spin-orbit interaction of nucleons, as well as restrictions on flows obtained in heavy-ion collisions, and fulfill constraints imposed by astrophysical observations of neutron stars.

In RMF models a significant decrease of the effective mass of the nucleon was found at a density of saturation. This effect was predicted purely phenomenologically. The development of QCD confirms the prediction and the effect has attracted much attention, since the decrease of the nucleon mass is connected to the partial restoration of chiral symmetry.

In the simplest version, the effective Lagrangian contains the nucleon fields and σ - and ω -mesons:

$$\begin{aligned} \mathcal{L} = & \bar{\Psi}(i\hat{\nabla} - m_N - g_\sigma\sigma - g_\omega\hat{\omega})\Psi \\ & + \frac{1}{2}(\nabla_\mu\sigma\nabla_\mu\sigma - m_\sigma^2\sigma^2) \\ & - \frac{1}{4}\mathcal{F}_{\mu\nu}\mathcal{F}_{\mu\nu} + \frac{1}{2}m_\omega^2\omega_\mu\omega_\mu, \end{aligned} \quad (\text{VIII.1})$$

where $\mathcal{F}_{\mu\nu} = \nabla_\nu\omega_\mu - \nabla_\mu\omega_\nu$, $\hat{\nabla} = \gamma_\mu\nabla_\mu$, etc.

Property of saturation is easily seen from the following argument: Suppose that low-density attraction of the scalar field dominates the ω exchange. With increasing density, the scalar charge of the nucleons, generating a scalar field, is suppressed by the Lorentz factor (The scalar charge of a particle placed in a box disappears in the ultrarelativistic limit. The vector charge, of course, remains constant.) In infinite-density limit, σ -meson decouples from the system of nucleons, but vector fields survive. As a result, the attraction at low densities is replaced by the ω -induced repulsion at high densities. In some intermediate-density regime, repulsion balances the attraction, this density is the density of saturation where the substance is in equilibrium. The coupling constants g_σ , g_ω , and the σ -meson mass are determined from fitting the properties of nuclear matter at saturation density.

RMF models offer low binding energy of nuclear matter at saturation due to cancellation between the strong repulsive vector and strong attractive scalar potentials. These two potentials are equal in magnitude to about a quarter of the nucleon rest mass. The scalar part reduces the nucleon mass and increases the influence of small components of the Dirac bispinors.

RMF models allow the most precise description of the nuclear properties with 5 - 15 parameters.

B. Dirac-Brueckner-Hartree-Fock approximation

DBHF approximation scheme is based on realistic meson-exchange models. As compared with the RMF model, it takes additional requirements of fermionic statistics and in-medium modification of two-body T -matrix into account. DBHF successfully reproduces the properties of nuclear matter at saturation mainly from first principles, using the interaction, based on data from nucleon-nucleon scattering.

Shown in Fig. 12 is the Bethe-Salpeter equation for the in-medium two-body scattering T -matrix (called reaction G -matrix). The difference from the vacuum equations is associated with the change of nucleon propagators in the loop and Pauli blocking, which restricts the admissible regions in the phase space of nucleons.

The nucleon self-energy can be found by solving equation shown in Fig. 13.

Equations in Figs. 12 and 13 constitute selfconsistent system of equations of the DBHF approximation.



FIG. 12: System of equations for in-medium T -matrix. V is meson-exchange potential. The bold lines in the loop are in-medium nucleon propagators.

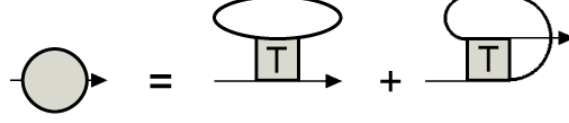


FIG. 13: System of equations for in-medium nucleon self-energy operator. The bold lines in the loops are in-medium nucleon propagators. T is in-medium T -matrix of Fig. 12.

Examples of the DBHF calculations can be found in Refs. [105–108]. DBHF scheme is phenomenological only marginally: The ladder approximation is used to solve the relativistic Bethe-Salpeter equation, negative-energy nucleons are neglected, nucleon resonances are neglected also.

C. Variational approach

Estimates of G -matrix with realistic potentials show that G -matrix has a sharp peak with respect to the difference of distances between the nucleons in the initial and final states. This means that in the process of scattering the distance between nucleons is not much changed, and for the variational calculations the dependence of the trial wave function on the relative momentum of the nucleon pairs can be neglected. The trial wave function has the form

$$\Psi = \prod_{i < j} \sum_{\ell} f^{\ell}(r_{ij}) \mathcal{P}^{\ell} \mathcal{A} \prod_k \phi_k(r_k), \quad (\text{VIII.2})$$

where \mathcal{P}^{ℓ} is projection operator to state of the pair ij with the orbital momentum ℓ , \mathcal{A} is the antisymmetrization operator, $\phi(r_k)$ are uncorrelated wave functions of the nucleons. The correlation function $f^{\ell}(r)$ is equal to one when the distance between the nucleons increases, but less than unity, when r is reduced.

The Jastrow wave function (VIII.2) is used for the calculation of the ground state energy from the cluster expansion

$$\begin{aligned} E &= \frac{\langle \Psi | H | \Psi \rangle}{\langle \Psi | \Psi \rangle} \\ &= \sum_i C_i + \frac{1}{2} \sum_{ij} C_{ij} + \dots, \end{aligned} \quad (\text{VIII.3})$$

where

$$\begin{aligned} C_k &= \langle \phi_k | \frac{p_k^2}{2m} | \phi_k \rangle, \\ C_{ij} &= \frac{\langle \phi_{ij} | H_2 | \phi_{ij} \rangle}{\langle \phi_{ij} | \phi_{ij} \rangle} - C_i - C_j, \end{aligned} \quad (\text{VIII.4})$$

etc. Here, H_2 is two-body Hamiltonian, ϕ_{ij} is two-body wave function.

The smallness of the correlation effect in the two-body nucleon wave function,

$$\rho_0 \sum_{\ell} \int d\mathbf{r} (1 - f^{\ell}(r))^2 \sim 0.1, \quad (\text{VIII.5})$$

at the saturation density $\rho_0 = 0.16 \text{ fm}^{-3}$ makes it possible to truncate the cluster expansion.

Recent examples of the variational calculations can be found in Refs. [109, 110].

D. In-medium modifications of hadrons

In-medium modification of the properties of hadrons affects the nuclear matter EoS. In the RMF models, vector mesons play a special role. The interaction mediated by vector mesons at high densities leads asymptotically to the stiffest EoS of nuclear matter. The effect of the vector meson on the energy density of nuclear matter can be estimated by averaging the Yukawa potential [100]

$$\varepsilon_I = \frac{1}{2V} \int d\mathbf{x}_1 d\mathbf{x}_2 \rho(\mathbf{x}_1) \frac{g^2}{4\pi} \frac{e^{-\mu r}}{r} \rho(\mathbf{x}_2), \quad (\text{VIII.6})$$

where $\rho(\mathbf{x}_1) = \rho(\mathbf{x}_2) \equiv \rho$ is baryon number density, $r = |\mathbf{x}_2 - \mathbf{x}_1|$, g is coupling constant, μ is vector meson mass, and V is normalization volume. A simple integration gives

$$\varepsilon_I = \frac{g^2 \rho^2}{2\mu^2}. \quad (\text{VIII.7})$$

The RMF models are used to study the modifications of the properties of vector mesons in nuclear medium [25, 111–113]. Assuming that the mass of mesons depends on the density, the contribution of the ω -meson to pressure can be found to be

$$P_I = \frac{g^2 \rho^2}{2\mu^2} \left(1 - \frac{2\rho}{\mu} \frac{\partial \mu}{\partial \rho} \right). \quad (\text{VIII.8})$$

This equation shows that the pressure decreases if the meson mass increases with density. The problem of modifying the mass of vector mesons in nuclear matter was studied in experiments on the dilepton production in heavy-ion collisions. Simulations of the dilepton production using transport models and the subsequent comparison with experiment gives a clear indication of the presence of collisional width, however, a noticeable shift of the masses of ρ - and ω -mesons is not registered [114].

IX. NUCLEAR MATTER WITH MULTIQUARK BARYONS. NONRELATIVISTIC TREATMENT

For two-nucleon contribution to the nuclear matter one starts with the Bethe-Brueckner series which is summed up by the operator equation [115]

$$G_2(W) = V_2 - V_2 Q_2 e_2^{-1} G_2(W) \quad (\text{IX.1})$$

where $G_2(W)$ is the reaction matrix of two nucleons in nuclear matter V_2 is the two-body interaction operator (potential), Q_2 is the projection operator on states outside of the Fermi sphere, and finally e_2 is energy denominator

$$e_2 |\mathbf{p}\mathbf{n}\rangle = (E_p + E_n - W) |\mathbf{p}\mathbf{n}\rangle. \quad (\text{IX.2})$$

Eq. (IX.1) is an equivalent of two-body t -matrix (Lippmann-Schwinger) equation for the case when two nucleons are inside nuclear matter.

One can also write equations for the pair wave functions. For the plane wave $\Phi_{\mathbf{p}\mathbf{n}}$ and actual w.f. $\Psi_{\mathbf{p}\mathbf{n}}$ one has

$$\Psi_{\mathbf{p}\mathbf{n}} = \Phi_{\mathbf{p}\mathbf{n}} - Q_2 e_2^{-1} G_2 \Phi_{\mathbf{p}\mathbf{n}} \quad (\text{IX.3})$$

Separating out the c.m. motion, $\Psi_{\mathbf{p}\mathbf{n}} = \frac{e^{i\mathbf{K}\mathbf{R}}}{V} \psi_{\mathbf{p}\mathbf{n}}$, and keeping only relative coordinates in $\psi_{\mathbf{p}\mathbf{n}}$, $\varphi_{\mathbf{p}\mathbf{n}} \equiv \exp(i\mathbf{k}\mathbf{r})$, one has the Bethe-Goldstone equation (for nonlocal in general interaction)

$$\psi_{\mathbf{p}\mathbf{n}}(\mathbf{r}) = e^{i\mathbf{k}\mathbf{r}} - \int F_2(\mathbf{r}, \mathbf{r}') V_2(\mathbf{r}', \mathbf{r}''; E) \psi_{\mathbf{p}\mathbf{n}}(\mathbf{r}'') d\mathbf{r}' d\mathbf{r}'' \quad (\text{IX.4})$$

where

$$F_2(\mathbf{r}, \mathbf{r}') \equiv \int \frac{d\mathbf{k}}{(2\pi)^3} Q_2(\mathbf{k}, \mathbf{K}) [e_2(\mathbf{k}, \mathbf{K})]^{-1} \exp[i\mathbf{k}(\mathbf{r} - \mathbf{r}')], \quad (\text{IX.5})$$

$$Q_2(\mathbf{k}, \mathbf{K}) |\mathbf{p}, \mathbf{n}\rangle = \begin{cases} |\mathbf{p}, \mathbf{n}\rangle, & \text{for } |\frac{1}{2}\mathbf{K} \pm \mathbf{k}| > k_F, \\ 0, & \text{otherwise,} \end{cases} \quad (\text{IX.6})$$

$$e_2 |\mathbf{p}\mathbf{n}\rangle = [E(\frac{\mathbf{K}}{2} + \mathbf{k}) + E(\frac{\mathbf{K}}{2} - \mathbf{k}) - W] |\mathbf{p}, \mathbf{n}\rangle \equiv e_2(\mathbf{k}, \mathbf{K}) |\mathbf{p}, \mathbf{n}\rangle, \quad (\text{IX.7})$$

and

$$\mathbf{K} = \mathbf{p} + \mathbf{n}, \quad \mathbf{k} = \frac{1}{2}(\mathbf{p} - \mathbf{n}). \quad (\text{IX.8})$$

From $\psi_{\mathbf{pn}}$ one easily finds the matrix G ,

$$\langle \mathbf{l}, \mathbf{m} | G_2 | \mathbf{k}, \mathbf{n} \rangle = \frac{1}{V} \delta_{\mathbf{K}\mathbf{K}'} \langle \mathbf{k}' | G_2 | \mathbf{k} \rangle \quad (\text{IX.9})$$

$$\langle \mathbf{k}' | G_2 | \mathbf{k} \rangle = \int e^{-i\mathbf{k}'\mathbf{r}} V_2(\mathbf{r}, \mathbf{r}') \psi_{\mathbf{pn}}(\mathbf{r}') d\mathbf{r} d\mathbf{r}'. \quad (\text{IX.10})$$

Inserting the separable interaction $V_2(\mathbf{r}, \mathbf{r}') = v_{hgh} = \sum_{\nu} \frac{f_{\nu}(\mathbf{r})f_{\nu}(\mathbf{r}')}{E-E_{\nu}}$, one obtains from (IX.4) the following system of algebraic equations

$$(f_{\nu}\psi) = f_{\nu}(\mathbf{k}) - \sum_{\nu'} \lambda_{\nu\nu'} (f_{\nu'}\psi) \quad (\text{IX.11})$$

where we have used notations

$$(f_{\nu}\psi) = \int d\mathbf{r} f_{\nu}(\mathbf{r}) \psi_{\mathbf{pn}}(\mathbf{r}), \quad f_{\nu}(\mathbf{k}) = \int d\mathbf{r} e^{i\mathbf{k}\mathbf{r}} f_{\nu}(\mathbf{r}), \quad (\text{IX.12})$$

$$\lambda_{\nu\nu'} = \frac{\int f_{\nu}(\mathbf{r}) F_2(\mathbf{r}, \mathbf{r}') f_{\nu'}(\mathbf{r}') d\mathbf{r} d\mathbf{r}'}{E - E_{\nu'}} \equiv \frac{\Lambda_{\nu\nu'}^{(2)}}{E - E_{\nu'}}. \quad (\text{IX.13})$$

In a similar way one easily calculates $\langle \mathbf{k}' | G | \mathbf{k} \rangle$,

$$\langle \mathbf{k}' | G_2 | \mathbf{k} \rangle = \sum_{\nu} \frac{f_{\nu}(\mathbf{k}') (f_{\nu}\psi)}{E - E_{\nu}}. \quad (\text{IX.14})$$

Keeping only one *MQS* level in (IX.11), (IX.14) one has

$$(F_{\nu}\psi) = \frac{f_{\nu}(\mathbf{k})}{1 + \lambda_{\nu\nu}}, \quad (\text{IX.15})$$

$$\langle \mathbf{k}' | G_2 | \mathbf{k} \rangle = \frac{f_{\nu}(\mathbf{k}') f_{\nu}(\mathbf{k})}{E - E_{\nu} + \Lambda_{\nu\nu}^{(2)}}. \quad (\text{IX.16})$$

The case of more *MQS* levels is discussed in the next sections. Note, that E in all equations in this paper denotes the total energy of two-nucleon system, including its masses, which finally in (IX.20) coincides with W , and one-particle energies $E(\mathbf{p})$ also include rest mass in kinetic term. To make (IX.1) selfconsistent, one should also define the single-particle energies E_n, E_p in (IX.2) through the same matrix operator G_2 [115].

$$E(\mathbf{p}) = T(\mathbf{p}) + U_2(\mathbf{p}, \rho) \quad (\text{IX.17})$$

$$U_2(\mathbf{p}, \rho) = \sum_{\mathbf{p}' \leq p_F} \langle \mathbf{pp}' | G_2(W = E(\mathbf{p}) + E(\mathbf{p}')) | \mathbf{pp}' \rangle_a \quad (\text{IX.18})$$

where subscript a implies antisymmetrization of state $(\mathbf{pp}')_>$.

To calculate the energy per nucleon one can use the BHF approximation

$$\frac{E}{A}(\rho) = \frac{\langle T \rangle}{A} + \frac{\langle U_2 \rangle}{2A} \quad (\text{IX.19})$$

where we have defined

$$\langle U_2 \rangle = \sum_{\mathbf{p}, \mathbf{p}' \leq p_F} \langle \mathbf{pp}' | G_2(E(\mathbf{p}) + E(\mathbf{p}')) | \mathbf{pp}' \rangle_a. \quad (\text{IX.20})$$

We now turn to the contribution of higher *MQS* states, and start with the case, when the only interaction present in nuclear matter is the *MQS* composed of $3N$ quarks, $N > 2$, while all other interactions with $N' \neq N$ are absent. Denoting the corresponding reaction matrix for N nucleons G_N , one can write similarly to (IX.1)

$$G_N(W) = V_N - V_N Q_N e_N^{-1} G_N(W) \quad (\text{IX.21})$$

where Q_N, e_N are natural generalizations of Q_2, e_2 and V_N is

$$V_N = \sum_{\nu} \frac{f_{\nu}^{(N)}(\mathbf{r}_1, \dots, \mathbf{r}_N) f_{\nu}^{(N)}(\mathbf{r}'_1, \dots, \mathbf{r}'_N)}{E - E_{\nu}} \quad (\text{IX.22})$$

It is clear, that generalization of Eqs. (IX.11-IX.16) to the case of N -nucleon interaction is straightforward if one replaces there one relative momentum \mathbf{k} by the set of $N - 1$ relative momenta $\{\mathbf{k}_{\alpha}\}, \alpha = 1, \dots, N - 1$, and similarly generalize $Q_2(\mathbf{k}, \mathbf{K})$ and $e_2(\mathbf{k}, \mathbf{K})$ to $Q_N(\{\mathbf{k}_{\alpha}\}, \mathbf{K})$, $e_N(\{\mathbf{k}_{\alpha}\}, \mathbf{K})$. For the function F_N one defines $N - 1$ relative coordinates $\{\mathbf{r}_{\alpha}\}, \alpha = 1, \dots, N - 1$, and one has instead of (IX.5)

$$F_n(\{\mathbf{r}_{\alpha}\}, \{\mathbf{r}'_{\alpha}\}) = \int \prod_{\alpha=1}^{N-1} \frac{d\mathbf{k}_{\alpha}}{(2\pi)^3} Q_N(\{\mathbf{k}_{\alpha}\}, \mathbf{K}) e_N^{-1}(\{\mathbf{k}_{\alpha}\}, \mathbf{K}) \exp(i \sum_{\alpha} \mathbf{k}_{\alpha} (\mathbf{r}_{\alpha} - \mathbf{r}'_{\alpha})). \quad (\text{IX.23})$$

The answer (IX.16) for the case of one *MQS* made of $3N$ quarks is

$$\langle \{\mathbf{k}'_{\alpha}\} | G_N | \{\mathbf{k}_{\beta}\} \rangle = \frac{f_{\nu}(\{\mathbf{k}'_{\alpha}\}) f_{\nu}(\{\mathbf{k}_{\beta}\})}{E - E_{\nu} + \Lambda_{\nu\nu}^{(N)}} \quad (\text{IX.24})$$

and $\Lambda_{\nu\nu}^{(N)}$ is expressed through F_N in the same way as in (IX.13) with the obtains replacement $\mathbf{r} \rightarrow \{\mathbf{r}_{\alpha}\}, \mathbf{r}' \rightarrow \{\mathbf{r}'_{\beta}\}$. Finally in (IX.19) one replaces $\frac{\langle U_2 \rangle}{2A}$ by $\frac{\langle U_N \rangle}{N!A}$, where $\langle U_N \rangle$ is

$$\langle U_N \rangle = \sum_{\{\mathbf{p}_i\} \leq p_F} \langle \{\mathbf{p}_i\} | G_N(W_N) | \{\mathbf{p}_i\} \rangle_a \quad (\text{IX.25})$$

and the set of one-particle momenta $\{\mathbf{p}_i\}$, $i = 1, \dots, N$ is inside the Fermi sphere, while $W_N = \sum_{i=1}^N E(p_i)$.

X. G MATRIX

Diagrams in Figs. 5, 7, and 8 show a closed system of equations that can be solved e.g. by iterations starting from the vacuum solution.

The projection operator Q_2 on states outside of the Fermi sphere influences scattering of the nucleons as described in Sect. IV. In the relativistic theory, the dibaryon self-energy Fig. 5 is represented in the form of dispersion integral. The phase space of two nucleons is restricted by Q_2 and weight of the dispersion integral modifies, accordingly. The invariant part of the dibaryon self-energy operator can be written in the form

$$\Pi_{IJ^P}(s, v) = \frac{1}{\pi} \int_{s_0}^{+\infty} B_F(s', v) \frac{\Im \Pi_{IJ^P}(s') ds'}{s' - s - i0} \quad (\text{X.1})$$

where B_F is the Pauli blocking factor and v is the dibaryon velocity. In terms of the nucleon momenta, the imaginary part of $\Pi_{IJ^P}(s)$ is the same as in the vacuum. The only modification of $\Pi_{IJ^P}(s)$ comes from $B_F \neq 1$ and the in-medium nucleon mass $m^* = m + \Sigma_S(p_+)$ where $p_+ = (\sqrt{m^{*2} + \mathbf{p}^2}, \mathbf{p})$.

A. Pauli blocking

One can give explicit relativistic form of the blocking factor (IX.6). It can be used with Eq. (X.1) for evaluation of the in-medium dibaryon self-energy.

In the rest frame, K , of the substance the Fermi sphere is described by equation

$$p_x^2 + p_y^2 + p_z^2 = p_F^2. \quad (\text{X.2})$$

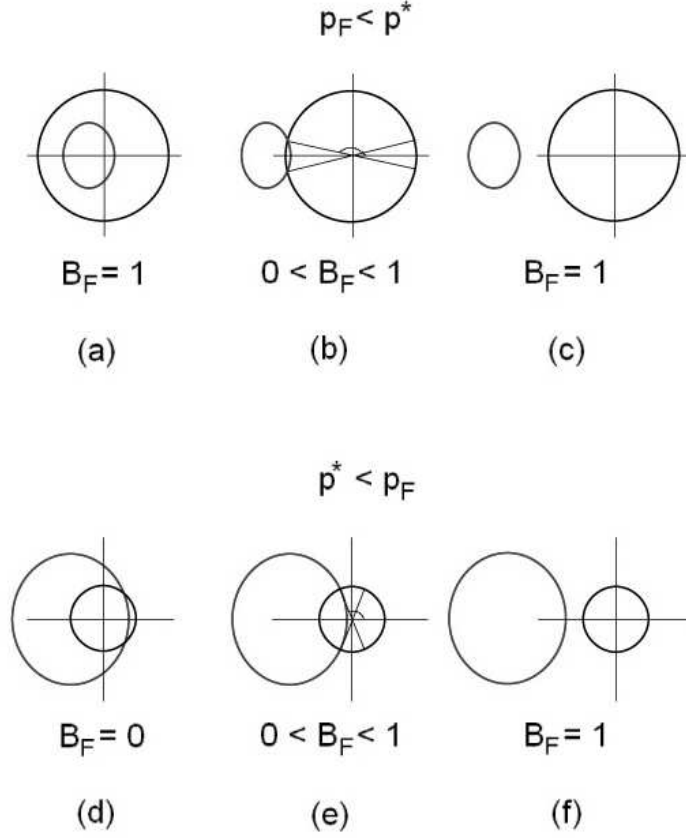


FIG. 14: Possible configurations of the boost-deformed Fermi sphere and the decay sphere in the rest frame of two nucleons. *Upper panel* $p_F < p^*$: Condition $-p^* < -\gamma(p_F + vE_F)$ is fulfilled in the case (a). The Fermi sphere is inside of the decay sphere. The decays are allowed and $B_F = 1$. The spheres intersect each other in the case (b) when $-\gamma(p_F + vE_F) \leq -p^* < \gamma(p_F - vE_F)$ and $0 < B_F < 1$. In the case (c), the relative velocity is high, $\gamma(p_F - vE_F) \leq -p^*$, the spheres do not intersect each other and the decays are allowed $B_F = 1$. *Lower panel* $p^* < p_F$: In the case of $p^* \leq \gamma(p_F - vE_F)$, the decay sphere is inside of the Fermi sphere and the decays are forbidden $B_F = 0$. The case (d) corresponds to intersection of the spheres for $\gamma(p_F - vE_F) < p^*$ and $E^* < E_F/\gamma$ where $B_F = 0$ also. In the case (e), $-p^* < \gamma(p_F - vE_F) < p^*$ and $E_F/\gamma < E^* < E_F$, the decays are possible and $0 < B_F < 1$. In the case (f), the relative velocity is high to provide $\gamma(p_F - vE_F) \leq -p^*$, in which case the spheres do not intersect and the decays are allowed $B_F = 1$.

In the co-moving frame, K' , of the dibaryon the decay products have momenta

$$p_x'^2 + p_y'^2 + p_z'^2 = p^{*2}. \quad (\text{X.3})$$

We assume that the dibaryon moves in the positive direction of the x -axis. Using boost along x , one can write equation for the Fermi sphere in K' :

$$\gamma^2(p_x' + vE')^2 + p_y'^2 + p_z'^2 = p_F^2,$$

where $v > 0$ and $p_x = \gamma(p_x' + vE')$, $p_y = p_y'$, $p_z = p_z'$. Since p' belongs to both the Fermi sphere and the decay sphere (X.3), $E' = E^* = \sqrt{m^{*2} + p^{*2}}$ and

$$\gamma^2(p_x' + vE^*)^2 + p^{*2} - p_x'^2 = p_F^2,$$

from which we derive

$$p'_{x\pm} = \frac{-E^* \pm E_F \sqrt{1 - v^2}}{v},$$

where $E_F = \sqrt{m^{*2} + p_F^2}$. Note that $p'_{x-} < -p^*$. There exists therefore only one intersection of the spheres. The nucleon self-energy depends on the absolute values of the momenta, so directions of the nucleon velocities have equal

weights. The modified dispersion law implies that the nucleon mass entering E^* and E_F is the effective nucleon mass m^* .

The critical values $p'_{x+} = \pm p^*$ at which the Fermi sphere touches the decay sphere give equations

$$\pm p^* = \frac{-E^* + E_F \sqrt{1 - v^2}}{v}.$$

The blocking factor is defined by fraction of the area of the decay sphere outside of the Fermi sphere. The possible cases are shown in Fig. 14. The blocking factor becomes

$$B_F = -\cos \theta_+, \quad (\text{X.4})$$

where

$$\cos \theta_+ = \max(-1, \min(0, \frac{p'_{x+}}{p^*})).$$

B. Heterophase nuclear matter with a Bose condensate of dibaryons

Small perturbations of s -channel NN interaction, as a rule, shift primitives from the unitary cut and turn them into resonances. One can expect therefore that the effects of the environment transform the primitives into the resonances. Such dibaryons can provide deep modification of nuclear matter at densities above the critical density for the formation of such dibaryons on mass shell. Before proceeding to discuss realistic models it is worthwhile to consider a mixed dibaryon-nucleon phase in ideal gas approximation.

Suppose that we fill the box with neutrons, as shown in Fig. 15. Pauli principle allows neutrons with increasing density consistently occupy higher energy levels. We can continue this process until the chemical potential of neutrons at the surface of the Fermi sphere will not be higher than half of dibaryon mass. In the approximation of an ideal gas, the chemical potential of fermions is equal to the Fermi energy, while the chemical potential of bosons is simply the mass of boson m_D .

When the Fermi energy of neutrons becomes higher than half the mass of the boson, it gets energetically advantageous for the two neutrons to merge and form a dibaryon. The critical density at which the process of the dibaryon condensation starts is thus determined by the mass of the lightest dibaryon. Above the critical density, the chemical potential of the nucleons μ_n is frozen at $\mu_n^{\text{max}} = m_D/2$ due to chemical equilibrium with respect to conversions $NN \leftrightarrow D$.

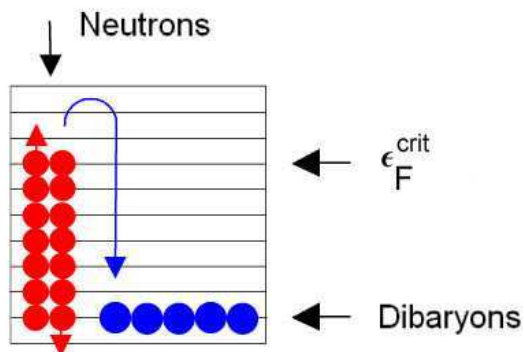


FIG. 15: Illustration of transition to the heterophase state of nuclear matter with an admixture of dibaryons.

Dibaryons are Bose particles and form a Bose condensate. Dibaryons in the condensate have zero velocity, so they do not collide with the boundary of the box and do not contribute to the pressure.

On the other hand, the Fermi energy of neutrons is frozen, so the pressure does not increase with increasing density (see Fig. 16). As a result, a binary mixture of neutrons and dibaryons loses its elasticity. Nuclear matter with such properties can not protect neutron stars against gravitational compression and the subsequent collapse.

Incompressibility of nuclear matter at saturation density is well known experimentally, it is certainly not equal to zero, so the dibaryon Bose condensate, apparently, does not exist in normal nuclei (at least in the ideal gas model and some simple modifications of this model, see below). Because of the charge symmetry of nuclei, $\mu_n = \mu_p$. Assuming further that the shell potential of dibaryons is two times deeper than for nucleons, we can conclude that the masses

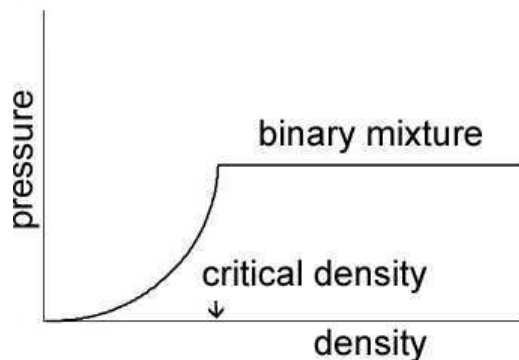


FIG. 16: Schematic view of EoS of the heterophase nuclear matter with an admixture of dibaryons in the absence of interactions.

of primitives (which turn in nuclear medium to dibaryons, i.e., resonances) associated with the NN -channel must be greater than

$$m_D > 2\varepsilon_F = 1.96 \text{ GeV}, \quad (\text{X.5})$$

where $\varepsilon_F = m_N + 40 \text{ MeV}$ is the Fermi energy of nucleons in nuclei. The primitive masses we derived earlier from the NN scattering, $m_D = 2047$ and 2006 MeV , satisfy this constraint.

In the nonrelativistic approximation, the evolution of the local velocity \mathbf{v} of matter inside the newly born protoneutron star is described by Euler's equation

$$\rho \frac{\partial \mathbf{v}}{\partial t} + \rho(\mathbf{v} \cdot \nabla)\mathbf{v} = -\nabla p - \rho \nabla \Phi,$$

where Φ is gravitational potential, ρ is density, and p is pressure. In the presence of the dibaryon Bose condensate, pressure remains constant, as indicated by the horizontal line in Fig. 16, and hence $\nabla p = 0$. Gauss' law implies that $\int d\mathbf{S} \cdot \nabla \Phi = 4\pi GM(r)$, where $M(r)$ is the mass inside a sphere of radius r , so $\nabla \Phi \neq 0$. Thus, we conclude that $\mathbf{v} \neq 0$. In the approximation of an ideal gas, the static solutions disappear because of formation of the dibaryon Bose condensate. These arguments are valid in the general relativity. Formation of the dibaryon condensate can be considered as a possible mechanism for the phase transition to quark matter.

Dibaryon-nucleon and dibaryon-dibaryon interactions contribute to the pressure. EoS of the binary mixture becomes stiffer, ensuring the stability of neutron stars in a certain range of densities. If the formation of the dibaryon Bose condensate is a first-order phase transition and the density jump $\Delta\rho$ at the phase transition is large enough, the neutron stars become unstable when the central density hits the critical value [60, 63, 116].

In a Bose gas of interacting bosons, a fraction of bosons is outside the condensate. These particles move, collide with a boundary, and contribute to the pressure. The stronger the repulsive interaction, the more stable can be a Bose gas of interacting bosons. With increasing density, the interaction energy is growing faster than the kinetic energy, so the difference between fermions and bosons becomes asymptotically less significant. Coupling constants and masses of dibaryons can be constrained from the existence and stability of massive neutron stars [45].

In the RMF model of Ref. [45] dibaryons with masses close to the ones we derived from the phase shifts analysis ($m_D = 2047$ and 2006 MeV in the 3S_1 and 1S_0 channels, respectively) with sufficiently weak σ -meson couplings (weak attraction force) appear at high densities without destabilizing neutron stars. Dibaryons with strong σ -meson couplings appear at densities below 0.3 fm^{-3} . Such dibaryons generate instability (square of sound velocity gets negative), providing phase transition to more dense phase of nuclear matter, e.g., quark matter.

There is therefore the interesting connection between parameters of the lightest dibaryons and structure and stability of neutron stars.

XI. NUCLEAR PHASE TRANSITION IN COLLAPSED STELLAR CORES

The behavior of stars under a phase transition instability is determined by the jump of density λ . If λ exceeds the critical value $\lambda_c = \frac{3}{2}$, the star becomes unstable at the moment the phase transition starts in the center. This result is remarkably independent on the specific properties of EoS. The magnitude of the density jump is the only relevant parameter [60].

In general, the problem of stellar stability with a phase transition is more complicated as discussed, for instance, in Refs. [63, 116]. A star can lose stability even when $\lambda < \frac{3}{2}$ (subcritical regime) on conditions that the interface between two phases is not exactly at the stellar center and a new-phase inner core of finite size has already been formed. The critical size of the new-phase core depends on the stiffness of EoS which is determined by the adiabatic index averaged over the star $\bar{\gamma}$. The lower the stability factor ($\bar{\gamma} - \frac{4}{3}$) the smaller density jump is required to destabilize the star. The hydrostatic equilibrium of a star at the boundary of stability ($\bar{\gamma} = \frac{4}{3}$) can be disturbed by phase transition with an arbitrary small jump of density.

A. Equation of state

Since our goal is to investigate only the main features of the hydrodynamic behavior of the instability we use a simplified approximation for EoS as described below.

The free energy is approximated in the following way

$$F_{L,H} = F_{id}(T, \xi) + \Delta F_{L,H}(n), \quad n = n_{id}(T, \xi), \quad (\text{XI.1})$$

where F is the specific (per particle) free energy, T is temperature, and n is the particle number density. The indices L and H correspond to low and high density phases, respectively. For simplicity, the matter is assumed to consist of neutrons only. The functions F_{id} and n_{id} are defined by the Fermi-Dirac statistics for ideal (noninteracting) nonrelativistic particles and depend on the temperature and parameter ξ that failing the interaction is simply the chemical potential.

The additive terms $\Delta F(n)$ in (XI.1) describe the interaction and depend only on n :

$$\Delta F_{L,H}(n) = C_{L,H} n^{\gamma_{L,H}-1} - C_{id} n^{2/3}. \quad (\text{XI.2})$$

Thus, Eqs. (XI.1,XI.2) define F as a function of n and T parametrically (parameter ξ). All the necessary for hydrodynamical calculations of thermodynamical quantities such as the pressure, internal energy, entropy, chemical potential etc. can be easily found from F by standard way. For example, the pressure P and chemical potential μ are

$$P = n^2 \left(\frac{\partial F}{\partial n} \right)_T, \quad \mu = F + \frac{P}{n}. \quad (\text{XI.3})$$

The region of transition between the two phases can be found from the equations of phase co-existence

$$P_L(T, n_L) = P_H(T, n_H), \quad \mu_L(T, n_L) = \mu_H(T, n_H), \quad (\text{XI.4})$$

which require the continuity of pressure and chemical potentials at the phase interface. These equations determine the particle density of the phase transition beginning n_L and that of its ending n_H , and so the magnitude of density jump $\lambda = n_H/n_L$, as functions of the temperature.

The constant C_{id} corresponds to ideal degenerate nonrelativistic neutron gas at zero temperature. Therefore, at $T = 0$ the second term in the right hand side of Eq. (XI.2) cancels the term F_{id} in Eq. (XI.1). Thus, at zero temperature we have a polytropic EoS (for both the phases) whereas for $T > 0$ it has more general form defined by Eq. (XI.1). What why we use the term ‘‘quasi-polytropic star’’.

We start hydrodynamic calculations from a hydrostatic configuration at $T = 0$. According to Eqs. (XI.1,XI.2,XI.3) at zero temperature we have

$$F_{L,H}(n) = C_{L,H} n^{\gamma_{L,H}-1}, \quad P_{L,H} = (\gamma_{L,H} - 1) C_{L,H} n^{\gamma_{L,H}}, \quad (\text{XI.5})$$

$$\mu_{L,H} = \frac{\gamma_{L,H}}{\gamma_{L,H} - 1} \frac{P_{L,H}}{n}. \quad (\text{XI.6})$$

From Eqs. (XI.4) it follows that for a polytropic EoS, such as given by Eqs. (XI.5,XI.6), the phase transition density jump λ is unambiguously determined by adiabatic indices of L and H phases:

$$\lambda \equiv \frac{n_H}{n_L} = \frac{\gamma_H(\gamma_L - 1)}{\gamma_L(\gamma_H - 1)}. \quad (\text{XI.7})$$

B. Initial model

Our calculations of the phase transition hydrodynamics were performed in dimensionless variables. Everywhere below (in the text and figures) the dimensionless values will be implied if not specified explicitly.

The following units for the temperature T , density ρ , velocity V , time t , pressure P , and energy E were used

$$\begin{aligned} T &: \left[\frac{m_u GM_s}{k_b R_s} \right], & \rho &: \left[\frac{M_s}{4\pi R_s^3} \right], & V &: \left[\sqrt{\frac{GM_s}{R_s}} \right], \\ t &: \left[\sqrt{\frac{R_s^3}{GM_s}} \right], & P &: \left[\frac{GM_s^2}{4\pi R_s^4} \right], & E &: \left[\frac{GM_s^2}{R_s} \right], \end{aligned} \quad (\text{XI.8})$$

where k_b is the Boltzmann constant, G — gravitational constant, M_s and R_s — the mass and initial radius of the star, respectively.

As an example, M_s and R_s for a hot protonneutron star formed in the collapse of the SN core in several tens of ms after bounce can be estimated as $M_s = 1.4M_\odot$ $R_s \approx 39$ km. Substituting these values for M_s and R_s in Eqs. (XI.8) we obtain

$$\begin{aligned} [T] &\approx 49 \text{ MeV}, & [\rho] &\approx 3.7 \times 10^{12} \text{ g/cm}^3, & [V] &\approx 69 \text{ 000 km/s}, \\ [t] &\approx 0.57 \text{ ms}, & [P] &\approx 1.7 \times 10^{32} \text{ erg/cm}^3, & [E] &\approx 1.3 \times 10^{53} \text{ erg}. \end{aligned} \quad (\text{XI.9})$$

Instead of the particle number density n , we will use hereafter the mass density ρ that is connected with n by the relation $\rho = m_u n$ where m_u is the atomic mass unit.

The initial configuration in our calculations was represented by a hydrostatically equilibrium star consisting of L-phase matter at $T = 0$ with the adiabatic index $\gamma_L = 5/3$. The dimensionless form of Eq. (XI.5) for pressure reads as

$$P = A \rho^{5/3}, \quad A = \frac{2}{3} \frac{C_L m_u^{5/3}}{G(4\pi)^{2/3} M_s^{1/3} R_s}. \quad (\text{XI.10})$$

So the initial model is a polytrope of index $k = 1.5$ with $A = 0.078484$ and dimensionless central density $\rho_c = 17.97$. The initial central density at $t = 0$ was assumed to be just at the beginning of the phase transition.

In order to simulate the fact that in a core-collapse SN the stellar core is actually rather hot and the pressure can exceed that for ideal Fermi gas at zero temperature, the factor C_L was chosen to be equal to $2.83 \times C_{id}$. If the density jump λ and γ_L are specified at $T = 0$ then one can find γ_H from Eq. (XI.7). Next, the factor C_H can be estimated from the relation

$$P_L(0, \rho_c) = P_H(0, \lambda \rho_c). \quad (\text{XI.11})$$

For the main value $\lambda = 1.525$ (at $T = 0$) in our calculations and $\gamma_L = 5/3$ one can derive from Eq. (XI.7) $\gamma_H \approx 1.355$.

In subsequent hydrodynamic calculations the quantities $C_{L,H}$ and $\gamma_{L,H}$ at any temperatures remain fixed and equal to their values estimated at $T = 0$ as is described above.

The only parameter that we change in different versions of our calculations is the value of λ at $T = 0$.

Figure 17 shows typical dependence of pressure on density at different dimensionless temperatures $T = 0$ (initial model), 1 and 2 (for version $\lambda = 1.525$ at $T = 0$).

An example of the phase diagram in our calculations is shown in Fig. 18 for $\lambda = 1.525$ at $T = 0$. The domains at the left of the solid curve and from the right of the dashed one cover the low-density and high-density single-phase states, respectively. The mixed-phase states occur everywhere over the region between those curves. Here the pressure does not depend on density at given temperature.

One can see that the density jump λ decreases with increasing temperature.

C. Results of hydrodynamical calculations

The hydrodynamic calculations were run with fully implicit Lagrangian code, the star being divided onto 1000 mass zones.

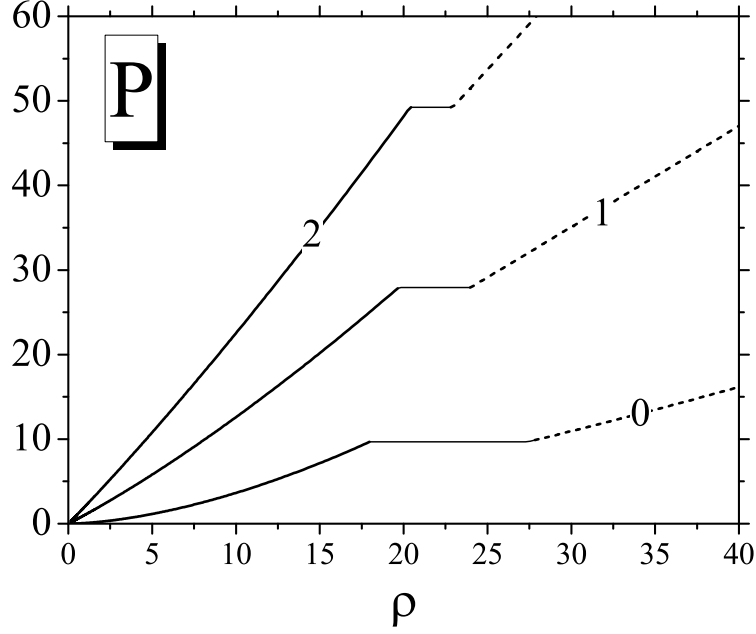


FIG. 17: Pressure as a function of density at different temperatures $T = 0, 1, 2$

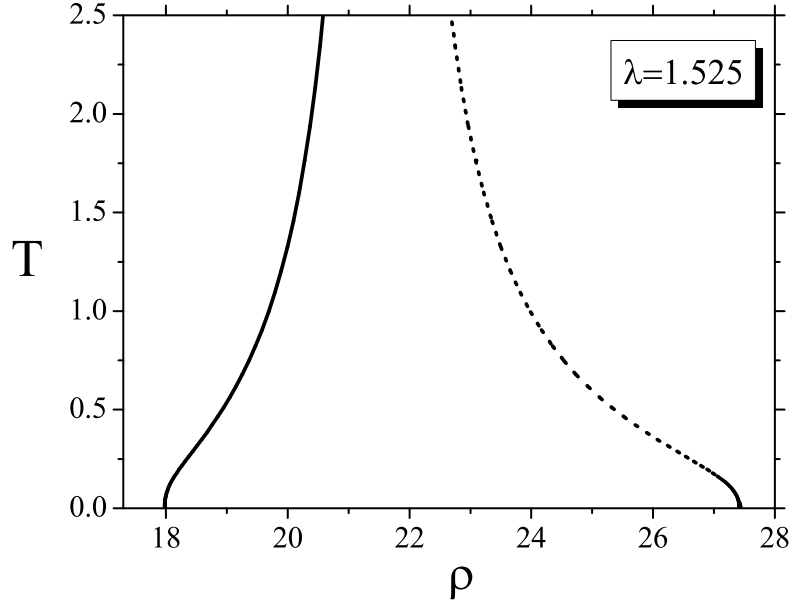


FIG. 18: The phase diagram for $\lambda = 1.525$ at $T = 0$

In order to activate the phase transition the hydrostatic equilibrium was perturbed by imposing a small inward velocity V_0 to stellar matter ($V_0 = -\alpha r$). The total kinetic energy injected in the star by such a perturbation was as small as 5×10^{-8} of the star gravitational energy E_g for $\lambda = 1.525$. In this way several models were calculated for different values of λ at $T = 0$. Below we discuss the results for the model with supercritical density jump $\lambda = 1.525$ at $T = 0$.

Figures 19–21 show the temporal evolution of density, temperature and velocity from the time of the loss of stability

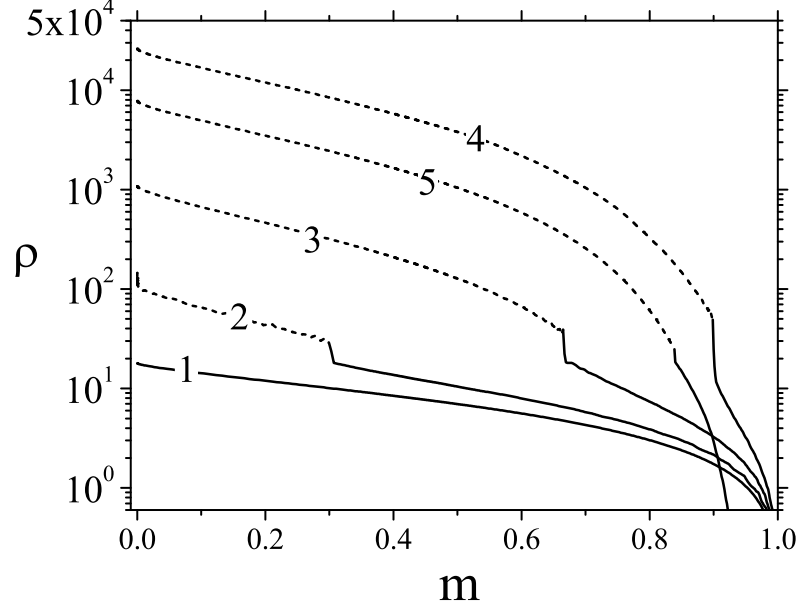


FIG. 19: Temporal evolution of density

$t = 0$ (curve labelled 1) on account of the appearance of new phase to the approach to final quasi-equilibrium configuration $t = 10$ (curve labelled 5). Intermediate curves correspond to times $t = 6.7$ (2), $t = 7.4$ (3), and $t = 7.7$ (4). Solid sections of the curves belong to domains contain low-density phase whereas dashed ones correspond to high-density phase. All the quantities are shown as the functions of dimensionless mass coordinate $0 \leq m \leq 1$.

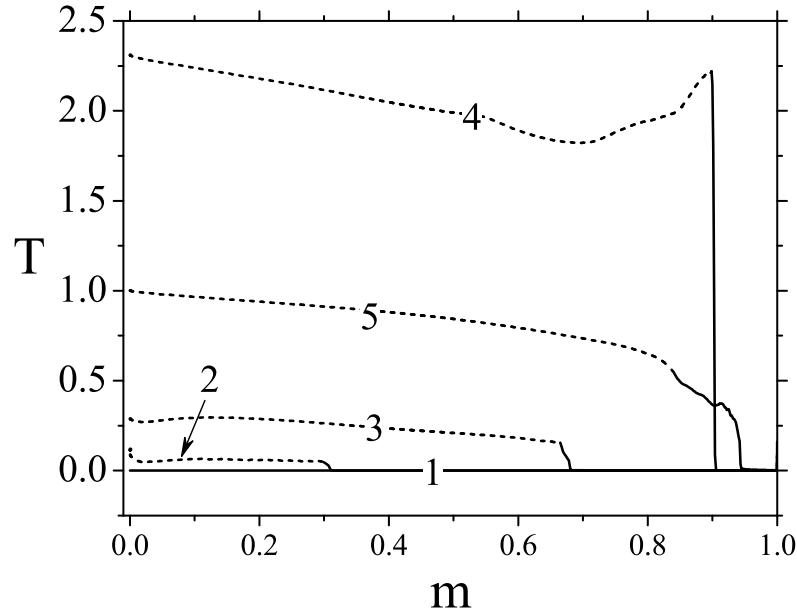


FIG. 20: Temporal evolution of temperature

One can clearly observe that the conversion of low-density matter into high-density one has a nature of mini

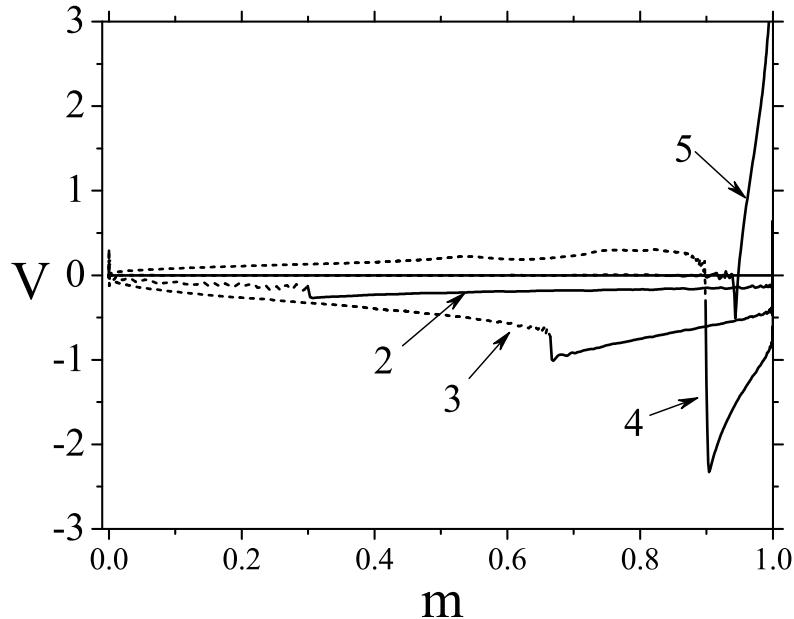


FIG. 21: Temporal evolution of velocity

collapse and finally results in hydrodynamic transition of the star into new equilibrium. The onset of a new phase at stellar center causes pulsational instability. The interface between two phases generates progressive waves that excite oscillation of the new-phase core. According to our numerical experiments, the heat-transport processes turn out to be of significant importance here for to convert the kinetic energy of pulsations in heat and to redistribute it in matter. To include convection in the mixing length approximation (see e.g. [117]) proves to be sufficient in our case.

As the core of new phase increases the collapse gathers strength and outgoing shock front appears at the phase interface. Both the density and temperature are growing quickly behind the front. This process becomes similar to standard bounce during the collapse of stellar cores without phase transition. Ultimately the core stops to compress and rebounds under the action of ram pressure creating outgoing shock wave that reaches outermost low density layers, cumulates and ejects the envelope of a mass $M_{ejc} \lesssim 0.05M_s$.

We have calculated a number of models with different values of the initial density jump λ at $T = 0$.

Figure 22 shows kinetic energy of ejected matter E_{ejc} in terms of the initial gravitational energy of the star as a function of λ . For $\lambda \gtrsim \frac{3}{2}$, E_{ejc} has virtually constant value of about 12% of initial gravitational energy since the initial configuration is a polytrope of index 1.5 with the dimensionless gravitational energy $E_g = -6/7$. When λ decreases below critical value $3/2$, E_{ejc} falls down abruptly — at subcritical $\lambda = 1.4$ it only amounts to 0.4%. It is significant that in the subcritical regime one has to increase the initial inward velocity in order to excite undamped (converting finally in collapse) oscillations of the new-phase core. For $\lambda = 1.4$ the kinetic energy of the initial perturbation of about $2 \times 10^{-5}|E_g|$ proved to be sufficient.

The lower λ , the larger the new-phase core should be. This is in full agreement with the work of Blinnikov [116]. If the mass of a subcritical core is not large enough the core remains stable. Moreover, for $\lambda < 3/2$ the ejection of stellar envelope proceeds owing to numerous pulsations each entailing small leakages of matter rather than a single outflow forced by a shock wave.

D. Discussion

Our calculations provide an example of hydrodynamical development of the phase transition-induced instability in collapsing stellar cores. The onset of the new-phase inner central core gives rise to a shock wave that ejects though low mass but of high velocity envelope. For our model the kinetic energy of the ejection can reach about 12% of the initial gravitational energy of the core. Taking into account the unit of energy from Eq. (XI.9) we obtain $E_{ejc} \approx 1.3 \times 10^{52}$ erg

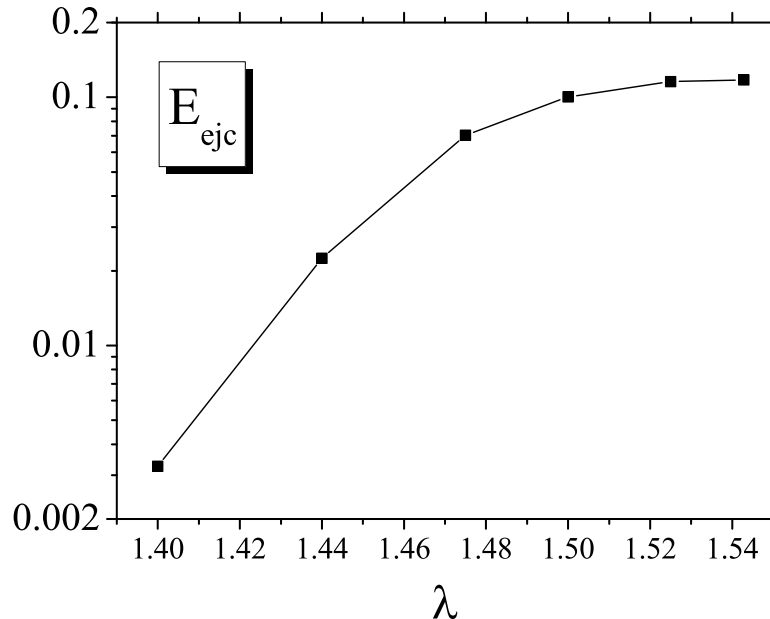


FIG. 22: Kinetic energy of ejected matter versus λ at $T = 0$

($\lambda = 1.525$). This is even more than necessary to conform to astronomical observations.

In reality the final ejection of SN envelope will occur after the following interaction of the phase transition induced shock wave with an outer standing accretion shock that decomposes infalling iron-peak nuclei into free nucleons. Thus, behind the accreting shock there exists a layer enriched with free neutrons and protons. When crossing this layer the phase transition shock has only to slightly accelerate it to cause its expansion accompanied by cooling and recombination of neutrons and proton back into heavy nuclei. The energy liberation due to such a recombination (about 7 – 8 MeV per recombined nucleon) could facilitate the final expulsion of SN envelope [118]. So, the phase transition shock can act at least as a trigger of the SN explosion.

The gravitational energy released in the hydrodynamical transition of the star into a new-phase state converts mostly to heat while the density increases by a factor of 10^3 (Figs. 19, 20). Therefore, the processes of heat transport becomes of primary importance. The major factors here are expected to be convection and neutrino transport in quark-gluon plasma. The latter was neglected in our calculations whereas convection was included. Hence, our explosion energy E_{ejc} seems to be underestimated because additional energy supply provided by neutrino heat transport to outer layers can only contribute to the ejection energy.

XII. CONCLUSIONS AND OUTLOOK

We briefly reviewed in this paper vast material related to the structure of QCD vacuum and the properties of neutron stars and presented new results on the physics of the density-induced deconfinement (Sect. III), relativistic QCB model (Sects.V-VII), EoS of nuclear matter with an admixture of MQS and possible phase transitions (Sects. IX-X), and finally and most importantly, we have considered in Section XI the evolution of newly born protoneutron stars under the influence of phase transition in nuclear matter.

We have shown that the phase transition curve in (μ, T) plane of states of the hadron-quark-gluon matter can be understood and predicted on the basis of the vacuum energy dominance in good agreement with available lattice data, however, the resulting critical density for $T \lesssim 20$ MeV is very high, $\rho_c \sim 30\rho_0$, which leaves room for possible intermediate phase transitions in normal nuclear matter below the deconfined quark phase.

To describe this region, one needs a more adequate description of the nucleon-nucleon forces, which includes quark degrees of freedom. We envisaged old QCB model, which was reformulated in modern relativistic form and well describes the experimental data. Having at hands new NN (and, in principle, $3N, 4N, \dots$) forces, we have formulated new system of equations for the EoS of nuclear matter with an admixture of 6QS, and here the main question is

whether MQS play a role of "primitives", i.e., the instantaneous objects generating hard NN repulsive cores, or they exist further in the environment on the mass shell and reveal themselves as a new physical component of high-density nuclear matter. We have shown that this new phase may appear when the density increases up to $(2 \div 3)\rho_0$, while more quantitative analysis is currently in progress. From this side, one can apply the resulting EoS to describe the interiors of neutron stars, the cumulative effect in reactions on nuclei, and study the role of MQS in phase transitions in nuclear matter.

One should emphasize a twofold role of the phase transition of the considered type in physics of supernovae. On the one hand, the phase transition could be a missing ingredient necessary to resolve a 30-years puzzle of supernova explosion in spherical symmetry. On the other hand, as demonstrated by recent calculations in Ref. [69], supernova outburst induced by the phase transition is accompanied by a second peak on its neutrino light curve that occurs in about 250 ms after core-collapse bounce. The temporal and neutrino-flavor properties of such a peak provide unique information about the EoS of superdense matter. Thus, nuclear and particle physicists have a good chance to experimentally check their findings in case of detection the neutrino signal from stellar core collapse in our Galaxy. As for astrophysicists, further detailed and systematic modeling of the phase transition effects in core-collapse supernovae is of great importance.

Acknowledgments

The authors wish to thank Natali Igunnova for help in preparation of the manuscript. D.K.N. and A.V.Yu. are supported by the SNSF grant (SCOPEs project No. IZ73Z0-128180/1) and Russian Federal Agency for Science and Innovations (Contract No. 02.740.11.0250). D.K.N. is supported by the RFBR grant No. 09-02-12168-ophi.m. M.I.K. is supported by the RFBR grant No. 09-02-91341 and DFG grant No. 436 RUS 113/721/0-3, Yu.A.S. and M.A.T. are supported by the RFBR grant No. 09-02-00629.

XIII. APPENDIX A: THE $6q$ DESCRIPTION OF 1S_0 AND 3S_1 STATES

We follow here results of Ref. [49] and the last reference in [51]. For 1S_0 and 3S_1 we neglect V_{hh} and keep only two levels of the $6qMS$. The following form of V_{hqh} is used

$$V_{hqh}(r, r') = \frac{[(E_1 - E)\eta_1(r) - c_1\delta(r - b)][(E_1 - E)\eta_1(r') - c_1\delta(r' - b)]}{E - E_1} + \frac{c_2^2\delta(r - b)\delta(r' - b)}{E - E_2}. \quad (\text{XIII.1})$$

The P -matrix for this potential has the form

$$P(b) = k + \frac{2\mu c_1}{\eta_1(b)} + \frac{2\mu c^2}{E - E_1} + \frac{2\mu c_2^2}{E - E_2}. \quad (\text{XIII.2})$$

The quantity k is defined due to orthogonality of $\eta_\nu(r)$ to be [51]

$$\frac{1}{\eta_\nu(r)} \frac{d}{dr} \eta_\nu(r) \Big|_{r=b} = k. \quad (\text{XIII.3})$$

From the Schrödinger equation for the total wave function $\psi(r)$ one obtains β_1

$$\eta_1(b)c_1 = -\frac{\beta_1^2}{2\mu} + E_1.$$

Then the values of all parameters reproducing the phases with good accuracy in the interval $0 \leq T_{Kin} \leq 515$ MeV are as follows

$$\begin{aligned} ^1S_0 : \quad & b = 7.42 \text{ GeV}^{-1}, \quad \beta_1 = 0.27 \text{ GeV}, \\ & c_1 = 0.34 \text{ GeV}^{1/2}, \quad c_2 = 0.371 \text{ GeV}^{1/2}, \\ & E_1 = 0.23 \text{ GeV}, \quad E_2 = 1 \text{ GeV}, \\ ^3S_1 : \quad & b = 7.025 \text{ GeV}^{-1}, \quad \beta_1 = 0.268 \text{ GeV}, \\ & c_1 = 0.343 \text{ GeV}^{1/2}, \quad c_2 = 0.445 \text{ GeV}^{1/2}, \\ & E_1 = 0.243 \text{ GeV}, \quad E_2 = 1 \text{ GeV}. \end{aligned}$$

XIV. APPENDIX B: TRANSFORMATION PROPERTIES OF DIBARYON CURRENTS

In this section, transformation properties of the nucleon wave functions and the operators O entering two-nucleon currents under the charge conjugation are given. The nucleon wave functions $\Psi = \psi \otimes \chi$ are products of bispinors ψ and isospinors χ .

A. Isospin C -parity

The isospin C -parity operator and its transformation properties under the main algebraic operations are given by

$$\begin{aligned} C_I &= i\tau^2 = \begin{pmatrix} 0 & 1 \\ -1 & 0 \end{pmatrix}, \\ C_I^T &= C_I^{-1} = C_I^+ = -C_I, \\ C_I^* &= C_I. \end{aligned}$$

The C -conjugation of isospinors is defined by

$$\begin{aligned} \chi_c &= C_I \chi^{+T}, \\ \chi_c^+ &\equiv (\chi_c)^+ = -\chi^T C_I. \end{aligned}$$

The isospin hermitian matrices are expanded over the set $\Xi = (1, \tau^\alpha)$, the components of the set transform as follows

$$C_I^T \begin{pmatrix} 1 \\ \tau^\alpha \end{pmatrix}^T C_I = \begin{pmatrix} 1 \\ -\tau^\alpha \end{pmatrix}. \quad (\text{XIV.1})$$

The equivalent form reads $C_I^T \Xi^T C_I = (-)^I \Xi$, where I is isospin of the element. If χ_1 and χ_2 are q -numbers,

$$\chi_{1c}^+ \Xi \chi_2 = \chi_{2c}^+ C_I^T \Xi^T C_I \chi_1 = (-)^I \chi_{2c}^+ \Xi \chi_1.$$

B. Lorentz C -parity:

In the standard representation [84], the C -conjugation matrix and its transformation properties under the main algebraic operations are given by

$$\begin{aligned} C_L &= -i\gamma^0\gamma^2 = -i\alpha^2 = -\begin{pmatrix} 0 & i\sigma^2 \\ i\sigma^2 & 0 \end{pmatrix}, \\ C_L^T &= C_L^{-1} = C_L^+ = -C_L, \\ C_L^* &= \bar{C}_L = C_L. \end{aligned}$$

The C -conjugated bispinors are defined as follows

$$\begin{aligned} \psi_c &= i\gamma^2\psi^* = C_L\bar{\psi}^T, \\ \bar{\psi}_c &\equiv \overline{(\psi_c)} = \psi^T C_L. \end{aligned}$$

Matrices acting on the bispinors can be expanded over the set $\Gamma = (1, \gamma_5, \gamma^\mu, \dots)$, the components of the set obey

$$C_L^T \begin{pmatrix} 1 \\ i\gamma_5 \\ \gamma^\mu \\ \gamma_5\gamma^\mu \\ \sigma_{\mu\nu} \\ i\gamma_5\sigma_{\mu\nu} \end{pmatrix}^T C_L = \begin{pmatrix} 1 \\ i\gamma_5 \\ -\gamma^\mu \\ \gamma_5\gamma^\mu \\ -\sigma_{\mu\nu} \\ -i\gamma_5\sigma_{\mu\nu} \end{pmatrix}. \quad (\text{XIV.2})$$

The bilinear forms are transformed as follows

$$\bar{\psi}_{1c}\Gamma\psi_2 = \bar{\psi}_{2c}C_L^T\Gamma^T C_L\psi_1 = \pm\bar{\psi}_{2c}\Gamma\psi_1,$$

the sign can be read off from Eq. (XIV.2).

C. Combined C -parity

The C -conjugation operator acting on the nucleon wave functions $\Psi = \psi \otimes \chi$ has the following properties:

$$\begin{aligned} C &= C_L C_I, \\ C^T &= C^{-1} = C^+ = C^* = C, \\ \bar{C} &= -C. \end{aligned}$$

The C -conjugated nucleon wave functions are given by

$$\begin{aligned} \Psi_c &= C\bar{\Psi}^T, \\ \bar{\Psi}_c &\equiv \overline{(\Psi_c)} = -\Psi^T C. \end{aligned}$$

The matrices O entering two-nucleon currents can be expanded over products of the matrices of Ξ and Γ . They transform according to the rule

$$C^T \Xi^T \Gamma^T C = \pm \Xi \Gamma.$$

The bilinear forms are transformed under the permutations as follows

$$\bar{\Psi}_{1c}\Xi\Gamma\Psi_2 = \bar{\Psi}_{2c}C^T\Xi^T\Gamma^TC\Psi_1 = \pm\bar{\Psi}_{2c}\Xi\Gamma\Psi_1.$$

The signs are fixed by Eqs. (XIV.1) and (XIV.2).

D. Even and odd bilinear forms

Using the above rules, one finds even bilinear forms under permutations of the nucleon fields. These forms are constructed using matrices

$$(1, i\gamma_5, \gamma_5\gamma_\mu), \\ \tau^\alpha(\gamma_\mu, \sigma_{\mu\nu}, i\gamma_5\sigma_{\mu\nu}).$$

The odd bilinear forms are constructed using matrices

$$\tau^\alpha(1, i\gamma_5, \gamma_5\gamma_\mu), \\ (\gamma_\mu, \sigma_{\mu\nu}, i\gamma_5\sigma_{\mu\nu}).$$

The odd structures including the first-order differential operator, that enter two-nucleon currents, are listed in Table V.

-
- [1] K. Yagi, T. Hatsuda and Y. Miake, *Quark-gluon plasma* (Cambridge Univ. Press, Cambridge 2005).
- [2] B. Müller, J. L. Nagle, *Ann. Rev. Nucl. Phys.* **56**, 93 (2006).
- [3] F. Karsch, E. Laermann, in “Hwa, R.C. (ed.) et al. : Quark-gluon plasma III”, pp. 1-59; arXiv:hep-lat/0305025 .
- [4] H. G. Dosch, *Phys. Lett. B* **190**, 177 (1987);
H. G. Dosch and Yu. A. Simonov, *Phys. Lett. B* **205**, 339 (1988);
Yu. A. Simonov, *Nucl. Phys. B* **307**, 512 (1988).
- [5] A. V. Nefediev, Yu. A. Simonov, M. A. Trusov, *Int. J. Mod. Phys. E* (in press); arXiv:
- [6] Yu. A. Simonov, M. A. Trusov, *Phys. Lett. B* **650**, 36 (2007); arXiv:hep-ph/0703277; *JETP Lett.* **85**, 730 (2007).
- [7] Yu. A. Simonov, *Phys. Lett. B* **619**, 293 (2005). ;
A. Di Giacomo, E. Meggiolaro, Yu. A. Simonov, A. I. Veselov, *Phys. Atom. Nucl.* **70**, 908 (2007);
P. Yu. Kulikov, Yu. A. Simonov, M. A. Trusov, (in preparation).
- [8] N. O. Agasian, B. O. Kerbikov and V. I. Shevchenko, *Phys. Rept.* **320**, 131 (1999).
- [9] L. A. Kondratyuk, M. M. Giannini, M. I. Krivoruchenko, *Phys. Lett. B* **269**, 139 (1991).
- [10] M. M. Giannini, L. A. Kondratyuk, M. I. Krivoruchenko, Talk given at 5th Workshop on Perspectives in Nuclear Physics at Intermediate Energies, ICTP, Trieste, Italy, May 6 - 10, 1991. Published in: *Perspectives in Nuclear Physics at Intermediate Energies*, Eds. S. Boffi, C. C. degli Atti, M. Giannini, (World Sci., Singapore 1992), pp. 48-57.
- [11] L. A. Kondratyuk, M. I. Krivoruchenko, *Z. Phys. A* **344**, 99 (1992).
- [12] S. Hands, S. Kim, J.-I. Skullerud, *Eur. Phys. J. C* **48**, 193 (2006).
- [13] H. Riff, H. Mütter, H. Herold, H. Ruder, *Matter at High Densities in Astrophysics. Compact stars and the Equation of State*, In Honor of Friedrich Hund’s 100th Birthday, *Springer Tracts in Modern Physics*, Vol. 133, Managing Ed. G. Höhler (Springer, Berlin 1996).
- [14] D. Barret, J. F. Olive and M. C. Miller, *Mon. Not. R. Astron. Soc.* **361**, 855 (2005).
- [15] F. Özel, *Nature*, **441**, 1115 (2006).
- [16] J. M. Lattimer, M. Prakash, *Phys. Rept.* **442**, 109 (2007).
- [17] D. Ivanenko, D. Kurdgelaidze, *Astrofizika* **1** 479, (1965); *Lett. Nuovo Cimento* **2**, 13 (1969).
- [18] F. Weber, *Prog. Part. Nucl. Phys.* **54** (2005) 193.
- [19] P. Danielewicz, R. Lacey, W. G. Lynch, *Science*, **298**, 1592 (2002).
- [20] C. Fuchs, *J. Phys. G* **35**, 014049 (2008).
- [21] H. Yukawa, *Proc. Phys. Math. Soc. Japan* **17**, 48 (1935).
- [22] G. Breit, *Proc. Nat. Acad. Sci. USA* **46** 746 (1960); *Phys. Rev.* **120**, 287 (1960); H. Bethe, “Theory of Nucl. Matter”.
- [23] C. Amsler et al. (Particle Data Group), *Phys. Lett. B* **667**, 1 (2008).
- [24] J. D. Walecka, *Annals Phys. (N.Y.)* **83**, 491 (1974).
- [25] S. A. Chin, *Annals Phys. (N.Y.)* **108**, 301 (1977).
- [26] V. R. Pandharipande, R. B. Wiringa, *Rev. Mod. Phys.* **51**, 821 (1979).
- [27] N. K. Glendenning and S. A. Moszkowski, *Phys. Rev. Lett.* **67**, 2414 (1991).
- [28] G. F. Burgio, H.-J. Schulze and F. Weber, *Astron. Astrophys.* **408**, 675 (2003).
- [29] C. Ishizuka et al., *J. Phys. G* **35**, 085201 (2008).
- [30] J. Schaffner-Bielich, *Nucl. Phys. A* **804**, 309 (2008).
- [31] H. Dapo, B.-J. Schaefer, and J. Wambach, arXiv:0811.2939v1 [nucl-th].
- [32] M. I. Krivoruchenko, F. Simkovic and A. Faessler, *Phys. Rev. D* **79**, 125023 (2009) [arXiv:0902.1825 [hep-ph]].
- [33] F. Özel, G. Baym and T. Guver, arXiv:1002.3153 [astro-ph.HE].
- [34] A. M. Baldin, A. V. Chizhov, R. G. Nazmitdinov, A. S. Shumovsky and V. I. Yukalov, *Dokl. Acad. Nauk SSSR* **279**, 602 (1984) [*Dokl. Acad. Sci. USSR* **279**, 602 (1984)].
- [35] R. G. Nazmitdinov, A. V. Chizhov, A. S. Shumovsky and V. I. Yukalov, *Nucl. Phys. A* **449**, 660 (1986).
- [36] N. K. Glendenning, *Phys. Rev.* **D46** (1992) 1274.
- [37] The MIT bag model has been proposed by physicists from The Massachusetts Institute of Technology: A. Chodos, R. L. Jaffe, K. Johnson, C. B. Thorn and V. F. Weisskopf, *Phys. Rev. D* **9**, 3471 (1974).
- [38] Yu. A. Simonov and V. I. Shevchenko, arXiv:0902.1405 [hep-ph].
- [39] Yu.S.Kalashnikova, I.M.Narodetski, Yu.A.Simonov, *Yad. Fiz.* **46** (1987) 1181.
- [40] Yu.A.Simonov, arXiv:hep-ph/0605022.
- [41] A. M. Baldin, *Short Communications in Physics, Lebedev Institute for Physics*, 1 (1971) 35; Yu. D. Bayukov et al., *Izvestia Akad. Nauk SSSR, Fizika*, **30** (1966) 521; *Yad. Fiz.* **18** (1973), 1246; G. A. Leksin, *Phys. Atom. Nucl.* **65**, 1985 (2002); I. G. Alekseev et al., *Phys. Atom. Nucl.* **71**, 1848 (2008); A. V. Akindinov, Yu. T. Kiselev et al., *JETP Lett.* **72**, 100 (2000); *ibid.* **85**, 142 (2007); Y. Sugaya, Yu. T. Kiselev et al., *Nucl. Phys. A* **634**, 115 (1998); S. V. Boyarinov et al., *Phys. Atom. Nucl.* **50**, 1605 (1989).
- [42] M. Bashkanov *et al.*, *Phys. Rev. Lett.* **102**, 052301 (2009) [arXiv:0806.4942 [nucl-ex]].
- [43] M. I. Krivoruchenko, *Pisma Zh. Eksp. Teor. Fiz.* **46**, 5 (1987) [*JETP Lett.* **46**, 3 (1987)].
- [44] A. Faessler, A. J. Buchmann, M. I. Krivoruchenko and B. V. Martemyanov, *Phys. Lett. B* **391**, 255 (1997) [arXiv:nucl-th/9611020].
- [45] A. Faessler, A. J. Buchmann and M. I. Krivoruchenko, *Phys. Rev. C* **56**, 1576 (1997) [arXiv:nucl-th/9706080].
- [46] A. J. Buchmann, A. Faessler and M. I. Krivoruchenko, *Annals Phys.* **254**, 109 (1997) [arXiv:nucl-th/9610024].

- [47] A. Faessler, A. J. Buchmann, M. I. Krivoruchenko and B. V. Martemyanov, J. Phys. G **24**, 791 (1998) [arXiv:nucl-th/9709030].
- [48] A. Faessler, A. J. Buchmann and M. I. Krivoruchenko, Phys. Rev. C **57**, 1458 (1998) [arXiv:nucl-th/9709028].
- [49] Yu.A.Simonov, Phys. Lett. B **107**, 1 (1981); Yad. Fiz. **36** (1982) 722; **38**, 1542 (1983); preprint ITEP-142 (1981); Nucl. Phys. A **416**, 109c (1984); ibid A **463**, 231c (1987).
- [50] R. L. Jaffe and F. E. Low, Phys. Rev. D **19**, 2105 (1979).
- [51] B. L. G. Bakker and I. M. Narodetskii, Adv. Nucl. Phys. **21** (1994) 1; Yu. A. Simonov, Lecture at the X School of Physics of ITEP (Moscow, Energoizdat 1983).
- [52] Yu. A. Simonov, Usp. Fiz. Nauk **136**, 215 (1982) [Sov. Phys. Usp. **25**, 99 (1982)].
- [53] V. S. Bhasin, V. K. Gupta, Phys. Rev. C **32**, 1187 (1985).
- [54] C. Fasano, T.-S. H. Lee, Phys. Rev. C **36**, 1906 (1987).
- [55] P. J. Mulders, Phys. Rev. D **26**, 3039 (1982); D **28**, 443 (1983).
- [56] M. I. Krivoruchenko, B. V. Martemyanov, Astrophys. J. **378**, 628 (1991); Nucl. Phys. B **24**, 134c (1991).
- [57] D.K. Nadyozhin and V.S. Imshennik, International Journal of Modern Physics A **20**, No. 29, p. 6597.6611 (2005).
- [58] D.K. Nadyozhin, arXiv:0804.4350v1 [astro-ph] (2008).
- [59] W.H. Ramsey, MNRAS **110**, 325 (1950).
- [60] M.J. Lighthill, MNRAS **110**, 339 (1950).
- [61] Z.F. Seidov, Astrofizika **3**, 189 (1967).
- [62] G.S. Bisnovatyi-Kogan, S.I. Blinnikov, É.É. Shnol', Sov. Astron. **19**, 559 (1976); Astron. Zh. **52**, 920 (1975) [in Russian].
- [63] G.S. Bisnovatyi-Kogan *Stellar physics*, Springer-Verlag (2001); *Physical processes of stellar evolution*, Moscow, "Nauka" pub. (1989) [in Russian].
- [64] Z. F. Seidov, arXiv:9912.039v1 [astro-ph] (1999).
- [65] Z. F. Seidov, arXiv:9911.489v1 [astro-ph] (1999).
- [66] M. Takahara and K. Sato, Astrophys. J. **335**, 301 (1988).
- [67] N.A. Gentile, M.B. Aufderheide, G.J. Mathews, F.D. Swesty, and G.M. Fuller, Astrophys. J. **414**, 701 (1993).
- [68] I. Sagert, M. Hempel, G. Pagliara, J. Schaffner-Bielich, T. Fischer, A. Mezzacappa, F.-K. Thielemann and M. Liebendörfer, arXiv:0902.2084v1 [astro-ph.HE] (2009).
- [69] I. Sagert, T. Fischer, M. Hempel, G. Pagliara, J. Schaffner-Bielich, A. Mezzacappa, F.-K. Thielemann, and M. Liebendörfer, Phys. Rev. Lett. **102**, 081101 (pp 4) (2009).
- [70] M. I. Krivoruchenko and B. V. Martemyanov, Yad. Fiz. **58**, 536 (1995) [Phys. Atom. Nucl. **58**, 484 (1995)].
- [71] M.Shifman, A.Vainshtein, V.Zakharov, Nucl. Phys. B **147**, 385, 448 (1979).
- [72] O.Andreev, V.I.Zakharov, Phys. Rev. D **76**, 047705 (2007).
- [73] Yu.A.Simonov, JETP Lett. **55**, 605 (1992); Phys. At. Nucl. **58**, 309 (1995).
- [74] M.D'Elia, A.DiGiacomo, and E.Meggiolaro, Phys. Lett. B **408**, 315 (1997); phys. Rev. D **67**, 114504 (2003); A.Di Giacomo, E.Meggiolaro and H.Panagopoulos, Nucl. Phys. B **483**, 371 (1997).
- [75] L. A. Kondratyuk, B. V. Martemyanov and M. I. Krivoruchenko, Z. Phys. C **52**, 563 (1991).
- [76] Yu.A.Simonov, Ann Phys. **323**, 783 (2008); E.V.Komarov, Yu.A.Simonov, Ann. Phys. **323**, 1230 (2008).
- [77] Yu.A.Simonov, Phys. Lett. B **619**, 293 (2005).
- [78] A.Di Giacomo, E.Meggiolaro, Yu.A.Simonov and A.I.Veselov, Phys. At Nucl. **70**, 908 (2007).
- [79] Yu.A.Simonov, Phys. Atom Nucl. **60**, 2069 (1997); Yu.A.Simonov, Phys. Rev. D **65**, 092018 (2002).
- [80] M.A.Trusov, Yu.A.Simonov, arXiv:0908.3276; Yu.A.Simonov hep-ph/0605022.
- [81] Yu.A.Simonov, Phys.Atom Nucl. **66**, 338 (2003).
- [82] K.Wildermuth and Y.C.Tang, Unified Theory of the Nucleus, Vieweg, Braunschweig, 1977.
- [83] Yu. A. Simonov, Few-Body Systems, Suppl. 2 (1987)228; Yu. S. Kalashnikova, I. M. Narodetskii, Journ. Mod. Phys. A **4** (1989) 335.
- [84] J. D. Bjorken and S. D. Drell, *Relativistic Quantum Mechanics*, (McGraw-Hill Book Co., N.Y., 1964).
- [85] L. Castillejo, R. Dalitz, F. Dyson, Phys. Rev. **101**, 543 (1956).
- [86] F. Dyson, Phys. Rev. **106**, 157 (1957).
- [87] T. D. Lee, Phys. Rev. **95**, 1329 (1954).
- [88] R. L. Jaffe and M. P. Shatz, preprint CALT-68-775 (1980).
- [89] M. Abramowitz and I. A. Stegun, *Handbook of Mathematical Functions: with Formulas, Graphs, and Mathematical Tables*, (Dover, New York, 1964).
- [90] S. Flügge, *Practical Quantum Mechanics*, (Springer-Verlag, Berlin, 1971).
- [91] F. E. Low, Phys. Rev. **97**, 1392 (1955).
- [92] M. I. Krivoruchenko, arXiv:1001.1659v1 [nucl-th] (2009).
- [93] Center for Nuclear Studies, The George Washington University, <http://gwdac.phys.gwu.edu/>.
- [94] M. I. Krivorucheko and Yu. A. Simonov, in preparation.
- [95] H. Clement *et al.* [CELSIUS-WASA Collaboration], To appear in the proceedings of International School of Nuclear Physics: 29th Course: Quarks in Hadrons and Nuclei, Erice, Sicily, Italy, 16-24 Sep 2007. e-Print: arXiv:0712.4125 [nucl-ex].
- [96] I. I. Sobelman, *Introduction to the Theory of Atomic Spectra*, (Pergamon Press, Oxford, 1972).
- [97] W.-D. Kraeft, D. Kremp, W. Ebeling, G. Roepke, *Quantum Statistics of Charged Particle Systems*, (Akademieverlag

Berlin and Plenum, London, New York, 1986).

- [98] F. Calogero, Yu. A. Simonov, Phys. Rev. Lett. **25**, 881 (1970); Nuovo Cim., **64B**, 337 (1969). See also: E. L. Surkov, Phys. Rev. C **5**, 1943 (1972).
- [99] Ya. B. Zel'dovich, UFN **86**, 303 (1965); Soviet Phys. Uspekhi **8**, 489 (1965).
- [100] Ya. B. Zel'dovich, ZhETF **41**, 1609 (1961).
- [101] H. Mütter, A. Polls, Prog. Part. Nucl. Phys. **45** (2000) 243.
- [102] P.-G. Reinhard, M. Bender, Lect. Notes Phys. **641** (2004) 249 (and references therein).
- [103] P. C. C. Freire, AIP Conf. Proc. **983**, 459 (2008);
P. C. C. Freire, S. M. Ransom, S. Begin, I. H. Stairs, J. W. T. Hessels, L. H. Frey and F. Camilo, AIP Conf. Proc. **983**, 604 (2008).
- [104] N. K. Glendenning, *Compact Stars: Nuclear Physics, Particle Physics and General Relativity*, (Springer-Verlag, N. Y., 1996).
- [105] T. Gross-Boelting, C. Fuchs, and A. Faessler, Nucl. Phys. A **648** (1999) 105.
- [106] C. Fuchs, Lect. Notes Phys. **641** (2004) 119 (and references therein).
- [107] E. van Dalen, C. Fuchs, A. Faessler, Nucl. Phys. A **744** (2004) 227.
- [108] E. N. E. van Dalen, C. Fuchs and A. Faessler, Phys. Rev. Lett. **95**, 022302 (2005) [arXiv:nucl-th/0502064].
- [109] A. Mukherjee and V. R. Pandharipande, Phys. Rev. C **75**, 035802 (2007) [arXiv:nucl-th/0609058].
- [110] A. Akmal, V.R. Pandharipande, D.G. Ravenhall, Phys. Rev. C **58** (1998) 1804.
- [111] A. Bhattacharyya, S. K. Ghosh and S. C. Phatak, Phys. Rev. **C60**, 044903 (1999).
- [112] A. Mishra, J. Reinhardt, H. Stocker, and W. Greiner, Phys. Rev. **C66**, 064902 (2002).
- [113] Ji-sheng Chen, Peng-fei Zhuang, Jia-rong Li, Phys. Rev. **C68**, 045209 (2003).
- [114] E. Santini, M. D. Cozma, A. Faessler, C. Fuchs, M. I. Krivoruchenko and B. Martemyanov, Phys. Rev. C **78**, 034910 (2008).
- [115] J. M. Eisenberg, W. Greiner, *Microscopic theory of the nucleus*, (North-Holland Publishing Company, Amsterdam-London, 1972).
- [116] S.I. Blinnikov, Sov. Astron. **19**, 151 (1975); Astron. Zh. **52**, 243 (1975) [in Russian].
- [117] A. Weiss, W. Hillebrandt, H.-C. Thomas and H. Ritter, *Cox & Guili's Principles of Stellar Structure*, Extended Second Edition, Cambridge Scientific Publishers, pp 767 (2004).
- [118] D.K. Nadyozhin, Astrophys. Space Sci. **53**, 131 (1978).